

Physicochemical Analysis of Bacterial and Firefly Bioluminescence

Dissertation

zur

Erlangung des Doktorgrades (Dr. rer. nat.)

der

Mathematisch-Naturwissenschaftlichen Fakultät

der

Rheinischen Friedrich-Wilhelms-Universität Bonn

vorgelegt von

Lydia Kammler

aus

Bonn-Duisdorf

Bonn 2013

Angefertigt mit Genehmigung der Mathematisch-Naturwissenschaftlichen Fakultät der
Rheinischen Friedrich-Wilhelms-Universität Bonn

1. Gutachter: Prof. Dr. Peter Vöhringer
2. Gutachter: PD. Dr. Maurice van Gastel

Tag der Promotion: 13.09.2013

Erscheinungsjahr: 2013

*Der Beginn aller Wissenschaften ist das Erstaunen,
dass die Dinge sind, wie sie sind.*

– Aristoteles zugeschrieben

Contents

1	Introduction.....	1
1.1	Bioluminescence.....	1
1.2	Bioluminescent model organisms.....	2
1.3	Chemical reaction of bioluminescence.....	3
1.4	Luciferin	5
1.5	Flavins and their abilities	7
1.6	Genetics, structure and function of bacterial luciferase.....	12
1.7	Bioluminescent reaction of firefly luciferase	17
1.8	Objective	18
2	Material and methods.....	20
2.1	Chemicals, enzymes, kits and other materials.....	20
2.2	Vectors and primers.....	23
2.3	Bacterial strains	25
2.4	Software and online tools	25
2.5	Microbiological methods.....	26
2.5.1	Cultivation of <i>Escherichia coli</i>	26
2.5.2	Cultivation of <i>V. fischeri</i>	27
2.5.3	Conservation of bacterial strains	27
2.5.4	Preparation of competent <i>E. coli</i> cells	27
2.5.5	Transformation of competent <i>E. coli</i> cells	27
2.6	Methods of molecular biology.....	28
2.6.1	Preparation of chromosomal DNA from <i>V. fischeri</i>	28
2.6.2	Isolation of plasmid DNA from <i>E. coli</i>	29
2.6.3	Photometric determination of DNA concentration and purity.....	29
2.6.4	DNA amplification <i>in vitro</i> by PCR.....	30
2.6.4.1	Standard-PCR.....	30
2.6.4.2	Colony PCR	31
2.6.4.3	Primer construction.....	32
2.6.5	DNA visualization	33
2.6.5.1	Agarose gel electrophoresis	33

2.6.5.2	Purification of DNA fragments from agarose gel.....	33
2.6.6	Enzymatic modification of DNA	34
2.6.6.1	Restriction of DNA	34
2.6.6.2	Ligation	34
2.7	Protein-biochemical methods	34
2.7.1	Homologous expression of bacterial luciferase	34
2.7.2	Heterologous expression of recombinant protein.....	35
2.7.3	Cell disruption	35
2.7.4	Chromatographic methods	36
2.7.4.1	Affinity chromatography of recombinant protein.....	36
2.7.4.2	Gel filtration chromatography.....	37
2.7.4.3	Ion exchange chromatography of homologous protein.....	39
2.7.5	Determination of protein concentration	40
2.7.6	Protein visualization.....	40
2.7.6.1	SDS-PAGE.....	40
2.7.6.2	Coomassie staining.....	42
2.8	Biophysical methods	42
2.8.1	UV/VIS spectroscopy.....	42
2.8.1.1	Theory.....	42
2.8.1.2	Flavin sample preparation	43
2.8.1.3	Oscillator strength determination	43
2.8.2	Fluorescence spectroscopy	44
2.8.2.1	Theory.....	44
2.8.2.2	Flavin sample preparation	45
2.8.2.3	Kinetic assays with luciferase	45
2.8.3	EPR spectroscopy	47
2.8.3.1	Theory.....	47
2.8.3.2	Spin trapping	49
2.8.3.3	Spin trapping sample preparation.....	51
2.8.3.4	Analysis of spin trapping samples by CW EPR	52
2.8.3.5	Triplet state of flavins.....	53
2.8.3.6	Sample preparation for excited triplet state measurements of FMN	56
2.8.3.7	Laser excitation of FMN and analysis by pulsed EPR.....	56
2.8.3.8	Simulations	57
2.8.4	Mass spectrometry	59
2.8.4.1	Theory.....	59
2.8.4.2	Recombinant LuxAB samples	60
2.8.4.3	Spin trapping samples	60
2.9	Theoretical calculations	60
3	Results	63
3.1	Electronic structure of FMN.....	64
3.1.1	UV/VIS spectra and calculations	64

3.1.2	EPR spectra and calculations	67
3.1.3	HOMO and LUMO calculations	73
3.2	Selective production and characterization of LuxAB from <i>V. fischeri</i>.....	79
3.2.1	Heterologous expression of recombinant LuxAB.....	79
3.2.2	Homologous purification of LuxAB	86
3.2.3	Optimum activity of LuxAB <i>in vitro</i>	87
3.2.4	Different substrates for bacterial bioluminescence.....	90
3.2.5	Kinetic assays with LuxAB <i>in vitro</i>	94
3.2.6	Radical intermediates in bacterial bioluminescence	97
3.3	Selective production and characterization of Luc from <i>P. pyralis</i>	102
3.3.1	Heterologous expression of recombinant Luc from <i>P. pyralis</i>	102
3.3.2	No radical intermediate detected.....	105
4	Discussion	106
4.1	Electronic structure of the lowest triplet state of bacterial luciferin.....	106
4.2	Purification and optimum activity conditions of bacterial luciferase.....	109
4.3	Affinity for different substrates	111
4.4	Kinetic assays <i>in vitro</i> ; aldehyde radicals and dithionite.....	114
4.5	Bacterial bioluminescence runs via a radical intermediate	116
5	Summary and outlook.....	120
6	References	123
	Appendix figures	145
	Publications.....	146
	Acknowledgment	148

Abbreviations

Amp	ampicillin
AmpR	ampicillin resistance
APS	adenosine-5'-phosphosulfate
ATP	adenosine triphosphate
a.u.	arbitrary units
bp	base pair(s)
BSA	bovine serum albumine
cDNA	chromosomal DNA
COSMO	conductor-like screening model
CV	column volume
CW	continous wave
Da	dalton
DEAE	diethylaminoethyl
DFT	density functional theory
DMPO	5,5-dimethyl-1-pyrrolin-N-oxide
DMSO	dimethylsulfoxide
DNA	deoxyribonucleic acid
EDTA	ethylenediaminetetraacetate
EPR	electron paramagnetic resonance
ESE	electron spin echo
ESI	electrospray-ionisation
FAD	flavin adenine dinucleotide
FMN	flavin mononucleotide
HEPES	N-[2-hydroxyethyl]-piperazine-N'-[2-ethanesulfonic acid]
HOMO	highest occupied molecular orbital
IPTG	isopropyl- β -S-thiogalactoside
ISC	intersystem crossing
kb	kilobases
Kan	kanamycin

KanR	kanamycin resistance
LUMO	lowest unoccupied molecular orbital
MALDI	matrix-assisted laser desorption/ionization
MW	molecular weight
MWCO	molecular weight cut off
NADH	reduced nicotinamide adenine dinucleotide
NADPH	reduced nicotinamide adenine dinucleotide phosphate
OD	optical density
PAGE	polyacrylamide gel electrophoresis
PCR	polymerase chain reaction
RIF	riboflavin
rpm	rounds per minute
RT	room temperature
S	standard
SDS	sodium dodecyl sulfate
SOC	spin-orbit-coupling
TEMED	N,N,N',N'-tetramethyldiamine
TEMPO	2,2,6,6-Tetramethylpiperidin-N-oxyl
TOF	time of flight
Tris	trishydroxymethylaminomethane
UV	ultraviolet
ZFS	zero field splitting

1 Introduction

1.1 Bioluminescence

The emission of light by a living organism is one of nature's most remarkable phenomena, first described several thousand years ago, when the ancient Chinese and Greeks referred to bioluminescent sightings. Aristotle noted in the 4th century B.C. that "some things though they are not in their nature fire, nor any species of fire, yet seem to produce light" [1]. The term 'luminescence' was first designated by Eilhardt Wiedemann in 1888 as the emission of light, which is not accompanied by a rise in temperature [2]. The description 'Bioluminescence' was proposed by Harvey in 1916, meaning the luminescence from living organisms [3]. The fact that the bioluminescent process neither requires nor generates much heat, referred to as 'cold light', makes this natural chemical reaction very interesting from a scientific and energy-saving perspective.

Although bioluminescence appears throughout the whole terrestrial and aquatic world, most of the light producing organisms live in saline waters. They are nearly absent in fresh water, except for some insect larvae and freshwater limpets. Bioluminescence evolved many times in many taxonomically distinct species [4], which is reflected in the innumerable appearance and diversity of different luminescent organisms. The morphology of bioluminescence is just as versatile as its function, ranging from communication to predator-prey interactions and reproduction. However, in some cases, e.g. several fungi, the function is still unknown. A number of animals developed highly complicated light organs, which are controlled by their nervous system and emit light only on stimulation (e.g. squids). In other organisms the light emission is continuous and originates from one single cell, such as in luminous bacteria and dinoflagellates [5]. The bioluminescence reaction is not only interesting from an energetic point of view, but also because it can be used as an analytical tool in various fields of science and technology. The firefly bioluminescence system for example requires adenosine 5'-triphosphate (ATP) and is therefore used as a method for measuring ATP concentrations as a scale for bacterial contamination in water pipes [6]. Luminescent dinoflagellates, which are responsible for the touristic 'bioluminescent bays' phenomenon in Puerto Rico and Jamaica, are sensitive to distinct toxins and are used as

biosensors in such a way that a change in their light emission intensity, which depends on toxin concentrations, can be detected. Another useful application are Ca^{2+} -sensitive photoproteins, which can be used for monitoring intracellular Ca^{2+} , like the aequorin from the jellyfish *Aequorea* [7]. Aequorin emits light in aqueous solutions by an intramolecular reaction only by the addition of Ca^{2+} . The total light emission is proportional to the amount of the applied protein.

The one thing that almost all bioluminescent reactions have in common is the necessity of a substance referred to as 'luciferin'. All known luciferin molecules contain an aromatic compound. By being oxidized and stimulated to a higher energy level, an excited state, they provide the energy for light emission in the visible range [8–13]. In most cases bioluminescence was found to be catalyzed enzymatically by a protein, 'luciferase'. In luminous fungi, however, there has no enzyme been detected that seems to be involved in the luminescent reaction.

1.2 Bioluminescent model organisms

A broad range of organisms are luminescent. Dubois first encountered in 1885 that two extracts prepared from the West Indies beetle *Pyrophorus* resulted in light emission when mixed together [14]. E. Newton Harvey made the biggest contribution to the scientific world. His lifelong study (1887-1959) and knowledge of bioluminescence and the various systems that it appears in are preserved in over 300 publications and his book 'Bioluminescence' [15]. He also discovered that the emitted light in salty water is mostly produced by bacteria. Until this day the most investigated and understood bioluminescence system is that of the bacteria. These microorganisms are only luminous when they have reached a sufficient concentration (10^8 cells/ml) to initiate the mechanism of 'quorum sensing' [16,17]. This term describes the regulation of gene expression in response to changes in cell density. Depending on the cell density, bacteria produce and release chemical signal molecules, termed autoinducers, which subsequently initiate or repress the expression of certain genes in all bacteria simultaneously. It is a common regulatory mechanism in gram-negative bacteria, especially amongst several pathogens [18]. Once this mechanism is initiated for

bioluminescence, light is emitted continuously rather than in discrete flashes. This occurrence is limited to bacteria and was first discovered in *Vibrio fischeri* [19]. Within the two existing phyla of bacteria, Archaea and Eubacteria, luminescent representatives are only known amongst the gram-negative γ -proteobacteria of the Eubacteria. The best-studied luminous representatives are *V. fischeri* and *Vibrio harveyi*. The latter is a mostly free-living species, whereas *V. fischeri* is additionally found as a symbiotic culture in light organs of various fish and squid [20]. McFall-Ngai and Ruby showed that the presence of these bacteria even induces the morphological development of the light organ in the bobtail squid *Euprymna scolopes* [21]. *V. fischeri* was isolated in 1889 by Martinus Willem Beijerinck [22]. It uses organic compounds exclusively as source of carbon and energy (heterotrophic) [23] and develops flagella as soon as it is removed from its symbiotic environment in the squid [24]. The complete genome has been sequenced in 2005 [25], which makes *V. fischeri* the ideal organism for the investigation of bacterial bioluminescence .

The most investigated luminescent organism outside the water environment is the North American firefly *Photinus pyralis* (Order *Coleoptera*, Family *Lampyridae*). Adult animals of this beetle are located in meadows, woodland edges and near streams from late spring to early fall [26]. Only the male individuals use their wings for flying, whereas the females have shorter wings and do not fly. Fireflies use bioluminescence in their abdominal organ to attract mating partners. The males locate the females by a combination of light flashes, to which the females reply with a delayed, coded flash [27]. *P. pyralis* possesses one of the most intense and brightest luminescence in the living world and therefore represents a scientifically interesting subject to study bioluminescence [28].

1.3 Chemical reaction of bioluminescence

Even though many methods have been developed that help to understand biological reactions, there is still very little known about the chemical reaction of bioluminescence on a molecular level. The energy for this light emitting reaction originates from the substrate luciferin. This molecule generates a distinct amount of energy when it is

oxidized, resulting in the transmission of light at a certain wavelength. Hence, most bioluminescence reactions have oxygen as a common reactant, but exhibit diverse reaction mechanisms to generate electronically excited molecule states capable of light emission. Figure 1-1 shows a small variety of the reaction diversity. The bacterial bioluminescence (Figure 1-1, A) uses reduced FMN as luciferin, which reacts with molecular oxygen and an aliphatic aldehyde [29]. This reaction is described in more detail elsewhere (cf. section 1.6).

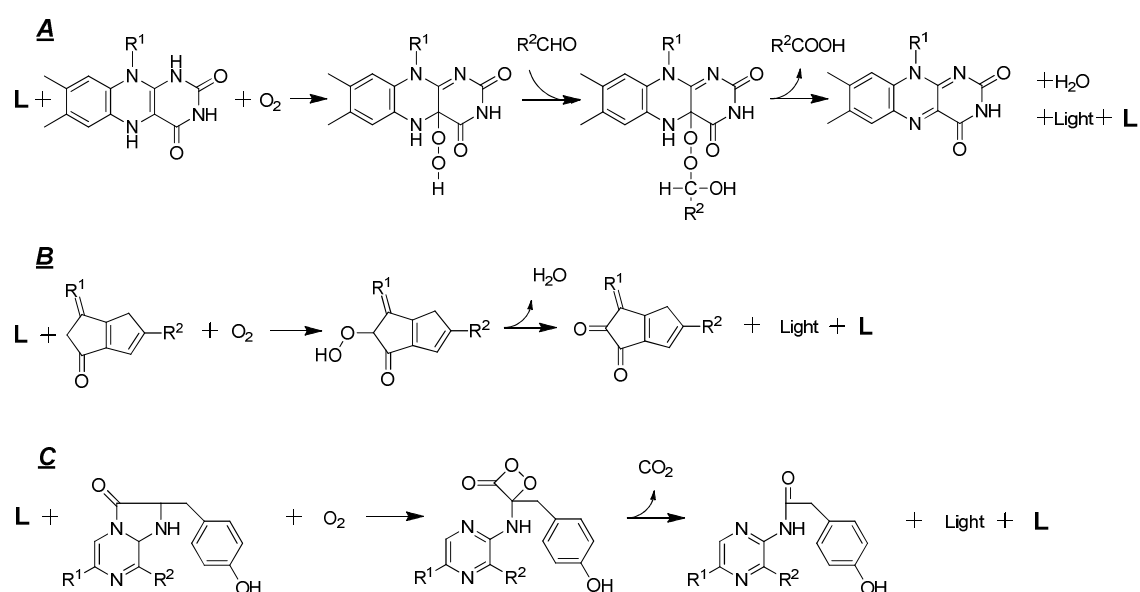


Figure 1-1: Examples of the chemical diversity in bioluminescence. A: bacteria, B: dinoflagellates, C: most oceanic phyla. The luciferase is indicated by the letter L. (illustration derived from Hastings and Krause [30])

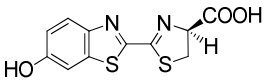
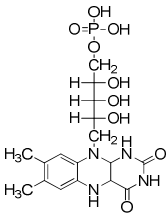
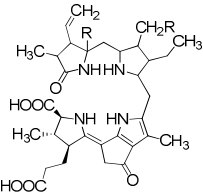
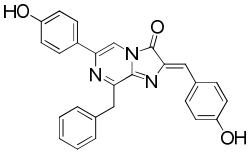
In dinoflagellates (Figure 1-1, B) the luciferin molecule is a tetrapyrrole with four five-membered rings (R_1 contains 2, R_2 contains 1) consisting of one nitrogen and four carbons [30]. The reaction presented in Figure 1-1 C is found in most oceanic phyla and involves the oxidation of the imidazolopyrazine bicyclic ring. Such coelenterazine centered luminescence occurs in jellyfish including *Aequorea* (jellyfish), *Cavernularia* (sea pansy) and *Renilla* (sea pen) [31]. *Aequorea* represents one rather untypical

bioluminescence mechanism (*vide supra*) with no need of oxygen, including a protein referred to as aequorin [7]. Aequorin leads to the emission of light simply by the addition of Ca^{2+} . Yet another distinctive feature is that the species *Aequorea aequorea* and *Aequorea victoria* emit green light *in situ*, whereas the aequorin protein from the same organism emits blue light *in vitro*. This is due to the presence of a green fluorescence protein (GFP) in the photogenic cells of *Aequorea*. A part of the energy, generated by bioluminescence, is transferred from the aequorin to the GFP, which subsequently emits green light [32,33]. Despite some exceptions, a luciferase protein and a luciferin substrate are involved in all natural bioluminescence reactions. The interaction of these two molecules has been of major interest. Especially for the bacterial bioluminescence this interaction has been well studied [4].

1.4 Luciferin

The term ‘luciferin’ derives from the Latin word ‘lucifer’, which means ‘light-bringer’. This appropriate description points out that the luciferin molecules are the key substance for the bioluminescence reaction. It is an organic compound that occurs in almost all luminous organisms and provides the energy for the light emitting reaction by being oxidized and promoted to an excited product state. The luciferin molecules are highly conserved across all phyla and can appear in both luminous and nonluminous organisms [34,35]. A multitude of molecules can serve as luciferin (Table 1-1). In luminescent bacteria reduced flavin mononucleotide, FMNH₂, serves as luciferin, dinoflagellates use a substituted open-chained tetrapyrrol [36]. Cnidaria and other marine organisms utilize an imidazolopyrazinone, also referred to as coelenterazine, which also exists with a number of different substitutes [37]. The most frequently described luciferin from the firefly *Photinus* is a benzothiazolylthiazole derivative, which reacts with ATP and forms luciferyl-AMP, before the actual luminescent reaction can occur [38].

Table 1-1: Diversity and discovery of natural luciferins.

Chemical structure	Description	Occurrence	Chemical identification
	D-Luciferin (benzothiazole)	Fireflies, beetles, railroad worms	Bitler 1957 [39] White 1961 [40] White 1963 [41]
	FMN (flavin)	Bacteria	McElroy 1955 [42]
	Tetrapyrrole	Dinoflagellates, krills	Nakamura 1989 [43]
	Coelenterazine	Widespread among oceanic phyla of eukaryotes	Hori 1973 [44]

This process is a distinctive feature of insect luciferins and has not been found in any other bioluminescent systems. Although these luciferin molecules seem to vary, they all have the common attribute of a mesomeric system, which stabilizes the obligatory excited state prior to light emission. Most luciferins even consist of several heterocyclic groups. The light-emitting species of the luciferin molecules is generally an excited

carbonyl-oxygen, which arises from a hydroperoxyl- or cyclic peroxide intermediate. The former appears as a 4a-hydroperoxy-FMNH in bacterial bioluminescence, the latter is associated with the oxidative cleavage of double bonds [37].

Interestingly, it has been shown that the radical pyrrol-cleavage of melatonin or other indolmetabolites leads to the emission of light [45]. The fact that some mesomeric metabolites emit light during the reaction with free radicals, might explain the occurrence of bioluminescence in different taxa with no evolutionary connection.

Immediate availability of luciferin is quite different in each organism. The ostracod *Cypridina* accumulates the luciferin molecules and the luciferase proteins in different parts of its salivary and mixes them only by secretion. Insect luciferin requires a pre-reaction with ATP and in some Cnidaria the light-emitting cells need to be stimulated by calcium before bioluminescence can occur. The present study is particularly focused on the investigation of the bacterial luciferin FMN. It belongs to the group of flavin molecules, which are described in more detail in the following section.

1.5 Flavins and their abilities

Flavins are a group of organic chromophores with fluorescent compounds involved in many biological processes, e.g. bacterial bioluminescence. Their name derives from the Latin word 'flavus', which means 'yellow' and describes the optical appearance of these yellow colored substances. Basic structure of all flavins is 7,8-dimethylisoalloxazine, a tricyclic heteronuclear organic ring that provides their main functional ability as redox active cofactors. It is reduced by one or two electrons to either the semiquinone or flavohydroquinone, respectively [46]. All three redox states exist in different protonation forms, depending on the effective pH (Figure 1-2) [47]. Neutral flavin is deprotonated at pH~10, semiquinone at pH~8, flavohydroquinone at pH~6, all forming different anions. The protonated conformations of neutral flavin and flavohydroquinone are formed at pH~0, of semiquinone at pH~2, all resulting in various cations.

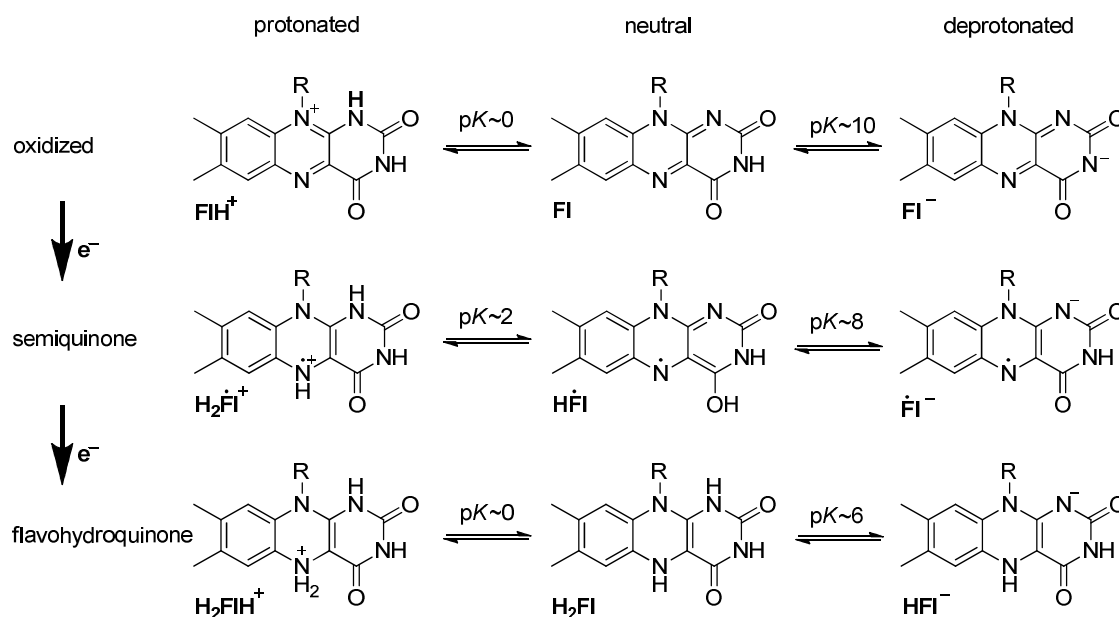


Figure 1-2: Redox and acid-base states of flavin; remodeled from Heelis [47]. The letter R indicates the flavin specific residue side chain.

Flavins differ in the composition of the side chain R at one nitrogen of the central ring (cf. Figure 1-2). A methyl group as residue side chain characterizes lumiflavin, whereas an extension of this methyl with $(\text{CHOH})_3\text{-CH}_2\text{OH}$ leads to a riboflavin (RIF) molecule, also known as vitamin B₂ and food additive E101. RIF represents the basic chemical structure of the two most important flavins, FMN and FAD (Figure 1-3). FMN and FAD are bound to proteins as mainly non-covalent, redox-active functional groups. They play essential roles in many biological, mostly electron-transfer related reactions, such as DNA repair mechanisms of photolyases [48–51] and programmed cell death (apoptosis) [52]. As components of cryptochromes they additionally function as blue-light photoreceptors [53] and bound to dehydrogenases and oxidases they are also highly involved in the oxidative metabolism and ATP production, which is the main source of chemical energy in biological systems [54,55]. A more detailed overview of different proteins that possess a flavin cofactor, named flavoproteins and flavoenzymes, is described elsewhere [56]. Some groups of flavoproteins have been shown to be radical enzymes [57], appearing as radical intermediates during the catalytic mechanism

and therefore providing excellent foundation for electron paramagnetic resonance (EPR) studies in order to analyze their electronic structure when bound to the enzyme. EPR research on flavoproteins has resulted in an increasing number of publications during the last decade [58–69].

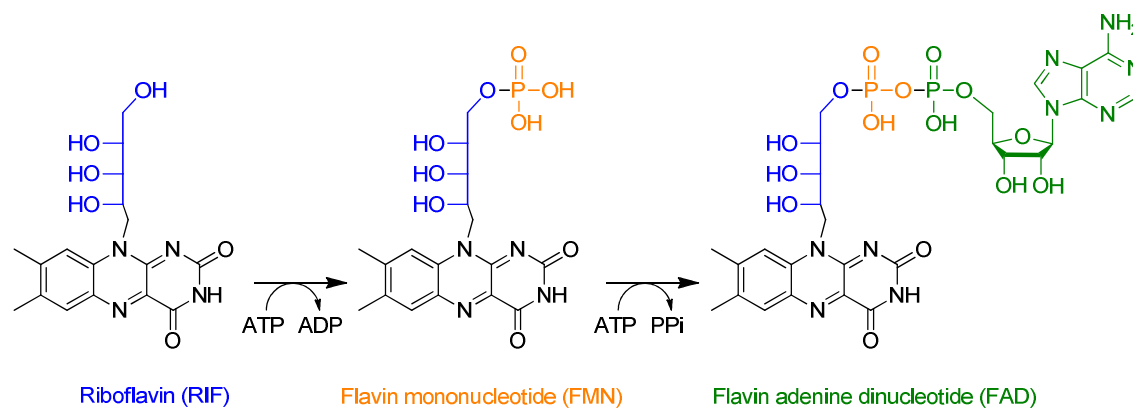


Figure 1-3: Conversion of riboflavin to FMN and FAD.

FMN is synthesized by phosphorylation of RIF at the last hydroxyl group of the side chain (Figure 1-3). In biological systems this ATP-dependent process is catalyzed by a group of phosphotransferases named riboflavin kinases [70,71]. Bound to the bacterial luciferase, FMN is majorly involved in the emission of light in bacterial bioluminescence by being the excited emitter [42]. FAD is synthesized from FMN by the addition of adenosine monophosphate (AMP), which is a nucleotide containing phosphoric ester of the nucleoside adenosine. As prosthetic group of the succinate dehydrogenase, complex II of the respiratory chain, FAD plays a major role in the electron transfer chain of mitochondria [72].

The fundamental role of flavins lies in their ability of being reversely reduced, which enables their main function as electron acceptor and donor in e.g. biological processes. This reduction step can be enforced chemically or photochemically by photo reduction [73,74]. The latter has been well studied for FMN and can cause photodegradation to

the primary photoproducts formylflavin, lumiflavin and lumichrome (Figure 1-4) derivatives in aqueous solutions [75].

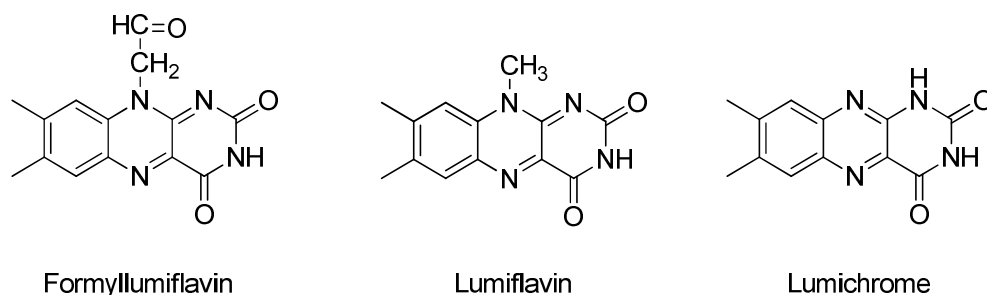


Figure 1-4: Primary photodegradation products of FMN [75].

Photophysical and photochemical properties of flavins have been of major scientific interest [76–80]. In particular, information about the electronic transitions of FMN in solution at different pH values have been provided by absorption spectra [81,82]. At neutral and high pH, two characteristic bands are present with maxima at about 375 nm and 450 nm, which exact wavelengths slightly depend on the pH value and temperature. Under acidic conditions, all bands come together and give rise to one large absorption band with a maximum at about 400 nm [81]. Time-dependent density functional theory (TDDFT) studies for oxidized and reduced lumiflavin have provided first insights into the orbital structure [83,84]. Both calculations and a high molar extinction coefficient of $> 10^4 \text{ M}^{-1}\text{cm}^{-1}$ [47] indicate that the bands at 375 and 400 nm can be classified as $\pi \rightarrow \pi^*$ transitions. A recent study confirms that the inclusion of environmental effects is essential in order to reproduce the experimental spectra [85], which was also reported in the *ab initio* study of a FAD-binding NAD(P)H:quinone oxidoreductase [86]. The yellow fluorescence of flavins shows its maximum at 520 nm in aqueous solutions [47,87]. The polarity of the solvent has an influence on the quantum yield (Q) of the flavins' fluorescence. It increases from $Q = 0.26$ in aqueous solutions to 0.47 in acetonitrile, which has been assumed to be caused by hydrogen bonding between the flavin and the solvent [88].

In addition, the intensity of fluorescence is influenced by the pH. Relative to the neutral form, a decreased intensity appears in the deprotonated form at high pH as well as in the protonated form at low pH (cf. Figure 1-2). In the presence of organic compounds, e.g. aromatic hydrocarbons and amino acids, the fluorescence is also considerably reduced, even more if the flavin is bound to an enzyme. This effect is assigned to an increased rigidity forced by the protein [87]. Flavin derived orange-red phosphorescence, which is the radiative decay of the triplet excited state to the ground state, displays a maximum at 600 nm [47,89]. It has a comparatively long lifetime of 0.1 to 0.2 seconds [90].

For organic chromophores, which are not paramagnetic, information about the electronic structure and catalytic cycle can still be obtained by EPR spectroscopy, if the molecule can be excited to a triplet state [91–93]. Triplet states ($S = 1$) contain two unpaired electrons and are therefore paramagnetic. The triplet state is usually reached upon promotion of an electron from a doubly occupied orbital into an empty orbital by excitation with light. Since the two unpaired electrons do not occupy the same orbital anymore, one spin may flip owing to spin-orbit coupling (SOC), thus generating the triplet state [94,95]. This mechanism of triplet formation is termed intersystem crossing (ISC) and described in more detail later (section 2.8.3.5). For a detailed comparison of the electronic structure of FMN in solution and bound to a protein, information by e.g. electron nuclear double resonance (ENDOR) spectroscopy of the photoexcited triplet state is required. ENDOR can provide steric information between the electron spins and the coupled nuclei. These examinations have not yet been carried out for FMN in frozen solution. One reason for the lack of such studies is the low spin polarization of the excited triplet state and an exceptionally long lifetime of one of the triplet sublevels of 100 ms, making measurements very time consuming [96–98]. The presence of a lifetime of 100 ms is indicative of a small SOC matrix element between the triplet state and the singlet ground state. The triplet state of FMN, however, has been reinvestigated and spin polarized triplet signals have been detected, despite low polarization [96]. The magnetic interaction between the two triplet electrons, zero field splitting (ZFS), and the decay kinetics of the triplet sublevels were found to depend on the protonation

state of FMN. Three protonation states have been investigated, in which the slowest decay was observed for the neutral FMN species [96].

1.6 Genetics, structure and function of bacterial luciferase

The gen loci and regulation of the bacterial bioluminescence has been studied in detail during the last decades [99–104]. The genes that are involved in bacterial bioluminescence are termed *lux* genes. *V. fischeri* shows at least eight *lux* genes organized in two loci with differing transcription patterns, the operon *luxICDABEG* and a single gene *luxR* (Figure 1-5).

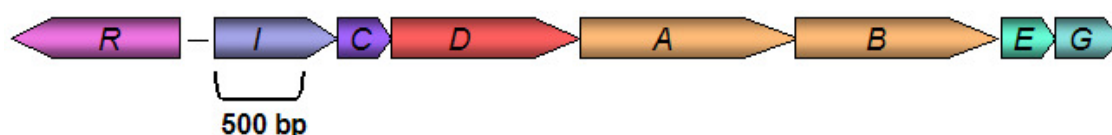


Figure 1-5: Schematic representation of the *lux* operon in *V. fischeri* (adapted from Ast and Dunlap [105]).

The enzyme required for the synthesis of the autoinducer is encoded by *luxI*. The quorum sensing in *V. fischeri* is controlled by a population density-responsive regulatory mechanism [106]. The protein encoded by *luxI* synthesizes only basic levels of the signal molecule, 3-oxohexanoyl-L-homoserine lactone, at low cell density. With increasing cell population this molecule assembles until a certain threshold concentration, which initiates its binding to LuxR, encoded by *luxR* as a transcriptional regulatory protein [107]. This complex directly induces the transcription of the *luxICDABEG* genes and the expression of the bioluminescence required proteins [16,104]. The genes *luxCDE* encode for proteins that are involved in the biosynthesis of a fatty aldehyde, which is the cosubstrate of bacterial bioluminescence and is oxidized to its corresponding fatty acid [108,109]. LuxC and LuxE are essential for the reduction of myristic acid (tetradecanoic acid) to a myristic aldehyde, whereas LuxD is supposedly involved in the transport of the fatty acid [110]. Up until today it is

unknown how the cell survives in the presence of reactive aldehyde species, also there has been no explanation for the transport of the aldehyde to the luciferase protein. The protein encoded by *luxG* is not essential for luminescence, but is assumed to enhance the synthesis of FMNH₂ *in vivo* in *V. fischeri* [111].

The luminescent reaction itself is catalyzed by the luciferase protein. Immunogold labeling on bacterial sections of *V. fischeri* and *V. harveyi* provided a predominantly association of the luciferase protein with the inner membrane of the bacterial cells, which enables an intense and more visible luminescence [112]. The luciferase consists of two subunits, α and β , encoded by the genes *luxA* and *luxB*. The two genes seem to have developed by gene duplication [113] due to their 32 % identity in the amino acid sequence in all luminescent bacteria [114]. The α subunit contains 29 additional amino acids inserted between the residues 258 and 259 of the β subunit [115], which causes an extended mobile loop exclusively on the α subunit [116,117]. The 77.6 kDa luciferase protein is a heterodimeric flavin-monooxygenase with molecular masses of 40.3 kDa for LuxA and 37.3 kDa for LuxB. The fundamental kinetic mechanism of the subunit folding and heterodimeric assembly has been cleared up [118]. Both subunits fold into highly similar $(\alpha/\beta)_8$ triosephosphateisomerase (TIM) barrel structures, which was shown by the description of the heterodimeric crystal structure at 2.5 Å and 1.5 Å resolution [115,119]. Eight parallel β -sheets are connected by eight α -helices and form a barrel-shaped structure. It was also described that the subunits interact across an extended amphipathic and planar interface and that the active site of the protein is formed by residues in the α subunit upon binding of FMNH₂. Directed and random mutagenesis experiments have been carried out on bacterial luciferase in order to elucidate the enzymatic function of the protein. A mutation of the His44 residue in the α subunit to an alanine resulted in an inactive enzyme [120], suggesting that this histidine residue is an essential component of the active center. A mobile loop of the protein between β strand 7 and α helix 7 of the α subunit was deleted using a genetic construct [116]. The approximately 10 % smaller protein was still folding and exhibiting bioluminescent activity, even though the total quantum yield was decreased

by two orders of magnitude. The β subunit most likely carries a supporting role for the α subunit and is essential for a high quantum yield of the enzyme [121].

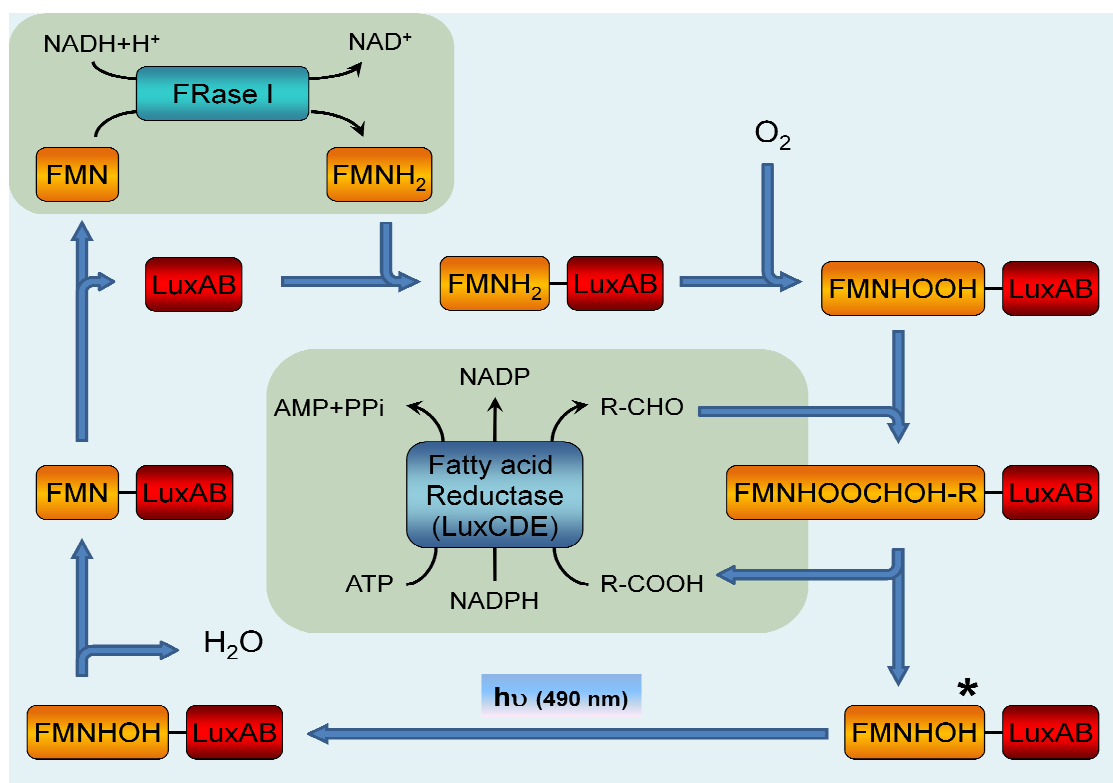


Figure 1-6: Schematic illustration of the cyclic enzyme reaction of bacterial bioluminescence in *V. fischeri*. FRase I provides FMNH₂ and the enzymatic complex LuxCDE provides the aldehyde. LuxAB binds FMNH₂ and catalyzes its reaction with molecular oxygen and the aldehyde with concomitantly emission of light. The reaction products are FMN, the corresponding acid of the aldehyde and water. (adapted from Bourgois [122])

Figure 1-6 gives an overview of the enzymatically catalyzed reactions during bacterial bioluminescence. The first step is the reduction of FMN to FMNH₂. Using either reduced nicotinamide adenine dinucleotide (NADH) or reduced nicotinamide adenine dinucleotide phosphate (NADPH) the species-specific flavin reductase catalyzes the reduction of FMN. The reductase ‘FRP’ in *V. harveyi* prefers NADPH as electron

donor [123,124], NAD(P)H:FMN oxidoreductase 'FRase I' from *V. fischeri* favors NADH [125]. The gene encoding for FRase I in *V. fischeri* ATCC 7744 has been identified and the crystal structure of the protein has been described in detail [111,126]. Nevertheless the transfer mechanism of flavin between FRase I and the luciferase still remains unclear, although the formation of a strong protein complex of these two proteins has already been demonstrated [127].

The first step in the mechanism cycle is the FMNH₂ binding of luciferase (cf. Figure 1-6). This process causes a structural change of the protein resulting in the protection of the enzyme from proteolytic inactivation [128,129]. Still it remains unclear how the flavin initiates the conformational change. Bound to the luciferase, FMNH₂ subsequently reacts with molecular oxygen and the second substrate, a long-chained aliphatic aldehyde (fatty aldehyde) [130,131]. The *in vivo* aldehyde substrate is tetradecanal, which originates metabolically from acyl-CoA [132,133]. During the bioluminescent reaction the aldehyde is oxidized into its corresponding fatty acid, which was deduced by means of mass spectrometry [134], of ³H-labeled and ¹⁴C-labeled decanal [135,136]. LuxCDE (fatty acid reductase) catalyzes the conversion of the fatty acid back into the aldehyde using ATP and NADPH [137]. The reaction of FMN with oxygen and aldehyde leads to a singlet excited state flavin molecule capable of light emission at 490 nm [138,139]. After the release of H₂O the luciferase dissociates the oxidized flavin, which is reduced again to FMNH₂ by FRase I and the bioluminescence reaction cycle starts over.

The detailed chemical transformation of the flavin is illustrated in Figure 1-7. After the reversible luciferase-binding of FMNH₂ (Figure 1-7, I), it reacts with molecular oxygen forming 4a-hydroperoxyflavin (Figure 1-7, II). Intermediate II is unusually stable with a lifetime of several minutes at 20 °C and several hours at subzero temperatures [140–143]. These long lifetimes enabled the characterization of intermediates I and II by means of NMR spectroscopy [144]. NMR also showed that the major flavin transformations are located on the C4a atom of the FMN's isoalloxazine moiety (cf. Figure 1-7, I). Intermediate II subsequently reacts with a long-chained aliphatic aldehyde, supposedly resulting in a flavin peroxyhemiacetal (Figure 1-7, III), which has

not been detected experimentally yet, but has been acknowledged as a presumably required step in the reaction [145]. The following transformation of intermediate III into an excited emitter has been speculated by many researchers. Most approaches describe a transition of several steps with radical intermediates by dissociative electron transfer [146], chemically initiated electron exchange luminescence (CIEEL) [147] or a dioxirane mechanism [148,149]; even a non radical transformation step with a second aldehyde molecule has been proposed [145]. However, there has been no experimental evidence for any proposition yet. Detailed information about the structure and further reaction of intermediate III remain unclear.

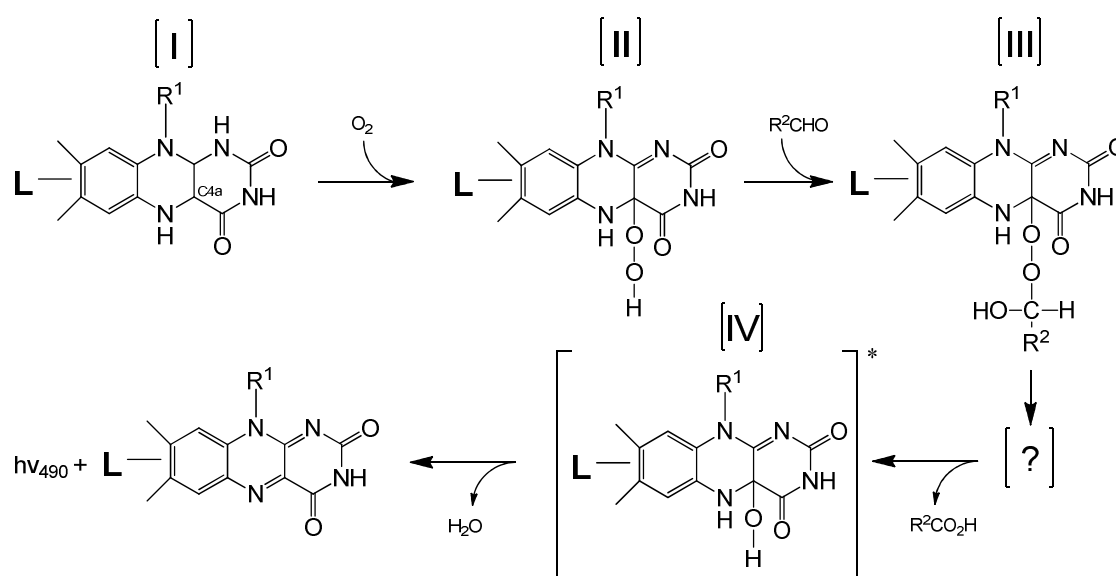


Figure 1-7: Simplified catalytic mechanism of bacterial bioluminescence and proposed intermediates of FMN (derived from Francisco [150]). The luciferase is indicated by the letter L. R^1 : side chain in FMN, R^2 : long chained aliphatic compound.

After the release of the fatty acid, the hydroxyhydroflavin intermediate (Figure 1-7, IV) has been generally accepted as bacterial bioluminescence excited emitter, which leads to the emission of light under H_2O release. The oxidized flavin dissociates from the luciferase, which then binds a $FMNH_2$ molecule to start this cyclic mechanism again.

The free energy produced during the oxidation processes of bacterial bioluminescence is estimated to be around 115 kcal/mol [122]. This amount of energy should be most likely enough to populate the excited hydroxyhydroflavin emitter, requiring 68 kcal/mol, and to produce a photon at 490 nm, which takes 60-80 kcal/mol [151–153]. The quantum yield in bacterial bioluminescence with decanal was determined to be at 0.16 [134].

1.7 Bioluminescent reaction of firefly luciferase

The firefly luciferase also functions as a monooxygenase and catalyzes the oxidation of luciferin in the presence of ATP, Mg^{2+} and molecular oxygen, resulting in oxyluciferin, CO_2 , AMP and the emission of light [154–156]. Figure 1-8 shows the schematic reaction as it appears in fireflies, beetles and railway worms. The ATP-dependent decarboxylation of luciferin forms an AMP derivative of luciferin, which subsequently reacts with molecular oxygen. The dioxetane decomposes, which is accompanied by the emission of light [30].

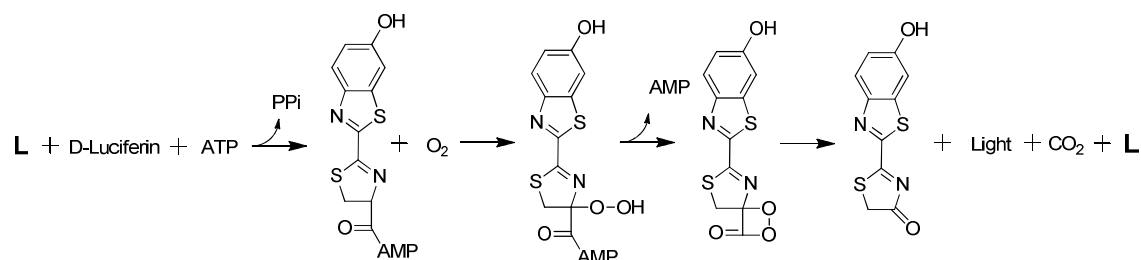


Figure 1-8: Reaction process of firefly bioluminescence; the luciferase is indicated by the letter *L*. (illustration derived from Hastings and Krause [30])

The *P. pyralis* luciferase was the first firefly luciferase that has been sequenced and cloned for heterologous expression [157]. Since then a great many of firefly luciferases have been equally investigated from organisms that appear in North and South America [158,159], Europe [160,161], Middle East [162] and Asia [163–165]. The monomeric protein from *P. pyralis* with a molecular weight of 62 kDa is encoded by the gene *luc*

[166]. Even though the molecular weight of approximately 60-62 kDa is equal among the firefly luciferases, the protein from *P. pyralis* shows the highest efficiency, even compared to all bioluminescent reactions, with almost one photon for each oxidized luciferin molecule [28]. The *P. pyralis* protein consists of a large N-terminal domain connected by a flexible linker to a small C-terminal domain. For the reaction the two domains get close to each other just enough to clasp around the substrates during the reaction [167]. The luciferin binding pocket has been located, with Arg218 in the N-terminal domain as essential residue of the luciferin binding site [168]. The emission spectrum of *P. pyralis* bioluminescence displays a broad signal with one maximum. Upon change of pH a shift in the maximum and therefore in the visible light color is observable. Under neutral or alkaline conditions, yellow-green light is emitted with a maximum at 560 nm. The color of the light changes into red under acidic conditions, with a maximum at 615 nm accompanied by a greatly decreased quantum yield [169]. A similar emission shift is also observed when the temperature is increased or at the presence of Zn^{2+} , Cd^{2+} or Hg^{2+} [170].

1.8 Objective

Since the first descriptions of bioluminescence, this visible phenomenon has been discovered in a number of different living organisms and has been an object of major scientific interest. Since these natural reactions, usually catalyzed by enzymes, show high energy efficiency without the concomitant production of heat, a better understanding of the reactions processes is advantageous. Though the reaction participants of these reactions have been mostly identified, only deficient information about the mechanism on an electronic level could be obtained up to now. The existence of a radical intermediate has been proposed for the bacterial bioluminescence reaction, yet there has been no successful approach providing evidence of such an intermediate state.

The main emphasis of this work lies on the investigation of the bacterial bioluminescence, primarily, and additionally the firefly bioluminescence by studying paramagnetic reaction intermediates with magnetic resonance techniques for a better

understanding of the detailed electronic processes of these reactions. For this purpose the two bioluminescence catalyzing luciferases from the bacterium *V. fischeri* and the firefly *P. pyralis* were cloned, recombinantly expressed in *E. coli* and purified by affinity chromatography using the Strep-tactin system. Native *V. fischeri* luciferase was additionally purified homologously by means of ion exchange chromatography. Kinetic measurements were used to display the catalyzing activity of the luciferases under different reaction conditions and with a multitude of reaction substrates. EPR spectroscopy was used for the investigation of paramagnetic reaction intermediates. The modern method of spin trapping in combination with EPR spectroscopy was applied in order to stabilize and analyze radical intermediates during bacterial and firefly bioluminescence.

The second aim of the present study was to obtain detailed information about the electronic structure of the luciferin molecule. As an organic compound that is present in almost all luminous organisms, it provides the energy for the light emitting reaction by being oxidized and promoted to an excited product state. The bacterial luciferin molecule, FMN, was investigated by EPR spectroscopy, optical spectroscopy and quantum chemistry. Since FMN in the ground state is not paramagnetic and therefore not detectable by EPR, a metastable paramagnetic triplet state was generated by means of laser excitation. Triplet EPR spectroscopy and optical absorption spectroscopy at different protonation states of FMN were combined with TDDFT calculations to obtain information about the molecular orbital structure of the luciferin. The effect of heavy atoms on the molecular orbital structure and the triplet formation of FMN was additionally analyzed.

2 Material and methods

Details about the applied methods and materials are described as they are relevant for this thesis. Elaborately information about the applied methods are given in the educational books mentioned below.

- Atherton, N. *Principles of Electron Spin Resonance*; Ellis Horwood PTR Prentice Hall: New York, 1993
- Cammann, K. *Instrumentelle Analytische Chemie*; Spektrum Akademischer Verlag: Heidelberg, Berlin, 2001
- Lakowicz, J.R. *Principles of Fluorescence Spectroscopy*; Kluwer Academic/Plenum Publisher: New York, Boston, Dordrecht, Moskau, 1999
- Schweiger, A., Jeschke, G. *Principles of Pulse Electron Paramagnetic Resonance*; Oxford University Press, 2001
- Skoog, D.A., Leary, J.J. *Analytische Chemie*; Springer-Verlag: Berlin, Heidelberg, New York, 1996
- Williams, D.H.; Fleming, I. *Spectroscopic Methods in Organic Chemistry*; McGraw-Hill Higher Education; 6th edition, 2007

2.1 Chemicals, enzymes, kits and other materials

Table 2-1: Suppliers

Name	Head office
Acros Organics	Geel, Belgium
Agilent Technologies	Waldbronn, Germany
AppliChem	Darmstadt, Germany
Bandelin	Berlin, Germany
Biorad	Munich, Germany
B Braun	Melsungen, Germany
Bruker BioSpin	Rheinstetten, Germany
Cambridge Isotope Laboratories	Saarbrücken, Germany
Clemens GmbH	Waldbüttelbrunn, Germany

DSMZ	Leipzig, Germany
Fermentas	St. Leon-Rot, Germany
Fluka	Taufkirchen, Germany
GE Healthcare Europe	Freiburg, Germany
IBA Bio Technology	Göttingen, Germany
IKA-Werke GmbH	Staufen, Germany
Life Technologies	Darmstadt, Germany
Merck	Darmstadt, Germany
Millipore	Schwalbach, Germany
MWG-Biotech AG	Ebersberg, Germany
PerkinElmer	Rodgau, Germany
Pharmacia	Uppsala, Sweden
Roth	Karlsruhe, Germany
Sigma	Steinheim, Germany
Thermo Fisher Scientific	Rockford, USA

Table 2-2: Chemicals

Name	Supplier
Acetaldehyde	Acros
Ampicillin	VWR
APS	Roth
Bromphenolblue	Roth
Cinnamaldehyde	Sigma
Citrate	Roth
Deuterium oxide (D ₂ O; ≥ 99 %)	Sigma
Decanal	Sigma
Di-potassium hydrogen	Roth
Deuterium-glycerol (98 %)	Cambridge Isotope Laboratories
Dodecanal	Roth
DTT	Roth
Deuterium chloride	Sigma
DMPO	Sigma
DMSO	Roth
EDTA	Roth
Ethidium bromide	Roth

FAD	Sigma
FMN	Fluka
Glycerol	Roth
Hydrogen chloride	Merck
HEPES	AppliChem
Hydrocinnamaldehyde	Sigma
Kanamycin	Merck
NADH	Roth
Sodium deuterium oxide	Sigma
Sodium hydroxide	Merck
Octanal	Sigma
Potassium dihydrogen	Roth
Riboflavin	Sigma
Sodium dithionite	Merck
TEMED	Roth
Tris-HCl	Roth
Vanillin	Sigma

Table 2-3: Enzymes

Name	Supplier
Lysozyme	Roth
Polymerases (<i>Pfu</i> , <i>Taq</i>)	Fermentas
Restriction endonucleases	Fermentas
T4 ligase	Fermentas

Table 2-4: Kits

Name	Supplier
GeneJet Gel Extraction Kit	Fermentas
GeneJet Plasmid Miniprep Kit	Fermentas

Table 2-5: Other materials

Name	Supplier
1 kb DNA ladder	Fermentas
6 x DNA loading dye	Fermentas
Agarose	Roth
Bradford reagent	Sigma
Cannulas	B Braun
Centriplus centrifugal filter	Millipore
DEAE 25	Pharmacia
DEAE 50	Pharmacia
DEAE cellulose	Pharmacia
DEAE sepharose	Pharmacia
Dialysis tubes visking, cellulose	Roth
Polypropylene columns	IBA Bio Technology
Prestained protein ladder	Roth
Q sepharose	Pharmacia
Sterile syringe filter	Roth
Strep-Tactin superflow	IBA Bio Technology
Superdex 75	Pharmacia
Syringes	B Braun
Zeba Spin Desalting Columns	Thermo Fisher Scientific

2.2 Vectors and primers

All constructed plasmids were analyzed by DNA sequencing by SeqLab (Göttingen, Germany).

Table 2-6: Plasmids used in this study.

Plasmid	Genotype or sequence	Source
pPR-IBA1	Ap ^r , C-terminal Strep tag II, T7 promotor	IBA
pET-28c(+)	Kan ^r , N-terminal His-tag/thrombin/T7-tag, C-terminal His-tag, T7 promotor	Merck

IBA1 <i>luxAB</i>	Ap ^r , <i>Bam</i> HI- <i>Sal</i> I fragment of PCR-amplified <i>luxAB</i> in pPR-IBA1 linked to a C-terminal Strep tag II, T7 promotor	This study
pET <i>luxA</i>	Kan ^r , <i>Bam</i> HI- <i>Sal</i> I fragment of PCR-amplified <i>luxA</i> in pET-28c, T7 promotor	This study
pGEM- <i>luc</i>	Ap ^r , <i>luc</i> from <i>P. pyralis</i>	Wood [171]
pPR-IBA2	Ap ^r , N-terminal Strep tag II, T7 promotor	IBA
IBA2 <i>luxAB</i>	Ap ^r , <i>Bam</i> HI- <i>Sal</i> I fragment of PCR-amplified <i>luxAB</i> in pPR-IBA1 linked to a N-terminal Strep tag II, T7 promotor	This study
IBA2 <i>luc</i>	Ap ^r , <i>Bam</i> HI- <i>Sal</i> I fragment of PCR-amplified <i>luc</i> in pPR-IBA2 linked to an N-terminal Strep tag II, T7 promotor	This study

Table 2-7: Primers used in this study; restriction sites are underlined; G: glycine, C: cysteine, A: adenine, T: thymine. Primers were obtained from MWG-Biotech AG.

Primer	Sequence (5' → 3')	Restriction site
<i>luxAB</i> _Vf7744_for	CACCAAGAAG <u>GGATCC</u> GAGTATG	<i>Bam</i> HI
<i>luxAB</i> _Vf7744_rev	CACCTAAT <u>GTCGAC</u> CAGAAATGC	<i>Sal</i> I
<i>luxAB</i> _strep_for	CACCACCATG <u>GGATCC</u> CAGTATGAAG	<i>Bam</i> HI
<i>luxAB</i> _strep2_rev	CGCTTAATT <u>GTCGAC</u> GGGTAGATTC	<i>Sal</i> I
<i>luxA</i> _long_Vf_for	CACCAC <u>CCATGG</u> GATCCAGTATGAAG	<i>Nco</i> I
<i>luxA</i> _long_Vf_rev	CTTGTTCCATTATTAT <u>GTCGAC</u> TATC	<i>Sal</i> I
<i>luc</i> _for	GAGGGCCC <u>GGATCC</u> AATGGAAG	<i>Bam</i> HI
<i>luc</i> _rev	GAATTT <u>C</u> <u>GTCGAC</u> GCTGAATACAG	<i>Sal</i> I

2.3 Bacterial strains

Table 2-8: Bacterial strains used in this study.

Bacterial strains	Genotype or phenotype	Source or reference
<i>E. coli</i> Dh5 α	F ⁻ endA1 glnV44 thi-1 recA1 relA1 gyrA96 deoR nupG Φ 80dlacZ Δ M15 Δ (lacZYA- argF)U169, hsdR17(r _K ⁻ m _K ⁺), λ -	Hanahan [172]
<i>E. coli</i> BL21 (DE3)	F ⁻ ompT gal dcm lon hsdS _B (r _B ⁻ m _B ⁻) λ (DE3 [lacI lacUV5-T7 gene 1 ind1 sam7 nin5])	Studier and Moffatt [173]
<i>V. fischeri</i> ATCC 7744	Wildtype (DSM 507)	DSMZ

2.4 Software and online tools

Table 2-9: Software used in this study.

Software	Function	Source
BLAST	Nucleotide or protein sequences database search	www.ncbi.nlm.nih.gov/ v/Blast
Cary WinFLR	Fluorescence spectrometer control software	Agilent Technologies
ChemDraw Pro 12.0	Chemical graph processing	PerkinElmer
ELEXSYS Series: Xepr	EPR spectrometer control software	Bruker
Expasy	DNA and protein analysis	www.expasy.ch
FL Winlab 4.00.00	Fluorescence spectrometer control software	PerkinElmer
Matlab 7.4.0	Kazan for data transcription	MathWorks

Microsoft Office 2007	Text and data processing	Microsoft
Origin Pro 8G	Data handling and analysis	OriginLab corporation
Reference Manager Version 12	Management of references	ISI ResearchSoft
Unicorn 5.11	ÄKTApurifier control software	GE Healthcare
UV Winlab 5.2.0.0646	UV/VIS spectrometer control software	PerkinElmer
Vector NTI Advanced 11	DNA Sequence processing	Life Technologies

2.5 Microbiological methods

2.5.1 Cultivation of *Escherichia coli*

Luria-Bertani (LB) medium: 10 g tryptone, 5 g yeast extract, 5 g NaCl, pH 7.5, ad 1 l H₂O_{demin}, pH 7.5 [174]

2 x YT medium: 16 g tryptone, 10 g yeast extract, 5 g NaCl, ad 1 l H₂O_{demin}, pH 7.0 [175]

E. coli was grown in autoclaved (20 min at 121 °C) liquid cultures of LB medium under aerobic conditions at 37 °C and 150 rpm. The nutrient-rich 2 x YT medium was used after transformation of vector DNA and for preparation of competent cells. 15 g agar was added to the medium for the preparation of solid medium plates. Antibiotics were added for the selection of plasmid containing cells. Final antibiotic concentrations of 100 µg/ml for ampicillin and 50 µg/ml for kanamycin were used in medium that was cooled down to at least 50 °C. Antibiotic stock solutions were run through a sterile syringe filter before further use. Cloning experiments were carried out in *E. coli* Dh5α whereas *E. coli* BL21 was used as recipient for expression plasmids.

2.5.2 Cultivation of *V. fischeri*

V. fischeri medium: 30 g NaCl, 7 g Na₂HPO₄ x 7 H₂O, 1 g KH₂PO₄, 0.5 g (NH₄)₂HPO₄, 0.1 g MgSO₄, 5 g tryptone, 3 g yeast extract, 2 ml glycerol, ad 1 l H₂O_{demin} [176]

V. fischeri was purchased as vacuum dried culture and removed from the vial as described by the manufacturer. The dried pellet was swollen in 0.5 ml medium for 30 min. 5 ml medium were then inoculated with this suspension and grown over night at 26 °C and 150 rpm.

2.5.3 Conservation of bacterial strains

For long term storage of *E. coli* and *V. fischeri* cells, aliquots of 0.5 ml of an overnight grown culture were mixed with a ratio of 3:2 with sterile glycerol, quick-frozen in liquid nitrogen and stored at –80°C.

2.5.4 Preparation of competent *E. coli* cells

Competent *E. coli* cells are capable of taking up external DNA. For this purpose the cells were prepared chemically using the calcium chloride method [177]. 70 ml 2 x YT medium were inoculated with 0.7 ml of a 5 ml *E. coli* preculture, grown in 2 x YT medium over night, and cultivated to an optical density at 600 nm (OD₆₀₀) of 0.4 – 0.6. The cells were centrifuged in sterile tubes at 1900 g (4°C, 6 min). The pellet was suspended in 10.5 ml iced 70 mM CaCl₂ / 20 mM MgSO₄ solution and incubated on ice for 40 min. The suspension was centrifuged again for 10 min and the cell pellet suspended in 3.5 ml 70 mM CaCl₂ / 20 mM MgSO₄ solution. After incubation on ice for 45 min 875 µl sterile glycerol was added to the cells, which were then stored in 100 µl aliquots at –80 °C.

2.5.5 Transformation of competent *E. coli* cells

Alien plasmid DNA was inserted into competent *E. coli* cells using transformation by heat shock. The cells were thawed on ice before use. After the addition of 5 – 10 ng

plasmid DNA the suspension was incubated on ice for 30 min. After a 42 °C heat shock of 90 sec the cells were again incubated on ice for 2 min. 500 µl 2 x YT-medium were added before an incubation at 37 °C for 60 min. The cells were then plated on LB plates with the respective antibiotic for the selective growth of the plasmid containing *E. coli* cells. In order to introduce a second plasmid into the same *E. coli* cell, the transformed cells were treated chemically as already described and transformed again with the second plasmid. The plasmids encode for two different antibiotic resistances, which enables the selection of the bacterial cells that contain both plasmids.

2.6 Methods of molecular biology

2.6.1 Preparation of chromosomal DNA from *V. fischeri*

TE buffer: 10 mM Tris-HCl, 1 mM EDTA, pH 8.0

TES buffer: 100 mM NaCl, 10 mM Tris-HCl, 1 mM EDTA, pH 8.0

Saccharose-TES buffer: 20 % (w/v) saccharose in TES buffer

Lysozyme-RNase solution: 20 mg/ml lysozyme, 1 mg/ml RNase

Sarcosine solution: 10 % (w/v) laurylsarcosine, 250 mM EDTA

Chromosomal DNA was isolated from the *V. fischeri* wild type strain using sarcosyl lysis based on Bazaral and Helsinki [178]. An overnight grown culture of 25 ml was harvested at 2500 g for 10 min. The pellet was suspended in 1 ml of 50 mM Tris-HCl pH 8.0 and centrifuged again at 14000 g for 5 min. The cell pellet was stored at 4 °C until further use. 50 – 100 mg of the frozen cell material was suspended in 2 ml iced TES buffer and sedimented for 10 min (14000 g, 4 °C). The pelleted cells were suspended in 250 µl saccharose-TES buffer and incubated on ice for 30 min. 250 µl freshly prepared lysozyme-RNase solution was added to the suspension before it was incubated in a gentle shaking water bath at 37 °C for 60 min. After the addition of 100 µl sarcosine solution the tube was inverted several times for gentle mixing. To achieve a shearing of the DNA the suspension was pressed through a sterile cannula

(1.2 x 40 mm) thrice. After 300 μ l of sterile H₂O_{demin} were added the chromosomal DNA was isolated from the residual cell material by phenol-chloroform-isoamylalcohol (P/C/I) extraction. An equal volume of P/C/I (25:24:1) was intensely mixed with the suspension and centrifuged (14000 g) for 5 min. The aqueous of the three phases was cautiously transferred into a new sterile reaction tube. This procedure was repeated at least thrice before a further extraction step using chloroform-isoamylalcohol (C/I) followed to remove traces of phenol. The C/I (24:1) was added with an equal volume and mixed intensely with the DNA containing solution. After the sample was centrifuged again for 5 min the aqueous phase was dialyzed against 1 l TE buffer for at least 3 hours and subsequently against 1 l high-purity H₂O for 2 hours. The chromosomal DNA was stored at 4 °C.

2.6.2 Isolation of plasmid DNA from *E. coli*

The preparation of plasmid DNA from *E. coli* cells was performed using the GeneJet Plasmid Miniprep Kit following the manufacturer's instructions. 4 ml of an overnight grown culture of plasmid DNA containing *E. coli* cells were used for plasmid separation. The plasmid DNA was stored at -20 °C.

2.6.3 Photometric determination of DNA concentration and purity

The determination of DNA concentration and purity was achieved by UV/VIS spectroscopy. Nucleic acids show an absorption maximum at 260 nm. At this wavelength an absorption value of 1.0 correlates with a double stranded DNA concentration of 50 μ g/ml [175]. The absorption maximum of proteins is located at 280 nm. The ratio of the absorption at these two wavelengths (A_{260}/A_{280}) therefore declares the purity of the DNA sample. Values higher than 2.0 imply a contamination with RNA, whereas lower values than 1.8 indicate a contamination with proteins or phenol.

2.6.4 DNA amplification *in vitro* by PCR

The well established method of polymerase chain reaction (PCR) can be used to amplify DNA *in vitro* by using only minimal concentrations of the template DNA. This enzymatic catalyzed reaction leads to an exponential duplication of a certain gene of interest by a cyclic process [179–182].

2.6.4.1 Standard-PCR

The PCR reaction consists of several consecutive molecular steps. It starts with the thermal denaturing of the double-stranded DNA template. The hydrogen bonds of the DNA break open at high temperatures, which lead to single-stranded nucleic acids. Short single-stranded DNA fragments, primers (oligonucleotides), that are complementary to the 3'- and 5'- end of a certain DNA fragment, bind to the template DNA and serve as starting points for DNA replication by a thermostable DNA polymerase. The success of the primer binding is temperature dependent and varies for every distinct PCR. The polymerase elongates the complementary DNA strand in 5'-3' direction, which eventually leads to double-stranded DNA. The repetition of denaturing, primer annealing and elongation by polymerase results in a useful amount of desired DNA that can be used for further molecular applications.

The PCR reaction was carried out in a PCR thermocycling system Primus 25 (Clemens). The thermostable DNA polymerase from *Pyrococcus furiosus* (*Pfu* polymerase) was used as enzyme for the elongation. Compared to the polymerase from *Thermus aquaticus* (*Taq* polymerase) the *Pfu* polymerase contains the ability of 3'-5' proofreading of the newly synthesized DNA during the elongation process, which decreases the number of falsely integrated nucleotides, resulting in a slower amplification rate of the polymerase. Therefore the *Pfu* polymerase was used for the creation of expression plasmids. The dNTP mixture contained dATP, dTTP, dCTP, dGTP with equal amounts. A standard PCR sample mixture and the applied PCR program are given in Table 2-10.

If chromosomal DNA was used as template, the PCR sample also contained 5 % dimethylsulfoxide (DMSO) in order to reduce the secondary structures of the DNA. In

that case the enzyme concentration was doubled. DNA amplifications by PCR were purified using the GeneJet Gel Extraction Kit following the manufacturer's instructions.

Table 2-10: PCR standard sample mixture and run program.

Standard PCR sample		Standard PCR program			
Polymerase specific buffer	1 x	1.	Initial denaturation	95 °C	3 min
Primer 5'-3'	50 pmol	2.	Denaturation	95 °C	30 sec
Primer 3'-5'	50 pmol	3.	Primer annealing	Primer dependent	1 min
Nucleotides (dNTP mixture)	200 µM each	4.	Elongation	72 °C	2 min/kb
DNA template	0.1 – 0.5 µg/µl	5.	Repetition step 2. - 4.	–	25 x
<i>Pfu</i> polymerase	1 U	6.	Final elongation	72 °C	7 min
Sterile H ₂ O	ad 50 µl	7.	Storage	4 °C	hold

2.6.4.2 Colony PCR

For a quick confirmation of recombinant *E. coli* mutants, PCR was carried out with whole cells instead of purified DNA template. The cell material was picked from LB plates containing the corresponding antibiotics and transferred into the PCR reaction

tube before the reaction components were added. The tube was shortly vortexed to ensure the mixing of the substances. *Taq* polymerase was used, since a proofreading capability is not necessary, with an elongation time of 1 min/kb. The denaturation time and the primer annealing time were decreased to 45 sec.

2.6.4.3 Primer construction

Oligonucleotides were constructed with attention to the following aspects. The primer should consist of 15 to 30 nucleotides with an optimal GC content of 40-60 %, whereat G and C should be distributed uniformly along the primer. One or two G or C were placed at the 3'-end of the primer to increase the binding strength to the DNA template due to the triple hydrogen bond. However, the primers should not contain more than four repetitions of the same base at any position to prevent frameshifts. Online tools (cf. Table 2-9) were used to check for self-complementarities and complementary sites between the primers. The melting temperature depends directly on length and composition of the primers. For oligonucleotides with 15 or less bases the temperature was calculated according to the Wallace formula [175]:

Formula 2-1

$$T_m \text{ [}^\circ\text{C]} = 4 \times (n_G + n_C) + 2 \times (n_A + n_T)$$

T_m = theoretical annealing temperature of primers

n = number of corresponding base

The following formula was used for nucleotides longer than 15 bases.

Formula 2-2

$$T_m \text{ [}^\circ\text{C]} = 69.3 + \frac{41 \times (n_G + n_C)}{s} - \frac{650}{s}$$

s = total number of bases

The annealing temperature for the PCR was chosen to be 5 °C below the lowest melting temperature leading to temperatures between 45 °C and 60 °C. Differences in melting temperature of the two primers should not exceed 5 °C. Restriction sites for subsequent cloning processes were tried to build in with at least 6 additional bases on each site to ensure restriction site identification of the restriction enzymes.

2.6.5 DNA visualization

2.6.5.1 Agarose gel electrophoresis

50 x TAE buffer: 2 M Tris-HCl, 1 M acetic acid, 50 mM EDTA, pH 8.0

6 x DNA loading dye: 10 mM Tris-HCl, pH 7.6, 0.03 % bromphenol blue (w/v),
0.03 % xylene cyanol FF, 60 % glycerol, 60 mM EDTA

DNA fragments were separated using gel electrophoresis according to Maniatis and coworkers [175]. The gel matrix consists of agarose, which is a long-chained polysaccharide of D-galactose and 3,6-anhydrogalactose. An electric potential is applied to the gel, which makes the negatively charged DNA molecules pass through the gel matrix and separate depending on their molecular size. 1 % gels were used by melting the agarose in a corresponding volume of 1 x TAE buffer and applying this agarose solution in a gel chamber. Wells for the DNA samples were included at one end of the gel. 1x TAE buffer containing 10 µg/ml ethidium bromide was used as running buffer. 1 µl of 6 x DNA loading dye was added to 5 µl of DNA sample before they were placed into the wells, including a DNA standard sample (1 kb DNA ladder) for later verification of the molecule sizes. A voltage of 100 V was applied to the gel chamber for 1 h. Due to the intercalation of the ethidium bromide molecules within the bases of the DNA and the orange colored fluorescence of ethidium bromide, the DNA fragments could be viewed using UV light.

2.6.5.2 Purification of DNA fragments from agarose gel

PCR fragments that have been run by gel electrophoresis were isolated from stained agarose gels for further use with a clean scalpel. To keep the DNA damaging low the

gel was exposed to UV light as short as possible. The excluded gel piece was applied to a Gel Extraction Kit following the manufacturer's instructions. The DNA fragments were stored at $-20\text{ }^{\circ}\text{C}$.

2.6.6 Enzymatic modification of DNA

2.6.6.1 Restriction of DNA

Restriction digestion of DNA was done by type II endonucleases following the manufacturer's instructions. Type II endonucleases make the cleavage within the palindromic recognition sequence, resulting in an absolute sequence specific restriction. 0.5-10 μg DNA was incubated with 3-5 U enzyme for 1 h. If the digested DNA was used for further cloning processes, the DNA was separated from the enzyme using the GeneJet Gel Extraction Kit following the manufacturer's instructions, except the first step of gel melting. Otherwise the digest sample was analyzed by gel electrophoresis for the determination of the molecular weight.

2.6.6.2 Ligation

The insertion of DNA fragments (inserts) into plasmid DNA was catalyzed by the ligase from the T4 bacteriophage of *E. coli*. The plasmid to insert ratio was approximately 1:3 and the ligation was carried out with 1 U ligase in 20 μl at 16°C over night. The sample was stored at $-20\text{ }^{\circ}\text{C}$.

2.7 Protein-biochemical methods

2.7.1 Homologous expression of bacterial luciferase

The *V. fischeri* cells were grown in 50 ml cultures over night at $26\text{ }^{\circ}\text{C}$ and 150 rpm, inoculated from a glycerol stock. 2 % of this preparatory culture were used to inoculate a 500 ml main culture, which was grown aerobically at $26\text{ }^{\circ}\text{C}$ and 200 rpm to an OD_{600} of 1.2. The cells were harvested at 10000 g for 15 min and stored at $-20\text{ }^{\circ}\text{C}$.

2.7.2 Heterologous expression of recombinant protein

E. coli strain BL21 was used for expression of recombinant luciferase. In previous cloning experiments the relevant genes (*luxAB* and *luc*) were amplified by PCR and integrated into the plasmids pPR-IBA1, pPR-IBA2 and pET-28c, respectively. Restriction sequences were included into the respective gene using mutagenic oligonucleotides in a way that prevents an alteration of the reading frame once the gene is located in the plasmid. In the plasmid pPR-IBA1 the expressed protein is fused to a C-terminal Strep-tactin affinity tag (Strep tag II), which was used for the expression of the bacterial luciferase. The expression with the plasmid pPR-IBA2 fuses the protein to an N-terminal Strep tag II, which was used for the firefly luciferase. The plasmid pET-28c was used for the expression of the LuxA subunit of the bacterial luciferase, whereas the protein was not fused with any affinity tag. All used plasmids are controlled by a T7 promotor and the protein expression was induced by IPTG in all cases.

10 ml LB medium with the respective antibiotics was inoculated with a single plasmid containing *E. coli* colony. This preparatory culture was incubated over night at 37 °C and 150 rpm and subsequently incubated in 500 ml main culture at 200 rpm. The cells were grown aerobically to an OD₆₀₀ of 0.6 – 0.8. After the addition of 0.5 mM IPTG, the bacterial LuxAB was expressed at 30 °C for 3 h whereas the eukaryotic Luc was expressed at 22 °C for 6 h. The cells were harvested at 6000 g for 15 min and stored at –20°C.

2.7.3 Cell disruption

Buffer L: 100 mM Tris-HCl, 150 mM NaCl, 1 mM EDTA, 1 mM DTT, 1mg/ml lysozyme, pH 8.0

Buffer P: 10 mM phosphate buffer, pH 7.0

Thawed cells of *E. coli* were dissolved in buffer L with 10 ml/g, incubated on ice for 30 min and subsequently disrupted by sonication (Sonopuls GM 2070, Bandelin) with 70 % power. The sonication was divided into 3 times of 4 min with 3 min of cooling on

ice in between. The crude extract was centrifuged at 40000 g for 15 min (4 °C) for the separation of cell debris. The supernatant (soluble fraction) contains the cytoplasmatic expressed recombinant protein and was separated from the pellet (insoluble fraction). The insoluble fraction was suspended in a buffer L volume equal to that of the soluble fraction for further analysis by SDS-Page. The soluble fraction, cleared lysate, was subsequently introduced into affinity chromatography for further purification steps.

Thawed cells of *V. fischeri* were dissolved in buffer P and disrupted by dispersing (Ultra Turrax, IKA-Werke GmbH) in liquid nitrogen. Cells were added in drops to the nitrogen and dispersed until a powdery sediment was visible. Cell fragments were dissolved in buffer P and centrifuged at 40000g for 15 min (4 °C). The supernatant was separated from the pellet and subsequently introduced into anion exchange chromatography (see section 2.7.4.3) for further purification steps.

2.7.4 Chromatographic methods

2.7.4.1 Affinity chromatography of recombinant protein

Buffer W: 100 mM Tris-HCl, 150 mM NaCl, 1 mM EDTA, 1 mM DTT, pH 8.0

Buffer E: 100 mM Tris-HCl, 150 mM NaCl, 1 mM EDTA, 1 mM DTT, 2.5 mM desthiobiotin, pH 8.0

Buffer R: 100 mM Tris-HCl, 150 mM NaCl, 1 mM EDTA, 1 mM HABA, pH 8.0

For the purification of heterologous expressed protein gravity flow (flow rate approx. 1 ml/min) affinity chromatography was applied. Due to cloning experiments the recombinant protein was linked to a Strep tag II, which consists of 8 amino acids (WSHPQFEK). It binds to Strep-tactin with high selectivity and a dissociation constant of 1 μ M. Once bound to the Strep-tactin the recombinant protein can be eluted using desthiobiotin, which possesses a higher affinity towards Strep-tactin therefore competes with the Strep tag for binding sites. A polypropylene column was packed with Strep-tactin Superflow and was applied as stationary phase of the chromatography process.

The following chromatography process is elucidated in Table 2-11. After use the column was stored in 20% ethanol at 4°C.

Table 2-11: Chromatography steps and applied solutions and their volume specified as column volumes (CV).

Chromatography step	Volume	Solution
Equilibration	2 x CV	Buffer W
Application of cleared lysate		
Washing	5 x CV	Buffer W
Elution	6 x ½ CV	Buffer E
Regeneration	3 x 5 CV	Buffer R
	2 x 4 CV	Buffer W
Storage (4 °C)	2 x CV	20 % Ethanol

The different fractions were subjected to SDS-PAGE (see section 2.7.6.1) in order to detect the protein containing fractions. The fractions containing purified luciferase were combined and dialyzed against buffer W using dialysis tubes (MWCO 14000) to dispose of desthiobiotin from the elution buffer and concentrated using Amicon protein centrifugal filter units (Millipore) with a molecular weight cutoff (MWCO) of 10 kDa. The protein samples were centrifuged according to the manufacturer's instructions until the desired volume was achieved. The protein samples were quick-frozen in liquid nitrogen and subsequently stored at -80 °C.

2.7.4.2 Gel filtration chromatography

The molecular mass of the heterologously expressed proteins was further analyzed by gel filtration chromatography. This method enables the separation of proteins by their molecular mass as they pass through a perforated solid column matrix. Smaller

molecules can pass through the internal matrix pores and therefore have to cover a higher distance than bigger molecules. Fast Pressure Liquid Chromatography (FPLC) was carried out with using an ÄKTApurifier. A 120 ml HiLoad 16/60 Superdex 75 prep grade column was used as matrix, run with 0.5 ml/min and calibrated with 2 CV buffer W (cf. section 2.7.4.1). The following standard proteins were used for calibration line: aldolase (160 kDa), BSA (66 kDa), chicken egg ovalbumin (45 kDa), myoglobin (17.8 kDa), horse heart cytochrome c (12.3 kDa), Chaperonin 10 (10 kDa). The K_{av} values of the standard proteins were plotted against the corresponding logarithm of their molecular weight. K_{av} is calculated with

Formula 2-3

$$K_{av} = \frac{V_e - V_0}{V_t - V_0}$$

V_e = elution volume of the protein

V_0 = column void volume (43 ml)

V_t = total bed volume (120 ml)

The K_{av} value of the protein of interest was determined and the formula of the calibration line was used to calculate the molecular weight. After use the column was stored in 20 % ethanol at 4 °C.

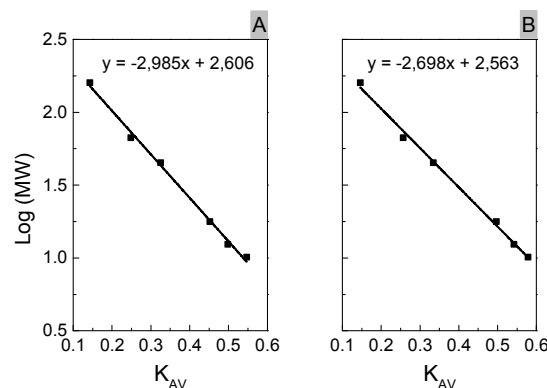


Figure 2-1: Gel filtration calibration line for the determination of the molecular weight of (A) bacterial LuxAB and (B) firefly Luc.

2.7.4.3 Ion exchange chromatography of homologous protein

The principle of ion exchange chromatography depends on charge-charge interactions between immobilized charges on a solid column and the protein of interest. A cation exchanger, in which the positively charged ions bind to negatively charged resin, is distinguished from an anion exchanger with a reversed charge situation. An increasing salt concentration in the used buffers elutes the bound molecules at certain ionic strength conditions. For the proper choice between anion and cation exchanger, the charge of your protein of interest at the applied pH condition needs to be known.

In order to determine the optimum ion exchanger matrix, different anion exchanger have been tested for the binding and purification of homologous luciferase. DEAE cellulose, DEAE sepharose, DEAE sephadex A-25, DEAE sephadex A-50 and Q sepharose were used to separate luciferase proteins from other proteins. After the disruption of the *V. fischeri* cells and the separation of the cell debris, 1 ml of the soluble proteins was added to 200 mg matrix in a column. The column was then washed with 1 ml buffer P (cf. section 2.7.3), in order to elute all protein that do not bind to the used matrix material (flowthrough). The following elution steps were carried out with increased phosphate buffer (pH 7.0) concentrations of 150 mM, 450 mM and 600 mM, each with 1 ml volume. The collected elution fractions, including the flowthrough were tested for the presence of active luciferase by visual luminescence, hence by the addition of 200 μ l reduced FMN and 50 μ l decanal. 5 ml of 5 mM FMN were chemically reduced with a spittle tip of $\text{Na}_2\text{S}_2\text{O}_4$. For anion exchange chromatography 200 ml of the optimum matrix material were filled into a glass column and a pericyclic pump (Cyclo II, Roth) was applied with a flow rate of 0.5 ml/min. The cleared lysate of *V. fischeri* cells, containing all soluble proteins, was applied to the column. A gradational increase of phosphate buffer (*vide supra*) was used to elute the protein. The elution was monitored by the absorption at 280 nm. Each buffer concentration was used until no elution of proteins was detectable. The collected fractions were subsequently tested for the presence of active luciferase by means of the above mentioned visual luminescence approach. Luciferase containing fractions were combined and dialyzed over night against an excess of buffer P at 4 °C.

Luciferase was then precipitated by the addition of solid ammonium sulfate, centrifuged at 16000 g for 30 min (4 °C) and precipitated repetitively until no protein precipitated any longer. The precipitates were suspended in buffer P and dialyzed against an excess of the same buffer overnight at 4 °C. Samples that showed luciferase activity were combined, quick-frozen in liquid nitrogen and stored at –80 °C.

2.7.5 Determination of protein concentration

The total protein concentration in samples was determined by the method of Bradford [183] using Bradford reagent as advised by the manufacturer. The assay is based on complex accumulation of the proteins with Brilliant Blue G, which can be followed at 595 nm. The Bradford reagent was suited for 1 – 1.4 mg/ml protein, therefore the standard was covering a range from 0 to 1.4 mg/ml bovine serum albumin (BSA).

2.7.6 Protein visualization

2.7.6.1 SDS-PAGE

Solution A:	1.5 M Tris-HCl, pH 8.8, 0.3 % SDS
Solution B:	0.5 M Tris-HCl, pH 6.8, 0.4 % SDS
5 x Electrophoresis buffer:	15 g Tris-HCl, 72 g glycine, 5 g SDS, ad 1 l H ₂ O _{demin}
APS solution:	10 % ammonium peroxodisulfate (w/v)
Acrylamide solution:	30 % acrylamide-bisacrylamide solution (37.5:1)
TEMED:	Tetramethylethylenediamine
Sample buffer:	100 mM Tris-HCl, 4 % (w/v) SDS, 20 % glycerol, 0.2 % (w/v) bromphenolblue

Protein samples were subjected to discontinuous SDS-polyacrylamide gel electrophoresis (SDS-PAGE) according to Laemmli [184] in order to achieve a separation of the proteins by molecular mass. A discontinuous gel consists of two

phases, a stacking gel and a running gel. A lower acrylamide concentration and a lower pH value in the stacking gel leads to an accumulation of each protein sample into a thin band before entering the running gel. A change in the acrylamide concentration in the running gel influences the intensity of the separation of the molecular masses of the different proteins. Table 2-12 shows the composition of the gels. Once the APS solution is added to the mixture the polymerization process starts. The two glass plates, serving as pour borders, were separated by a 1 cm spacer. After the running gel mixture was filled between the glass plates, H_2O_{demin} was carefully added on top of it to achieve a straight-lined gel surface. After the polymerization was completed the water was removed and the mixture for the stacking gel was filled on top of the running gel and a well comb was placed within to form sample slots. Dilution series of the protein samples were mixed with sample buffer (1:1) and incubated at 100 °C for 5 min. 1 x electrophoresis buffer was used as running buffer. A protein mass marker was placed in one slot for subsequent estimation of the molecular masses. After the gels have been run at 30 mA they were stained with Coomassie Blue (see section 2.7.6.2).

Table 2-12: Composition of SDS gels with different acrylamide concentrations of running gels. The shown amounts are adequate for two gels in a Mini-PROTEAN 3 System gel chamber (Biorad).

	Running gel		Stacking gel
	10 %	15 %	4.5 %
Acrylamide solution	4 ml	6 ml	0.75 ml
Ultra pure H_2O	5 ml	3 ml	3 ml
Solution A	3 ml	3 ml	–
Solution B	–	–	1.25 ml
APS solution	100 μ l	100 μ l	100 μ l
TEMED	5 μ l	5 μ l	5 μ l

2.7.6.2 Coomassie staining

Coomassie staining solution: 50 % methanol, 10 % acetic acid, 0.25 % Coomassie Brilliant Blue R 250 (w/v), 40 % H₂O_{demin}

Decolorizing solution: 20 % methanol, 10 % acetic acid, 70 % H₂O_{demin}

Electrophoretically run protein gels were stained using Coomassie Blue according to Blum and coworkers [185]. The running gel was separated from the stacking gel and incubated in Coomassie staining solution for at least 1 h under continuous slewing. Subsequently the gel was incubated in decolorizing solution until protein bands were clearly visible in the gel (~ 30 min).

2.8 Biophysical methods

2.8.1 UV/VIS spectroscopy

2.8.1.1 Theory

The absorption of electromagnetic radiation in an ultraviolet (UV; 200 – 400 nm) and visible (VIS; 400 – 800 nm) range results in the excitation of valence electrons within a molecule. The molecule takes up energy in form of photons and is transferred from the electronic ground state to the electronic excited state. Compared to atoms, the different electronic states in molecules exhibit relatively broad energy ranges caused by overlaid vibrational and rotational levels. Therefore spectra of molecules show a band spectrum and not a distinct line spectrum.

Quantitative information about the absorbing compound can be obtained from the Lambert-Beer(-Bouguer)'s law (Formula 2–4). These correlations only apply for diluted solutions, since only then the molecules of the analyte are solvated with and without any interaction among themselves. Additionally, the concentration of the analyte must be adapted to the sensitivity of the spectrometer.

Formula 2-4

$$E = \frac{\log I_0}{I} = \varepsilon(\lambda) \times c \times d$$

E = extinction

I_0 = intensity of the irradiate measuring beam

I = intensity of the eradiate measuring beam

$\varepsilon(\lambda)$ = extinction coefficient

c = concentration of the analyte

d = path length

2.8.1.2 Flavin sample preparation

Dry FMN, FAD and riboflavin were dissolved in H₂O_{demin}, D₂O or the corresponding buffer. For the measurements at low and high pH, the flavins were dissolved in 37% HCl and 5 M NaOH solutions, respectively. For experiments in D₂O 35% DCl and 5M NaOD was used. Preparations of reduced FMN contained sodium dithionite as a chemically reducing agent or EDTA, which enabled the photoreduction of FMN using UV light [74]. AgNO₃ was added and mixed by vortex at neutral pH to a final concentration of 10 M. UV/VIS spectra have been recorded on a Beckman DU-64 UV/VIS spectrometer and a PerkinElmer Lambda 35 spectrometer at room temperature (RT).

2.8.1.3 Oscillator strength determination

The oscillator strength f_{osc} is a dimensionless quantity that is used to estimate the relative strength of the electronic transitions within a molecular system and that gives information about the transitions probabilities. It can be determined experimentally by integration of an absorption band and is related to the experimental quantity, the extinction coefficient ε of absorption, by the following term:

Formula 2-5

$$f_{osc} = 4.3 \times 10^{-5} \int \frac{\varepsilon(\bar{\nu}) d\nu}{M^{-1}cm^{-1}\mu m^{-1}}$$

ε = extinction coefficient

$\bar{\nu}$ = energy of the absorption in wavenumbers

The integrated absorption coefficient, $\varepsilon(\bar{\nu}) d\nu$, is an experimental measure of transition intensity, because it describes the area under the spectral absorption curve in the UV/VIS spectrum. The area under an absorption band in a UV/VIS spectrum was integrated using the Origin Pro software under assumption of Gaussian distribution. If the band data consisted of multiple or overlapping peaks, the data was separated to obtain the area of the peak of interest.

2.8.2 Fluorescence spectroscopy

2.8.2.1 Theory

Similarly, to the UV/VIS spectroscopy the absorption of photons is the basic requirement for fluorescence spectroscopy. The molecule is transferred to an excited electronic level by a photon and subsequently drops back into the ground state, simultaneously emitting photons. The emission radiation can be of the same energy as the excitation radiation (resonance fluorescence) or can be of lower energy. The difference between these two radiations is referred to as Stokes' shift and is caused by the additional vibrational excitation (Franck-Condon principle). The vibrational states relaxation is much faster than the emission of light, meaning that the relaxation to the electronic ground state always originates from the vibrational ground state of an excited electronic state. In case of bioluminescence the excited state is generated chemically (chemiluminescence) and not by radiation. Thus the amount of emitted photons exhibits direct information about the chemical reaction.

2.8.2.2 Flavin sample preparation

FMN was dissolved in $\text{H}_2\text{O}_{\text{demin}}$ or buffer for fluorescence measurements. Fluorescence spectra have been recorded on a PerkinElmer LS55 spectrometer, detector R928 (red-sensitive photomultiplier), at room temperature. The excitation wavelength was adapted to the absorption maxima of FMN, which were obtained by UV/VIS spectroscopy. For measurements of reduced FMN the flavin was either chemically reduced by sodium dithionite or photochemically by the addition of EDTA and illumination with UV light.

2.8.2.3 Kinetic assays with luciferase

The activity of the bacterial and the eukaryotic luciferase was investigated by fluorescence spectroscopy. The photons emitted during the enzymatically catalyzed reaction are generated chemically, therefore no light excitation was necessary. The detected photons provide direct information about the activity of the protein under respective conditions since only with the enzymatic activity of the luciferase photons are emitted.

The reaction of the bacterial bioluminescence requires reduced flavin as luciferin, aldehyde and the luciferase protein. For emission measurements flavin was reduced chemically by sodium dithionite ($\text{Na}_2\text{S}_2\text{O}_4$), which was dissolved in vacuum-vented $\text{H}_2\text{O}_{\text{demin}}$ in order to stabilize the reducing capacity. The flavin (FMN, FAD, riboflavin) was dissolved in $\text{H}_2\text{O}_{\text{demin}}$. Different aldehydes (dodecanal, decanal, octanal, cinnamaldehyde, hydrocinnamaldehyde, vanillin, acetaldehyde) were tested as possible substrate for the bacterial bioluminescent reaction.

Reaction batch:	100 mM	Buffer (pH 5.5 - 9.0)
	0.05 – 4 μM	LuxAB
	25 – 200 μM	Flavin
	0.1 – 20 mM	$\text{Na}_2\text{S}_2\text{O}_4$
	0.2 – 10 mM	Aldehyde

It was obligatory to associate the protein with the reduced flavin before the aldehyde, because a partly inhibiting complex can be formed if the luciferase is first exposed to the aldehyde prior to the flavin [186,187], which leads to the inactivation of the protein. Also after the addition of $\text{Na}_2\text{S}_2\text{O}_4$ the sample was mixed by inversion until the flavin was visibly reduced. The aldehyde was filled into a quartz cuvette before the rest of the sample was added to the cuvette at once, which started the reaction. During measurements the sample was air-bubbled with 18 ml/min flow rate to ensure the exposure to O_2 , which is required for the reaction. For the determination of the pH optimum of the protein different buffers (citrate, phosphate, HEPES, Tris-HCl) were used as solvent for the reaction batch to cover a pH range of 5.5 – 9.0. Since the definite protein concentration of homologically purified bacterial luciferase could not be determined, 20 μl of the same storage batch were applied to reaction samples.

Emission spectra have been recorded on a Cary Eclipse Fluorescence Spectrometer (High performance R928 photomultiplier detector) at room temperature. Emission spectra in a wavelength range from 400 nm to 650 nm were acquired as well as time resolved spectra at 490 nm, which were recorded with a time interval of 0.01 min (Δt). Signal averaging was done with 100 ms (gatetime). The time resolved spectra are comparable given that the same Δt was used in all measurements.

Additionally, kinetic experiments of firefly bioluminescence with D-luciferin and ATP as substrates have been performed. In the presence of MgCl_2 the firefly luciferase catalyzes the emission of light using these reacting agents, which were dissolved in $\text{H}_2\text{O}_{\text{demin}}$.

Reaction batch:	100 mM	Buffer (pH 5.5 - 9.0)
	0.1 μM	Luc
	100 μM	D-luciferin
	10 mM	MgCl_2
	250 μM	ATP

For emission measurements the reaction was started by mixing Luc, MgCl₂ and ATP in the respective buffer and adding it to the D-luciferin, which was applied to the quartz cuvette beforehand. Due to the necessity of O₂ for the bioluminescent reaction the sample was air-bubbled during measurements. Emission spectra with Luc were recorded from 450 to 700 nm.

2.8.3 EPR spectroscopy

2.8.3.1 Theory

Electron paramagnetic resonance (EPR) spectroscopy is a technique for the detection and investigation of paramagnetic compounds - species with unpaired electrons. Paramagnetic compounds are present in many systems containing metallic ions, i.e. cofactors of proteins, or organic radicals that occur during a chemical reaction. Electrons have a quantum mechanical intrinsic angular momentum, an electron spin S , which interacts with an applied external magnetic field, shown by the Stern-Gerlach experiment [188]. In EPR the interaction of electron spins with an applied magnetic field is analyzed to obtain information about the identity and structure of the paramagnetic species. In an external magnetic field the electron spin of a system with a single unpaired electron ($S=1/2$) can orientate either parallel or antiparallel to the magnetic field (Zeeman interaction). Accordingly, the magnetic quantum number m_s has two distinct values, $m_s = -1/2$ and $m_s = +1/2$. The electron spin energy levels are:

Formula 2-6

$$E\left(m_s \pm \frac{1}{2}\right) = \pm \frac{1}{2} g_e \mu_B B_0$$

g_e = g-factor for free electrons

μ_B = Bohr magneton

B_0 = magnetic field strength

The energy difference between these two levels is defined as:

Formula 2-7

$$\Delta E = g_e \mu_B B_0$$

A transition of the electron spin between the two energy levels occurs, if an irradiation of microwaves with respective frequency is applied. These considerations apply accordingly for the nuclear spins. This resonance condition is fulfilled when Formula 2-8 is satisfied.

Formula 2-8

$$\Delta E = g_e \mu_B B_0 = h \cdot \nu$$

h = Planck's constant

ν = frequency of microwave radiation

A simple Lorentzian line shape signal is observed when in the applied magnetic field the energy difference of two spin states matches the energy of the microwave radiation (Figure 2-2).

In CW (continuous wave) EPR spectroscopy the sample is irradiated with a fixed microwave frequency (GHz range) whereas the magnetic field is consistently swept. Since the position of the absorption band in the EPR spectrum depends only on the g -factor, it makes g a characteristic value for each analyzed analyte. A free electron displays a g value of $g_e = 2.0023$.

The influence of nearby nuclei on the electron also needs to be considered. Since some nuclei have a magnetic moment as well, they can generate a local magnetic field B_1 , which influences the electron. This interaction is termed hyperfine interaction, leading to a splitting of the lines in the EPR spectrum. Additional information can be collected from this interaction concerning the identity and number of atoms and their distance

from the unpaired electron. The number of signals in the EPR absorption spectrum increases exponentially as the number of nuclei gets larger.

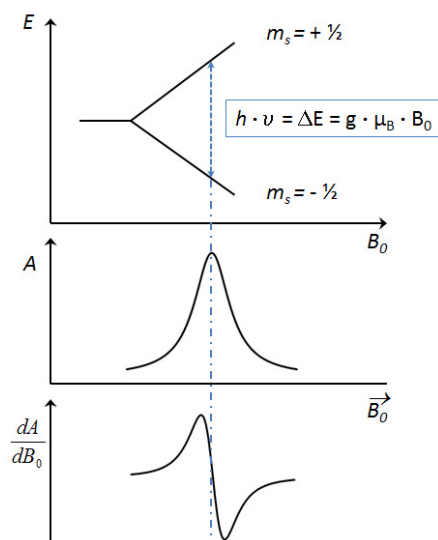


Figure 2-2: Formation of EPR signal with (top) splitting of the energy levels of an electron spin subjected to a magnetic field, (middle) Lorentzian absorption and (bottom) its first derivative as observed in CW EPR.

2.8.3.2 Spin trapping

A well established method for the detection of short-lived radicals *in vitro* is spin trapping [189]. The used spin traps are molecules that can capture short-lived radicals by taking over the unpaired electron and forming a stable EPR-visible adduct. There are different spin trap molecules that can be used for this purpose, but they all share a nitrogen oxide group stabilized in a heterocyclus. Each spin trap has its own properties concerning the affinity towards different radicals. Whereas 2,2,6,6-tetramethylpiperidin-N-oxyl (TEMPO) and its accordant 4-hydroxy compound (TEMPOH) are often used to capture alkyl radicals ($R\bullet$) [190,191], 5,5-dimethyl-1-pyrrolin-N-oxide (DMPO) has a high affinity towards radicals localized on oxygen atoms [192]. For example, DMPO has been used to capture hydroxyl radicals ($HO\bullet$), superoxyl ($O_2^-\bullet$) and hydroperoxy

radicals ($\text{HOO}\bullet$) [193,194], as well as alkoxy ($\text{RO}\bullet$) and peroxy radicals ($\text{ROO}\bullet$) [195]. Additionally, DMPO possesses low cytotoxicity, good reception by living cells and a high rate constant for the reaction with OH radicals [192,196].

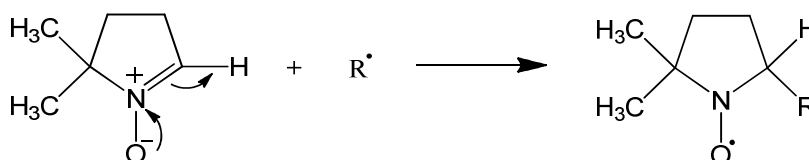


Figure 2-3: Schematic reaction mechanism of spin trapping with DMPO.

The short-lived radical is added by nucleophilic attack of the C=N double bond of the DMPO and homolytic opening of this bond followed by the formation of a nitroxide radical to which the original radical is covalently attached (Figure 2-3). The originated DMPO adduct is stabilized due to the delocalization of the unpaired electron. Since this radical, like all radicals, holds a paramagnetic character, it is directly accessible by EPR spectroscopy.

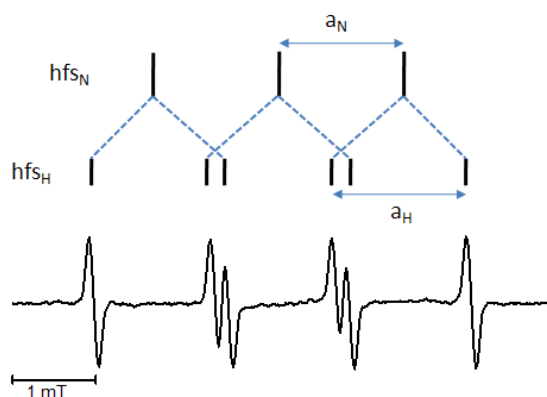


Figure 2-4: Example of DMPO adduct signals in CW EPR. Hyperfine splitting, due to interactions with nuclear spins of nitrogen (hfs_N) and neighboring hydrogen (hfs_H) generates an EPR spectrum with 6 signals. Hyperfine coupling constants a_N and a_H can be determined directly from EPR spectra.

Interactions with the nuclear spins of the nitrogen atom and neighboring hydrogen atom of DMPO result in hyperfine splitting. The EPR spectra show a characteristic primary triplet coupling splitting from the nitrogen nucleus of the nitroxide group (hfs_N) (Figure 2-4). Additional hyperfine interaction with neighboring hydrogen (hfs_H) atom leads to an EPR signal appearance of a triplet of doublets. Detailed information about the spin adducts are provided by the magnitude of the hyperfine splitting - hyperfine coupling constants a_H and a_N . The hyperfine coupling constants are determined experimentally from EPR spectra.

2.8.3.3 Spin trapping sample preparation

For the preparation of spin trapping samples FMN was reduced photochemically. During irradiation with UV light or blue light the lowest excited triplet state of FMN is generated, which subsequently abstracts electrons from a reducing agent, such as EDTA or NADH [74,197].

Samples containing bacterial luciferase were prepared in potassium phosphate buffer (100 mM, pH 7.5). The total volume of all samples was 1 ml containing 0.25 - 5 μ M purified heterologous luciferase protein. Reduced FMN and 20 mM DMPO was added to the respective solutions and the samples were subsequently mixed by several inversions to ensure a homogeneous mixture of all components. The light emitting reaction was initiated with the rapid injection of the respective aldehyde. When the flavin was reduced chemically, 20 mM sodium dithionite was added to 0.2 - 1 mM FMN. For the photochemical reduction 200 μ M FMN were mixed with 8 mM EDTA or NADH and illuminated using a 150W xenon lamp (Hamamatsu). A lens was used to focus the illumination on a quartz cuvette containing the sample and a second cuvette with H₂O was placed between the lens and the sample cuvette to avoid additional heating of the sample due to infrared radiation (Figure 2-5). The sample was illuminated and air-bubbled (18 ml/min flow rate) using a cannula (0.6 x 30 mm) for 20 - 40 min. Spin trapping samples with firefly luciferase were prepared as described for kinetic experiments in section 2.8.2.3, including 5 - 30 mM DMPO. Due to the necessity of O₂ for the luminescent reaction, the sample was also carefully air-bubbled at 18 ml/min for various time intervals. All samples were analyzed by CW EPR. The samples were

measured in a suprasil quartz flat cell, which minimizes the absorption of microwaves by aqueous samples.

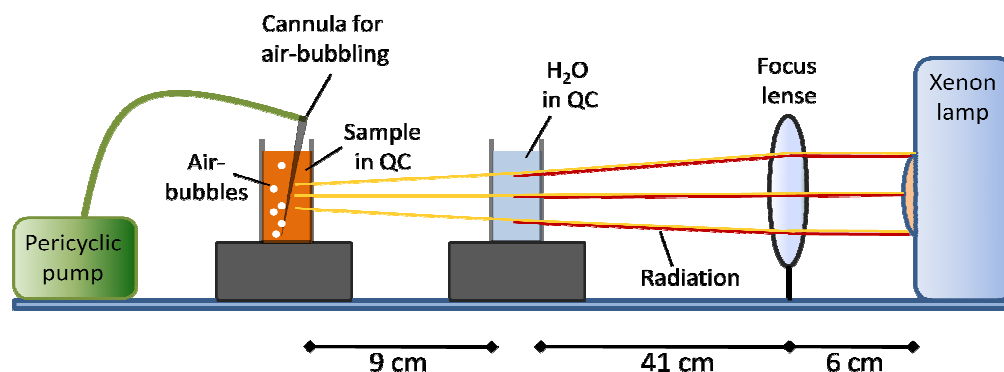


Figure 2-5: Schematic view of the illumination setup. Xenon lamp light is focused through a focus lens on the quartz cuvette (QC) containing the sample. The radiation is guided through a QC filled with water to eliminate infrared radiation and to avoid additional heating of the sample. The sample is carefully air-bubbled using a cannula and pericyclic pump.

2.8.3.4 Analysis of spin trapping samples by CW EPR

CW EPR experiments were carried out on a Bruker ESP 300E EPR spectrometer. In CW experiments the spectrum is generated by continuous application of microwave irradiation at constant frequency while the magnetic field is slowly swept. The microwave irradiation is provided up by a Gunn diode. An attenuator controls the amount of microwave power that reaches the sample, which is localized in a resonant cavity. The wavelength of the microwave radiation fits to the cavity dimensions, building up a standing wave, which results in an increased level of the microwave radiation in the sample. The electrical properties of the investigated sample determine the frequency at which the cavity is resonant. The cavity together with a sample is tuned so that all microwave power enters the cavity and that reflection is minimized. The applied magnetic field is slowly swept until the difference in the energy of two spin levels in the investigated sample is on resonance with the microwave radiation. At this point, the additional absorption of microwaves by the sample creates a small detuning

of the resonator. Hence more microwave power is reflected by the resonator, which is detected as resonance signal.

2.8.3.5 Triplet state of flavins

The electronic ground state in almost all organic molecules is a singlet state, S_0 (Figure 2-6). Illumination of these molecules results in the formation of an excited singlet state with spin preservation. One of the unpaired electrons may then flip the spin, most notably by SOC [198], which leads to the formation of a triplet state T_1 with the spin quantum number $S = 1$. This mechanism of triplet formation is known as ISC. The triplet state is an electronically excited state with an even number of electrons and two parallel unpaired electron spins. In most cases the lowest triplet state is lower in energy than the first excited singlet state. Besides radiationless decay of S_1 or T_1 the relaxation $T_1 \rightarrow S_0$ can only occur very slowly, because of spin interdiction, and therefore differs from the relaxation $S_1 \rightarrow S_0$, which is accompanied by spontaneous emission. The relaxation $S_1 \rightarrow S_0$, referred to as fluorescence, is a fast process in the pico- to nanosecond range, whereas the relaxation $T_1 \rightarrow S_0$, termed phosphorescence, is considerably slower and takes place in the micro- to millisecond range. Hence a continuous illumination of the system would result in the population of T_1 , depending on ISC and decay rate of the triplet state.

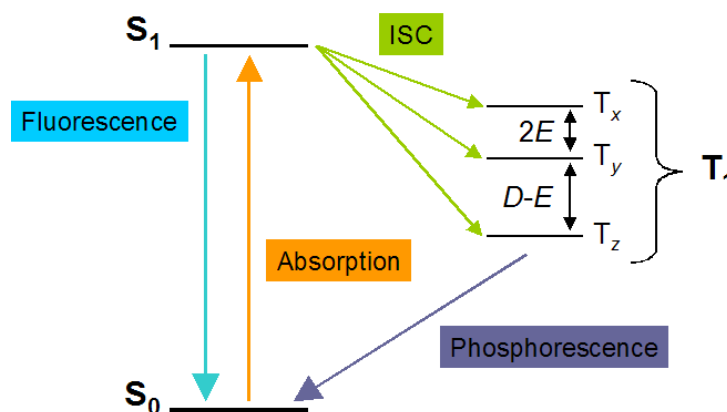


Figure 2-6: Scheme of the lowest electronic levels in an organic molecule. S_0 : singlet ground state; S_1 : singlet excited state; T_1 : triplet excited state including the spin sublevels T_x , T_y and T_z .

Molecules with a total electron spin of $S \geq 1$ possess split electron spin energy levels even when no external magnetic field is applied. In the case of an excited triplet state three distinct spin sublevels T_x , T_y , T_z (cf. Figure 2-6) constitute the energy level pattern, termed ZFS. Even in absence of a magnetic field, the relaxation probability from each of the three sublevels to S_0 differ, mainly due to the magnetic dipole-dipole interactions between the unpaired electrons, the ZFS. The sublevels are labeled according to the molecular axes, with X having its spin polarized in the (Y,Z)-plane, orthogonal to the X axis. The energy splitting between T_z and the middle between T_x and T_y , is defined as D parameter (Figure 2-7) and is typically in the range of a few GHz. Half of the energy splitting between T_x and T_y is specified as E parameter, which is mostly less than a GHz and ranges from 0 to $1/3 D$. ZFS parameters D and E contain information about the electron spin density distribution of the molecule in the triplet state. Parameter D describes the effective distance between the two unpaired electrons and is inversely proportional to the third power of that distance ($D \propto r^3$). The parameter E contains information about the deviation of the electron spin density distribution from the axial symmetry.

The ZFS Hamiltonian is defined as

Formula 2-9

$$H_{ZFS} = D \left\{ S_z^2 - \frac{1}{3} S(S+1) \right\} + E (S_x^2 - S_y^2)$$

The eigenvalues of the ZFS Hamiltonian are the following:

$$E_x = \frac{1}{3} D + E$$

$$E_y = \frac{1}{3} D - E$$

$$E_z = -\frac{2}{3} D$$

The ZFS parameters D and E can be obtained from the EPR spectrum. The width of the spectrum equals $2D$. Parameter E can be observed from the inner transitions that are visible in the spectrum. The separation between the transitions that originate from the canonical orientation for which the molecules oriented with their X principal axis parallel to the magnetic field, equals $D + 3E$. These parameters can also be determined by simulation of the EPR spectra or DFT calculations as described later (sections 2.8.3.8 and 2.9).

The relative populations of the energy sublevels affect the EPR transition [199]. It becomes either emissive or absorptive (E = emissive, A = absorptive). The transitions occur between the energy levels 0, +1 and 0, -1, as indicated in Figure 2-7, showing two EPR lines for one canonical orientation. The occurring order of emissive and absorptive transitions obtained from all 6 canonical orientations provides information about the triplet formation. Since SOC depends on the spin orientation with respect to the orbital, the population rates of T_x , T_y , T_z differ from the excited singlet, whereas T_z is mostly less coupled than the other two.

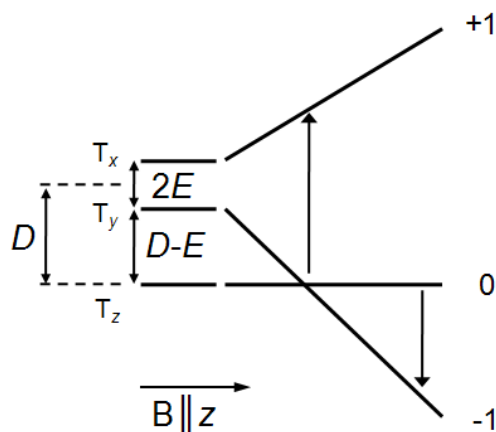


Figure 2-7: Scheme of the energy sublevels of a triplet state T_x , T_y and T_z , including the ZFS parameters D and E . The direction of the magnetic field is parallel to the Z principal axis.

EPR studies of triplet states are much less common than those of doublet state radicals, for the obvious reason that most radical species concern ground states of molecules, whereas triplet states are mostly metastable and typically have lifetimes in the microsecond range. The lifetimes of the three magnetic sublevels furthermore depend on SOC, and because SOC is a spin-selective interaction, the lifetimes are usually different. Often, the magnetic sublevel that attains most population also decays most rapidly. The amplitude of the EPR signal in the triplet state depends on the population difference of the resonant sublevels. Large EPR signals are present if the triplet state is fully polarized, ideally with only one triplet sublevel containing all the population. Since intersystem crossing competes with fluorescence and radiationless decay of the excited singlet state, which typically occurs on a nanosecond time scale, the absolute population or yield of the triplet state may be increased if the SOC interaction is maximized. The present thesis looks into this approach by the addition of heavy atoms (silver).

2.8.3.6 Sample preparation for excited triplet state measurements of FMN

1 mM and 10 mM FMN was dissolved in H₂O_{demin} or D₂O. The solutions contained 50 % (v/v) glycerol or D-glycerol in order to obtain an optically transparent frozen solution. For measurements at low and high pH, FMN was dissolved in 37 % HCl or 5 M NaOH solutions. For experiments in D₂O 35 % DCl and 5 M NaOD were used. For the investigation of the influence of heavy atoms on the SOC, AgNO₃ was added at neutral pH to a final concentration of 10 M. All samples were subsequently transferred to a Q-band EPR tube (outer diameter 2 mm) and were initially frozen at -20 °C and subsequently rapidly frozen and stored in liquid nitrogen.

2.8.3.7 Laser excitation of FMN and analysis by pulsed EPR

Light-induced triplet signals of FMN have been measured at which a laser pulse has been used for an excitation of samples placed inside the cryostat of the EPR spectrometer. The ZFS constants *D* and *E* can be derived from pulsed EPR spectra and can give information about the effective distance between the triplet electrons. Compared to CW EPR, which uses continuous microwave radiation, pulsed EPR is performed by the application of short intense microwave pulses, followed by the

detection of a Hahn echo [200]. A $\pi/2$ pulse rotates the initial magnetization by 90 degrees (Figure 2-8) in such a way that it lies along the y-axis. During the time τ the spin packets dephase in the transversal xy-plane. The following π pulse flips the magnetization by 180 degrees entirely so that after a second time period τ it is aligned along the y-axis, where it can be detected as a spin echo.

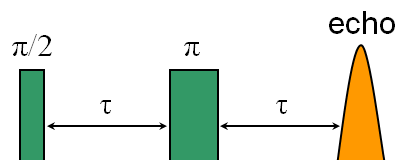


Figure 2-8: Scheme of a two-pulsed Hahn echo sequence containing π and $\pi/2$ pulses. τ : time between pulses and echo.

The microwave pulses were triggered by laser flashes and a magnetic field was sweeping constantly while microwave pulses were applied. In an electron spin echo (ESE) measurement the absorption signal is detected directly. ESE measurements were carried out on a Bruker Elexsys E580 FT EPR spectrometer equipped with a Q-band EPR/ENDOR resonator and an Oxford CF935 helium gas flow cryostat at 30 K. A Hahn echo pulse sequence with pulse lengths for $\pi/2$ of 30 ns and for π of 60 ns and a delay between pulses of $\tau = 600$ ns was applied. Laser excitation was performed by an OPO (Optical Parametric Oscillator) Plus laser pumped by a Continuum Surelite II laser. Irradiation at a wavelength of 450 nm was applied to excite the sample with energy of 10 mJ/pulse. The repetition rate of the laser was 10 Hz. The laser radiation was focused on the sample using an adjustable lens system.

2.8.3.8 Simulations

EPR spectra have been simulated with a self-written program by Dr. Maurice van Gastel based on the formalism developed by Dauw and coworkers [199]. In this formalism, each zero field sublevel (T_x , T_y , T_z) is ascribed a fractional population (p_x , p_y , p_z) with

Formula 2-10

$$p_x + p_y + p_z = 1$$

An orientational average is performed over all possible orientations of the molecule in frozen solution, the spin Hamiltonian

Formula 2-11

$$H = \mu_B \vec{B} \cdot \vec{g} \cdot \hat{S} + \hat{S} \cdot \vec{D} \cdot \hat{S}$$

B = magnetic field

\vec{g} = g tensor

\vec{D} = zero field splitting tensor

is diagonalized using the principal axis system of \vec{D} as a reference. The g tensor is described by the principal values (g_x, g_y, g_z) and \vec{D} is the traceless zero field splitting tensor with principal values $(-(1/3)D + E, -(1/3)D - E, (2/3)D)$. For each orientation the population of the magnetic sublevels $|M_S\rangle$ ($M_S = 1, 0, -1$) is given by

Formula 2-12

$$p_{M_S} = \sum_{i=x,y,z} |C_{iM_S}|^2 p_i$$

p_{M_S} = population of the M_S sublevel

C_{iM_S} = coefficient of the mixing zero field states in the magnetic field

p_i = population of one of the three zero field levels

where the coefficients C_{iM_S} are the eigenvectors of H .

2.8.4 Mass spectrometry

2.8.4.1 Theory

Besides liquid chromatography (UV/VIS, fluorescence) mass spectrometry gives amendatory information about the analyte. Compared to optical detection techniques the mass spectrometric detection can help to identify unknown compounds by their mass-to-charge ratio (m/z). The basic idea is the molecular weight determination of free ions in high-vacuum conditions, which include three main steps: (1) Ionization and acceleration by means of an ion source; (2) m/z separation of the generated ions in a mass analyzer; (3) detection of ions and their concentrations, which can be plotted against m/z .

The organic mass spectrometry was limited on small molecules up to the 80th when MALDI (Matrix-assisted laser-desorption ionization) and ESI (electrospray ionization) were established as ionization techniques [201–203], which enabled the analysis of larger molecules like proteins. From this time on, proteins could be transferred from the solid (MALDI) or the condensed (ESI) state into the gas phase and ionized, which makes mass spectrometry to one of the most important techniques for protein analytics.

For the protein analysis using MALDI – TOF (time of flight) the sample is incorporated into an organic matrix, which increases the signal intensity of the sample during measurements. Applied to a metallic carrier plate, the protein and the matrix are cocrystallizing, whereat one or two protons are transferred to the protein. Under high-vacuum conditions the protein and matrix ions are sublimated by a short-wave laser. Due to their electronic charge the protein ions are accelerated towards an electrode and are separated by their m/z value. A detector records the time of flight, which can be used to determine the m/z by known acceleration voltage and distance of flight.

In ESI the liquid sample is atomized using a thin capillary. The difference in potential of 3-6 kV between the capillary's needle point and the backplate electrode causes charging of the atomized sample components once they exit the capillary. The type of voltage that is applied to the capillary determines the charge of the generated ions. A positive voltage generates positive ions and a negative voltage generates negatively

charged ions. The following evaporation results in a decreasing volume and an increasing volumic charge. Once the Coulomb repulsion gets larger than the surface tension of the sample components, they dissociate in even smaller particles. The latter process repeats until only highly solvated analyte ions are present. A part of these ions access the analyzer through a small gap in the backplate electrode, where the separation by mass-to-charge ratio occurs. The chemical properties and the polarity of the adjacent volumic charge influence the positive or negative charge of the ions. ESI is a gentle method for exact molecular weight determination, since the fragmentation of the analyte is greatly reduced.

2.8.4.2 Recombinant LuxAB samples

The heterologously expressed heterodimer LuxAB from *V. fischeri* was further analyzed by mass spectrometry to monitor the presence of both subunits. MALDI-TOF can be used to analyze the molecular mass of peptides and proteins and was therefore applied for this purpose. The small sample volume required for this method is a big advantage, since the protein yield of conventional gravity flow affinity chromatography is rather low. The samples containing purified protein were desalted prior to mass spectrometry analysis using Zebra Spin Desalting Columns (MWCO: 7 kDa). DHAP (2',4'-Dihydroxyacetophenone) was used as organic matrix.

2.8.4.3 Spin trapping samples

The spin trapping samples for EPR measurements were subsequently analyzed by mass spectrometry in order to monitor the reaction products, including any spin trapping complexes. The sample preparation was done as described in more detail in section 2.8.3.3. The samples were analyzed by ESI. The charge of the generated ions during ESI depends on the applied voltage. Since some molecules are better detected carrying a positive charge, whereas others are better detected with a negative charge, all samples were analyzed with both applied voltages.

2.9 Theoretical calculations

Density functional theory (DFT) is a method, based on position-dependent electron density, to describe the quantum mechanical state of a system with a large number

of electrons. DFT is used to evaluate the basic properties, such as bond lengths and energies, of molecules and solid state bodies. Since this method is based on the idea that the complete solution of the Schrödinger equation is not required due to the use of an approximation procedure, it presents an efficient possibility to calculate chemical properties of large systems.

DFT calculations have been performed together with Dr. Maurice van Gastel using the ORCA program system [204]. The model for FMN includes the complete molecule given in Figure 3-5. The goal of the theoretical investigation is to obtain chemical and physical insights into the orbital structure of FMN. In order to mimic acidic conditions, the chromophore was protonated at position 1. For alkaline conditions, the chromophore was deprotonated at position 3 and extended with a Na^+ counterion. All calculations employ the TZVP basis set [205] and the B3LYP functional [206,207]. The spin-spin part of the ZFS has been calculated with a wave function obtained from a spin-restricted open shell calculation (ROKS), since it is known that the spin contamination, even if small, inherent to unrestricted DFT formalism gives rise to ZFS parameters of moderate precision [208]. The part of the ZFS resulting from spin polarization has been calculated manually according to a physically transparent formalism described by van Gastel [209] in analogy to the widely used McConnell theory for hyperfine interactions [210]. In order to model the binding of silver, the geometry was augmented with an Ag^+ ion bound trigonally: to the oxygen atom at position 4, to the nitrogen atom at position 5 and to an additional water molecule [211,212]. Additionally, the effect of the solvent was investigated for the deprotonated chromophore without the sodium ion and with inclusion of one or two additional water molecules and the COSMO (conductor-like screening model) [213] for solvation, using a dielectric constant of 80. All models have been fully geometry optimized.

In the ground state, the highest occupied molecular orbital (HOMO) is doubly occupied and the lowest unoccupied molecular orbital (LUMO) is empty. For the lowest triplet state both orbitals harbor one electron, referred to as singly occupied molecular orbitals (SOMOs). In this thesis they will be referred to as HOMO and LUMO. For the model,

which includes Ag^+ , the contribution of SOC at Ag^+ to the ZFS has been estimated manually by calculating the matrix elements

Formula 2-13

$$\vec{D} = \frac{\zeta^2}{E_n - E_k} \langle n | \vec{L} \cdot \vec{S} | k \rangle \langle k | \vec{L} \cdot \vec{S} | n \rangle$$

where $|n\rangle$ represents the Ag part of the wave function of the lowest triplet state and $|k\rangle$ the first excited triplet state, obtained by promotion of an electron from the HOMO – 1 to the HOMO. The HOMO contains 0.30% d_{xz} character at Ag and the HOMO – 1 contains 0.67% $d_{x^2-y^2}$ and 0.23% d_{xy} character at Ag (Löwdin spin populations). The energy difference $E_n - E_k$ is taken as equal to the difference in orbital energies of the HOMO – 1 and the HOMO from the ROKS calculation, -17650 cm^{-1} . The SOC parameter ζ for silver amounts to 0.27 eV (2194 cm^{-1}) [214]. After subtracting the trace, the D_{zz} element amounts to $+24 \cdot 10^{-4} \text{ cm}^{-1}$, giving rise to a contribution by SOC equal to $D_{soc} = (3/2) D_{zz} = +36 \cdot 10^{-4} \text{ cm}^{-1}$. The population of the triplet y level is expected to become much lower, since the contribution by SOC to the ZFS is largest along the y -direction, whose orbital angular momentum operator connects the d_{xz} orbital and the $d_{x^2-y^2}$ orbital. No symmetry constraints were imposed on the molecule in any calculation. The g values have been calculated with a spin-unrestricted formalism. Calculations of the electronic transitions were performed with TDDFT (Time dependent DFT), a spin-restricted formalism, and the B3LYP functional, since Neiss and coworkers have shown that this method produces reasonably accurate results for uracil and lumiflavin [83].

3 Results

Flavins are functionally relevant molecules, especially in electron-transfer related reactions in biological processes, e.g. FMN as a major component in the bacterial bioluminescence reaction. Bound to the luciferase protein as FMNH₂, it is majorly involved in the emission of light by being the excited emitter. Investigations about the electronic structure of FMN help to understand its function as light emitter on an electronic level. Prior findings on free FMN may be useful when compared with luciferase-bound FMN. Hence, the electronic structure of FMN was analyzed by means of EPR and UV/VIS measurements in combination with DFT and TDDFT calculations. Since flavins are not paramagnetic species, EPR investigations can only carry information, if the molecule reaches a radical state during a reaction or if it is excited to a triplet state. The latter is not easily accessible by EPR, since triplet states are metastable and typically have lifetimes in the microsecond range. The amount of the molecules in the triplet state may be increased, if the SOC interaction is maximized and the competition between ISC, fluorescence and radiationless decay shifts in favor of the first. In this study, the influence of the SOC interaction by the presence of heavy atoms, in particular AgNO₃, was analyzed, in order to increase the amount of flavin molecules in the triplet state.

Furthermore, a radical intermediate has been proposed for the bacterial bioluminescence reaction, but no experimental approach directly confirmed their presence yet. An initial investigation of the presence of radical intermediates was performed in this study by using spin trapping in combination with EPR spectroscopy. Therefore heterologous and homologous bacterial luciferase from *V. fischeri* was purified. The activity of the purified protein was additionally analyzed by fluorescence measurements with a multitude of aldehydes and flavins as luminescent substrates. Firefly bioluminescence was also analyzed by spin trapping in order to detect radical intermediates of the reaction. For this purpose, firefly luciferase from *P. pyralis* was purified heterologously.

3.1 Electronic structure of FMN

3.1.1 UV/VIS spectra and calculations

Different protonation states of FMN were measured by UV/VIS at low, neutral and high pH values in aqueous solutions of H₂O and D₂O, respectively (Figure 3-1). The substitution of protons by deuterium is reasonable for EPR measurements (*vide infra*) and was performed for UV/VIS measurements for reasons of completeness. The absorption maxima occur at 357 and 452 nm at high pH, and at 372 and 445 nm at neutral pH. It is apparent that the separation of these bands is largest at high pH and becomes smaller at neutral pH. The 450 nm band images a poorly resolved shoulder at about 480 nm. At low pH, the two bands fall together forming one unstructured band with doubled amplitude and an absorption maximum at 396 nm. The spectra in D₂O are very similar to the ones in H₂O, except that the bands at about 450 and 396 nm become less intense and broader.

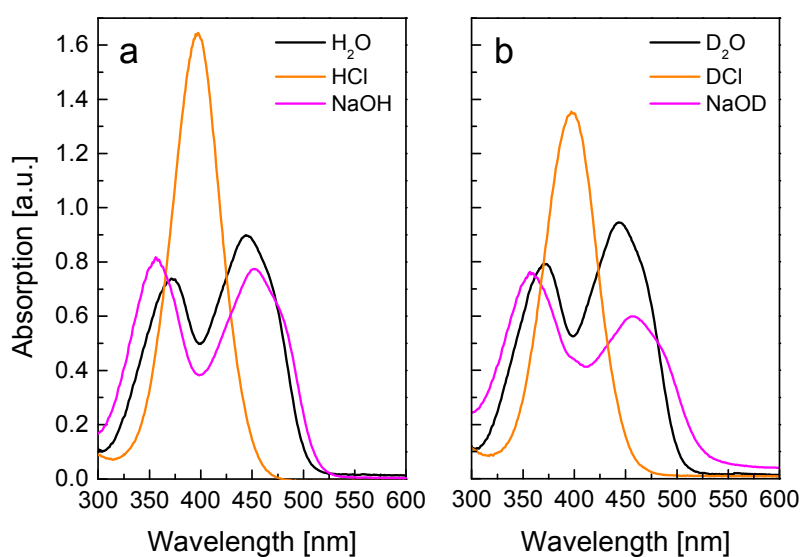


Figure 3-1: UV/VIS spectra at RT of (a) 0.1 mM FMN in H₂O, 37% HCl and 5 M NaOH, respectively, and (b) 0.1 mM FMN in D₂O, 37% DCl and NaOD, respectively.

Figure 3-2 shows UV/VIS spectra of FMN in the presence of AgNO_3 . After the addition of 1 M AgNO_3 the yellow colored FMN solution becomes initially more reddish, but at concentrations of 10 M AgNO_3 the color becomes yellow again. The two main absorption bands show bathochromic shifts from 372 to 384 nm and from 445 to 467 nm with respect to FMN at neutral pH.

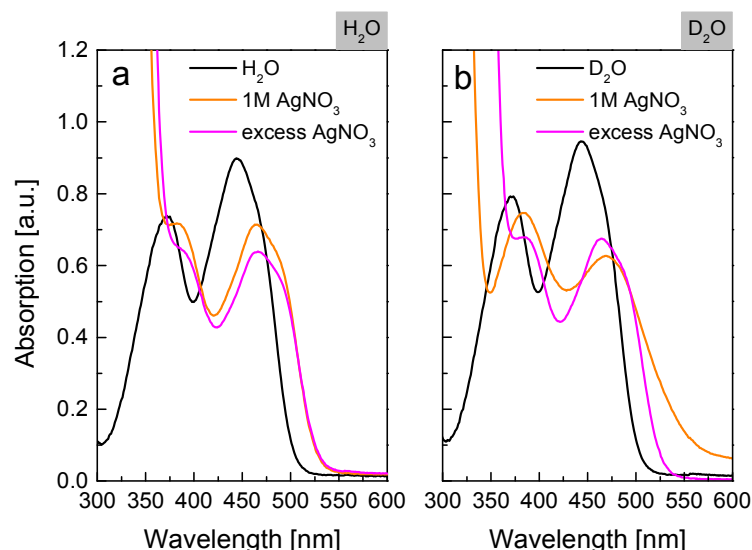
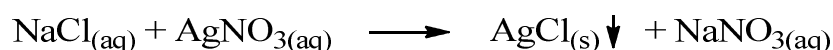


Figure 3-2: UV/VIS spectra at RT of 0.1 mM FMN with the addition of 1 M AgNO_3 and AgNO_3 in excess respectively in (a) H_2O and (b) D_2O .

Interestingly, the absorption band at 465 nm shows a variation at 1 M AgNO_3 in deuterated solvent in such a way that it is red shifted, broader and lower in intensity than the corresponding band in H_2O . Additionally, upon addition of AgNO_3 the presence of increased absorption at longer wavelengths than 500 nm is noticeable. Spectra at different pH could not be measured in the presence of AgNO_3 due to precipitation. The addition of HCl leads to the accumulation of hardly soluble AgCl and the addition of NaOH to insoluble Ag_2O . The chemical reaction equations are:



The electronic transitions of FMN under acidic, neutral and alkaline conditions, as well as in the presence of AgNO_3 , have been calculated by TDDFT formalism and are given in Table 3-1. Additionally, the experimental and calculated oscillator strengths are reported in round brackets.

Table 3-1: Experimental and calculated electronic transitions [nm] and oscillator strengths (in braces) of FMN under acidic, neutral and alkaline conditions, and in the presence of AgNO_3 at pH 7.

pH 7		pH 0	
Exp	Calc	Exp	Calc
467 (0.026)	485 (0.116)		
445 (0.082)	430 (0.143)		459 (0.042)
	381 (0.138)		
372 (0.172)	375 (0.116)	396 (0.267)	395 (0.430)
pH 13		AgNO_3	
Exp	Calc	Exp	Calc
			618 (0.058)
479 (0.022)	447 (0.245)	497 (0.010)	
452 (0.089)	393 (0.169)	467 (0.072)	499 (0.334)
357 (0.196)	363 (0.167)		363 (0.015)
		384 (0.143)	357 (0.080)

The electronic transitions that have been experimentally observed at 467, 445 and 372 nm in the UV/VIS spectrum of FMN at neutral pH in Figure 3-1 are well reproduced within the TDDFT formalism at 485 and 430 nm and two bands at 381 and 375 nm. The oscillator strengths are in reasonable although not perfect agreement with

experiment, which is consistent with the accuracy level of the TDDFT formalism. TDDFT calculations of FMN cation display only one strong band at 395 nm, since the oscillator strength for the band at 459 nm is considerably small. This is in line with the experimental data of FMN at low pH, in which all bands come together at 396 nm to one very strong signal. At high pH, however, the calculated electron transitions are in somewhat poor agreement with the experimental data. In general, the calculated transitions seem to reproduce the experimentally observed absorption maxima. The same observation holds for the calculations and absorption maxima for FMN in the presence of AgNO₃.

3.1.2 EPR spectra and calculations

To gain further insight into the electronic structure of FMN at different pH values or in the presence of AgNO₃, ESE detected EPR measurements of photoinduced triplet states of FMN have been carried out. If calculations reproduce the experimentally observed ZFS parameters from EPR spectra and electronic transitions from UV/VIS, the calculated wave functions can be used to describe the electronic orbital structure.

Light with a wavelength of 450 nm was used to excite the sample with energy of 10 mJ/pulse. This wavelength corresponds to the highest UV/VIS absorption maximum of FMN. Figure 3-3 shows spectra of triplet signals in presence and in absence of AgNO₃ in H₂O and D₂O, respectively. The substitution of protons, that are in immediate proximity to the electron spin, by deuterium, leads to a better defined separation of matrix effects and smaller couplings close by the paramagnetic centre. When AgNO₃ is absent, the EPR spectra display a polarization pattern of EEEAAA (E = emissive, A = absorptive).

The triplet EPR spectra of FMN at different pH values show the same polarization pattern, independent from the excitation wavelength. With lower or higher excitation wavelengths the EPR signals only decreased in amplitude. Upon addition of AgNO₃ the polarization pattern changes to EAEAEA. In H₂O and D₂O the widths of the spectra remain the same.

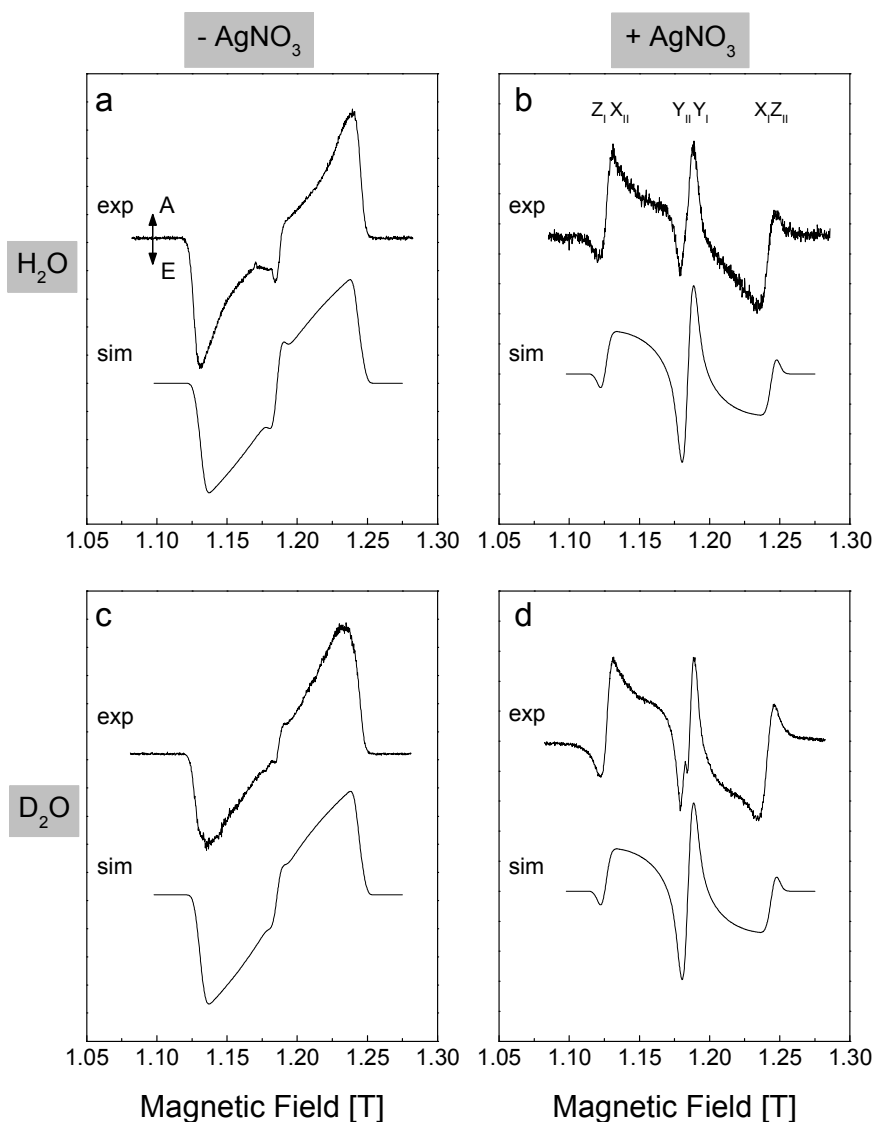


Figure 3-3: Q-Band ESE detected triplet EPR spectra at pH 7 and excited at 450 nm of (a) 1 mM FMN in H_2O , (b) 1 mM FMN and 10 M $AgNO_3$ in H_2O , (c) 1 mM FMN in D_2O and (d) 1 mM FMN and 10 M $AgNO_3$ in D_2O . Simulations are included in the figure. Experimental conditions: $T = 30$ K, Hahn echo pulse sequence: 30 ns – 400 ns – 60 ns, microwave frequency 33.260 GHz. The canonical orientations, for which molecules in the frozen solution oriented with their X, Y or Z principal axis of the D tensor parallel to the magnetic field, are included in (b). The divergence of absorptive and emissive transitions is indicated in (a).

The EPR spectra have been simulated as described in section 2.8.3. The parameters with which all spectra can be well simulated are given in

Table 3-2. The ZFS parameters D and E , determined by simulation, are slightly larger when silver nitrate is present. However, the spectra show anisotropy of the line width, which grows larger at the edges of the spectrum. An additional effective hyperfine coupling constant A_{zz} of 100 MHz has been included in the simulation for the Z canonical orientation, in order to reproduce the experimentally observed spectra.

Table 3-2: ZFS parameters D and E [10^{-4} cm^{-1}], populations of the zero-field triplet sublevels p_x , p_y and p_z for the triplet states of FMN and FMN with AgNO_3 at pH 7, as obtained from simulations. The line width was 2.5 mT; a hyperfine interaction A_{zz} of 100 MHz is included to take into account the anisotropy of the line width.

	FMN	FMN + AgNO_3
D [10^{-4} cm^{-1}]	535	579
E [10^{-4} cm^{-1}]	167	178
p_x	0.5	1.0
p_y	0.4	0.0
p_z	0.0	0.0
g_x	2.0050	2.0023
g_y	2.0037	2.0023
g_z	2.0023	2.0023

The line shape at the X canonical orientation shows a discrepancy between experiment and simulation. The experimentally observed spectra show a rather peak shaped intensity compared to the simulation. The reason for this discrepancy is likely related to the fact that the excitation by laser light in principle does not allow electric dipole transitions in the propagation direction of the laser light, thus giving an additional constraint in the orientation selection. In this study, this constraint was not included,

since the large amount of scattering in the sample largely but not completely covers this factor. In Figure 3-4 the spectra of FMN in HCl and NaOH are compared.

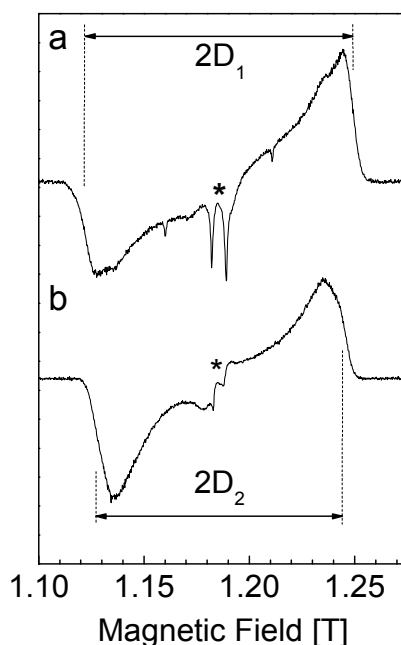


Figure 3-4: Q-Band ESE detected triplet EPR spectra of 10mM FMN in (a) 37% HCl and (b) 5 M NaOH, excited at 450 nm. The signals marked with * derive from photogenerated radicals. Experimental conditions: $T = 30$ K, Hahn echo pulse sequence: 30 ns – 400 ns – 60 ns, microwave frequency 33.260 GHz. Simulations give rise to the following D values: $D_1 = 603 \cdot 10^{-4} \text{ cm}^{-1}$, $D_2 = 541 \cdot 10^{-4} \text{ cm}^{-1}$.

At high pH the width of the spectrum is smaller than at low pH. This results in a smaller D parameter at high pH ($541 \cdot 10^{-4} \text{ cm}^{-1}$) than at low pH ($603 \cdot 10^{-4} \text{ cm}^{-1}$), indicating that the effective distance between the triplet electrons is largest at high pH.

The calculated ZFS parameters D and E are listed in Table 3-3. Three principal contributions to the ZFS arise: the direct magnetic dipole-dipole interaction between the two triplet electrons, a second order contribution by SOC (see section 2.9) and a contribution by spin polarization. The contributions to D are referred to here as D_{dir} ,

D_{soc} , and D_{pol} . The contribution by spin polarization arises in the following manner. The first triplet π electron (assumed to be a spin-up (α) electron) causes the σ electrons of a C-H or N-H bond to be polarized by the exchange interaction such that the α electron density of the σ -electron pair increases at the carbon or nitrogen atom and the spin-down (β) electron density increases at the proton. This causes additional spin density and a negative isotropic hyperfine interaction at the proton, which is a well-known phenomenon that is well described by the McConnell equation [210]. The second triplet electron then magnetically interacts with the additional σ spin density caused by the first electron and vice versa. The contribution to the ZFS by spin polarization may be in the order of 20 % of the total ZFS and therefore not negligible [209].

Table 3-3: Calculated ZFS parameters D and E , and g values for FMN with and without AgNO_3 . The ZFS parameter D is specified in terms of the contribution by the direct dipole-dipole interaction, the contribution by spin polarization and by SOC.

	FMN pH 7	FMN + AgNO_3	FMN pH 0	FMN pH 13
D [10^{-4} cm^{-1}]	540	564	550	579
D_{dir} [10^{-4} cm^{-1}]	477	442	480	493
D_{pol} [10^{-4} cm^{-1}]	63	86	70	86
D_{soc} [10^{-4} cm^{-1}]	0	36	0	0
E [10^{-4} cm^{-1}]	131	111	160	138
g_x	2.0059	2.0128	2.0046	2.0057
g_y	2.0046	2.0047	2.0038	2.0047
g_z	2.0022	2.0023	2.0022	2.0023

For FMN the calculated dipol-dipol interaction of the two triplet electrons add up to $477 \cdot 10^{-4} \text{ cm}^{-1}$ and the contribution by spin polarization amounts to $63 \cdot 10^{-4} \text{ cm}^{-1}$. For light atoms like carbon and nitrogen the second order contribution by SOC is

$< 10^{-4} \text{ cm}^{-1}$ and therefore insignificantly small. This gives rise to a total D value of $540 \cdot 10^{-4} \text{ cm}^{-1}$, which is in excellent agreement with experiment. Thus the contribution of the spin polarization contributes up to 12 % to the total ZFS for the triplet state of FMN.

The calculated D parameter of $564 \cdot 10^{-4} \text{ cm}^{-1}$ for the model of FMN and AgNO_3 is also in good agreement with experiment. Since calculation indicates that about 3% of the total spin density is present at Ag^+ in this model, and since the SOC parameter at Ag^+ is substantial (2200 cm^{-1}) [214], its contribution cannot be neglected. The contribution of SOC has been calculated using Formula 2-13 (section 2.9) and amounts to $36 \cdot 10^{-4} \text{ cm}^{-1}$. Moreover, the spectrum for FMN and AgNO_3 is best simulated with population only in the T_x level, which is in line with the observation that the contribution of SOC to the ZFS tensor is about 5 times larger along the y direction than along the x direction (see section 2.9), thus reducing the relaxation time and population of the T_y sublevel with respect to T_x . The models for high and low pH give rise to larger D parameters, which was also observed in experiment.

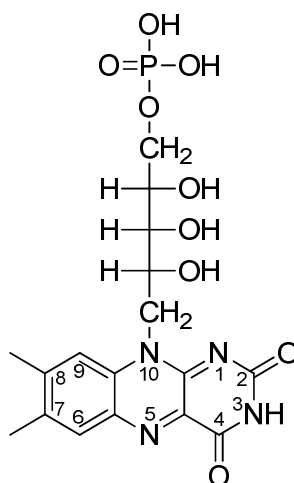


Figure 3-5: Structure and IUPAC numbering scheme of neutral FMN.

Concerning ^{14}N hyperfine interactions, the nitrogen atoms N1, N5 and N10 (Figure 3-5) all have A_{zz} values of 20 MHz, giving rise to a combined total hyperfine broadening

of 60 MHz. Their in-plane components are smaller than 2 MHz, as are all components of the hyperfine tensor of nitrogen atom N3. The calculated hyperfine broadening of 60 MHz is thus able to explain the observed differences in the ZFS parameter D when measured at 9 GHz (X-band) [96] or at 34 GHz (Q-band). In summary, since the calculations are able to largely reproduce the experimentally observed electronic transitions in the UV/VIS spectrum, as well as the ZFS parameters from EPR spectroscopy, the calculated wave function was used in order to describe the electronic orbital structure of the FMN molecule in the following section.

3.1.3 HOMO and LUMO calculations

For the simulation of the electron density distribution in FMN under acidic (cation), neutral and alkaline (anion) conditions, DFT calculations have been performed. Figure 3-6 displays the calculated results of the HOMOs and LUMOs. For all models, the frontier orbitals concern π orbitals of the isoalloxazine moiety. In pursuance of the calculations particularly the $2p_z$ orbitals at the carbon atoms C4a, C5a, C9a and C10a contribute a lot to the HOMO of FMN. In calculations done by Neiss and coworkers [215] the contribution of these orbitals to the HOMO of 10-methylisoalloxazine is much less. Also the electron density for the LUMO at the carbon atoms 2 and 7 (see Figure 3-5 for stereoscopic orientation) is negligible for 10-methylisoalloxazine, whereas the calculations for FMN in the present study show definite density at these atoms.

Under acidic, neutral and alkaline conditions the HOMO and LUMO compositions seem to be largely unaffected by the protonation state of FMN. The only notable difference in the HOMO occurs under acidic and neutral conditions at the nitrogen atom N1. Here the protonation leads to a stabilization of the local N1($2p_z$) orbital and a reduced contribution of this orbital to the HOMO composition. Under alkaline conditions the FMN molecule is deprotonated at the nitrogen atom N3 resulting in a FMN anion (Figure 3-6). Without inclusion of mechanisms to stabilize the negative charge, the HOMO and LUMO change drastically (Figure 3-7) and become incompatible with experiment (cf. Figure 3-6). As an alternative to inclusion of sodium counterions, water molecules have been added and solvent effects have been included

by the COSMO model (Figure 3-7), in order to stabilize the negative charge and to keep the calculations as close as possible to experimental conditions. Only with explicit inclusion of two water molecules and further solvation effects with COSMO the frontier orbital structure was found to be recovered as under alkaline pH conditions (Figure 3-6, right). These findings suggest that environmental effects have a large influence on the electronic structure of FMN.

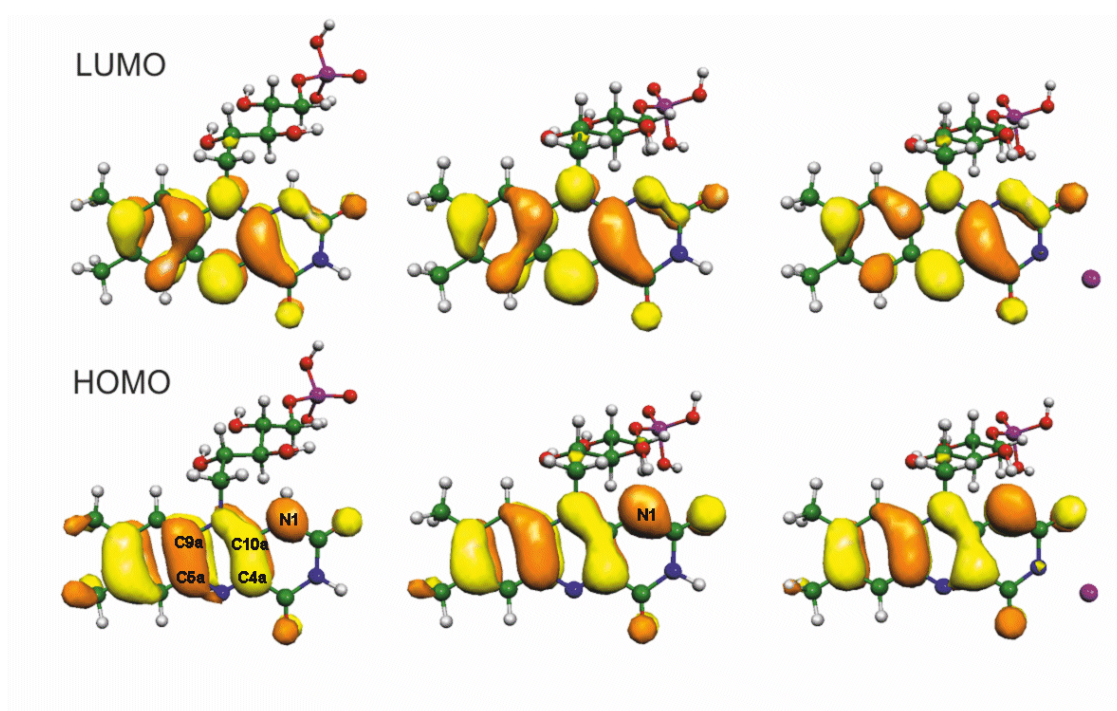


Figure 3-6: Calculated LUMO (top) and HOMO (bottom) for FMN under acidic (left), neutral (middle) and alkaline (right) conditions.

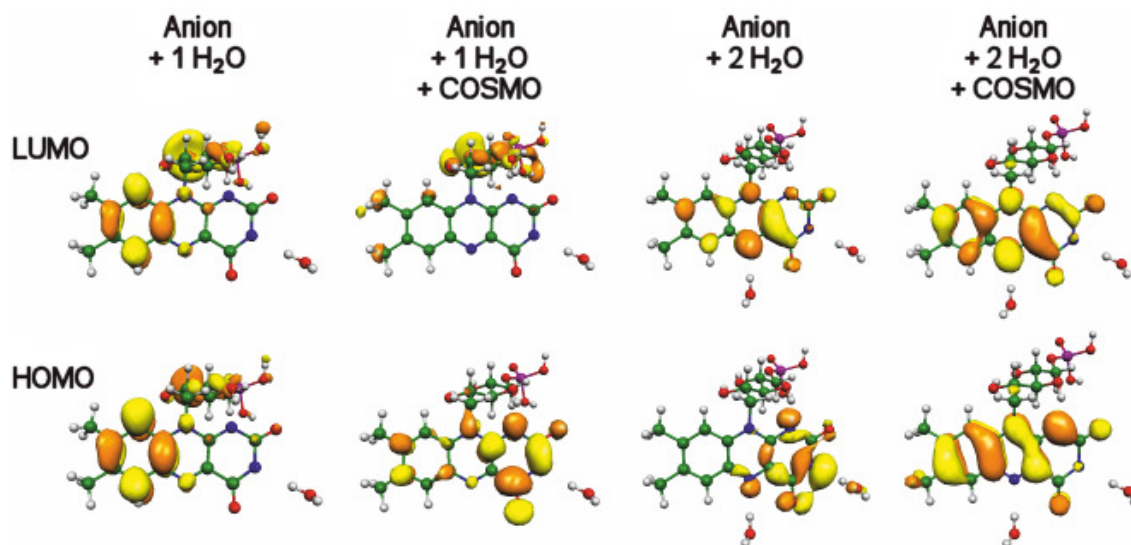


Figure 3-7: HOMO and LUMO for anionic FMN models with one water molecule or two water molecules, with and without taking into account further solvation effect by the COSMO model ($\epsilon = 80$).

The following section contains the examination of the electronic wave function in more detail. The composition of the frontier orbitals was investigated, especially in terms of pH changes. Triplet EPR spectra of FMN at alkaline, neutral and acidic conditions already revealed high similarity and D values change only by 13 %. Hence there is no high sensitivity to pH changes being expected from the HOMO and LUMO. Rather, the lower-lying doubly occupied orbitals are expected to respond more to changes in pH and thereby the protonation state of FMN. Figure 3-8 gives an overview of the doubly occupied molecular orbitals for the models of neutral FMN and the FMN cation, enumerated as LUMO, HOMO – 1 to HOMO – 7. Unlike in previous calculations [83–85] the ribose chain was included here. A certain participation of the side chain in some of the orbitals, especially the HOMO – 4 and HOMO – 6 of the neutral FMN, is noticeable.

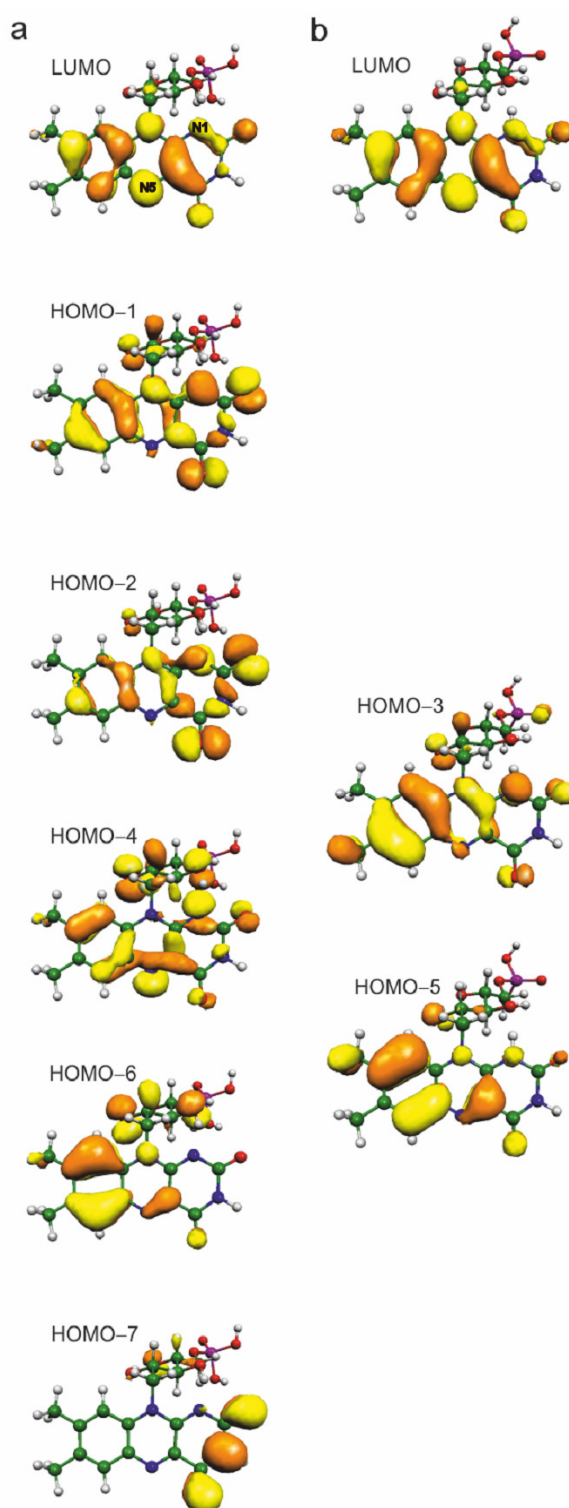


Figure 3-8: Overview of the molecular orbitals of (a) neutral FMN and (b) cationic FMN that are involved in the electronic transitions in the visible range.

The electronic transitions from the TDDFT calculations are listed in Table 3-4.

Table 3-4: Decomposition [%] of the calculated electronic transitions (ET) [nm] of neutral FMN and the FMN cation by TDDFT in terms of single excitations of electrons from doubly occupied orbitals given in Figure 3-8 (vide supra) to the LUMO.

ET [nm]	HOMO -1	HOMO -2	HOMO -3	HOMO -4	HOMO -5	HOMO -6	HOMO -7
	[%]						
FMN neutral							
485	38.3	31.9					
430	10.4	7.4		31.8		25.9	
381	3.8	1.7		5.8		17.1	64.2
375				9.2		42.4	24.1
FMN cation							
395			13.1		54.9		

The information is cut down to the contributions of single excitations, e.g. promotion of an electron from the HOMO – 1 to the LUMO. Generally, π and σ orbitals cannot mix, but since no symmetry constraints are imposed and since symmetry is also formally broken owing to the ribose side chain, π and σ orbitals can mix. The calculations show that the density at N1 of FMN, where the positive charge upon protonation is localized, helps to understand the changes in the UV/VIS spectra with changing pH. For neutral FMN, the HOMO – 1, HOMO – 2 and HOMO – 4 all have large densities at N1. The promotion of an electron from these three orbitals to the LUMO is found to dominate the electronic transitions calculated at 485 and 430 nm. The density at N1 in the LUMO, however, is small and completely absent in the HOMO – 6 and HOMO – 7. The excitations from these two orbitals to the LUMO dominate the calculated transitions at 381 and 375 nm.

Upon lowering the pH, the electronic transitions all come together and give rise to one large band found experimentally at 396 nm and calculated at 395 nm. In other words, the calculated transitions at 485 and 430 nm at neutral pH become blue shifted upon lowering the pH and the ones at 381 and 375 nm become red shifted. This is completely in line with a protonation of N1 upon lowering the pH: the HOMO – 1, HOMO – 2 and HOMO – 4 all become stabilized. The energy gap with the LUMO increases and the electronic transition shifts into the blue. Similarly, the energy of the HOMO – 6 and HOMO – 7 is unaffected by protonation of N1, whereas the LUMO becomes slightly stabilized owing to the small density at N1. The energy gap thus decreases and the electronic transitions shift into the red. Since these doubly occupied orbitals become more degenerate, they also mix. The remaining transitions responsible for the oscillator strength at 395 nm in the FMN cation are derived from electronic excitations from the HOMO – 3 and HOMO – 5 to the LUMO. These orbitals are all π orbitals. Upon comparison, the HOMO – 3 of the cation roughly equals the sum with equal weights of the HOMO – 1 and HOMO – 2 of the neutral FMN and the HOMO – 5 of the cation equals the sum with equal weights of the HOMO – 4 and HOMO – 6 of the neutral FMN. In order to understand the changes in the UV/VIS spectrum upon addition of AgNO_3 , the density at N5 is of critical importance. Experimentally, all bands are red shifted upon addition of AgNO_3 , indicating that the energy gap of the involved orbitals of the electronic transition decreases. Upon inspection of the orbitals for neutral FMN in Figure 3-8, the LUMO is found to have a large density at N5. Of the doubly occupied orbitals, only the HOMO – 4 has significant electron density at N5. Thus, when a positive charge, in this case Ag^+ , binds to N5, the LUMO is dominantly stabilized over the doubly occupied orbitals, and all transitions undergo a bathochromic shift.

In summary, triplet EPR spectra and optical absorption spectra at different pH values in combination with TDDFT calculations reveal that the HOMO and LUMO of FMN are largely unaffected by changes in the protonation state of FMN. Rather, the orbital structure of the lower lying doubly occupied orbitals changes dramatically. Additional EPR experiments have been carried out in the presence of AgNO_3 , which allows the formation of an Ag-FMN triplet state with different zero field splitting parameters and

population and depopulation rates. Addition of AgNO₃ only induces small changes in the optical spectrum, indicating that the Ag⁺ ion only contributes to the ZFS by second order SOC and leaves the orbital structure unaffected.

3.2 Selective production and characterization of LuxAB from *V. fischeri*

A radical intermediate has been proposed for the bacterial bioluminescence reaction, yet there has been no successful approach providing evidence of such an intermediate state. For the investigation of this reaction on an electrochemical level by means of EPR spectroscopy and for kinetic experiments, the genes encoding the luciferase protein from *V. fischeri* were cloned, heterologously expressed in *E. coli* and purified by affinity chromatography. Heterologous expression enables the purification of the desired protein with high yield and exceptionally high purity, which makes it best suited for kinetic and EPR measurements. Additionally, homologous luciferase was purified from *V. fischeri* cells for comparison with heterologous luciferase, to ensure correct function of the heterologous protein.

3.2.1 Heterologous expression of recombinant LuxAB

For cloning experiments the adjacent genes *luxA* and *luxB*, which encode for the heterodimeric bacterial luciferase, were amplified together by means of the PCR method (Figure 3-9), using the mutagenic oligonucleotides *luxAB_Vf7744_for* and *luxAB_Vf7744_rev* (cf. Table 2-7). The GenBank accession number for the nucleotide sequence of the *lux* operon of *V. fischeri* ATCC7744 is AY341062.2. Chromosomal DNA (cDNA), isolated from *V. fischeri* ATCC 7744 cells as described in section 2.6.1, was only stable for approximately 48 h when stored at either 4 °C or –80 °C. Hence, template cDNA was used subsequently after preparation. The primers border nucleotide positions 980 – 3143 (bp) of the *lux* operon and include restriction sites *Bam*HI and *Sal*I, respectively. The annealing temperature was set to 54 °C. In order to reduce secondary structures of the cDNA, which inhibits gene amplification, 5% DMSO was added to the PCR sample.

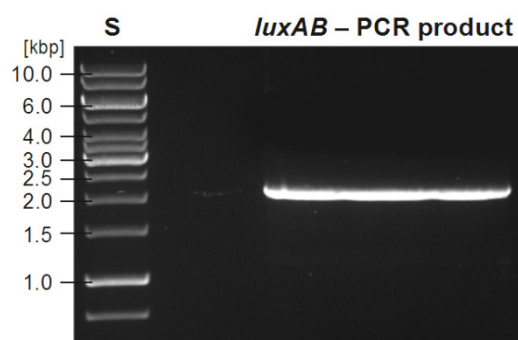


Figure 3-9: Electrophoresis gel of the luciferase gene complex *LuxAB* from *V. fischeri* amplified by PCR. Primers *luxAB_Vf7744_for* and *luxAB_Vf7744_rev* were used to amplify the adjacent genes *luxA* and *luxB* from cDNA with a molecular weight of 2163 Da. MW: molecular weight; S: standard.

LuxAB was cloned into plasmid pPR-IBA2, which was digested with the same restriction enzymes as the PCR product. The created vector was analyzed by DNA sequencing and enzyme digestion with *Hind*III to ensure correct ligation of the *lux* genes and the plasmid matrix. The expression of heterodimeric *LuxAB* from IBA2*luxAB* was performed in *E. coli* BL21 as described in section 2.7.2. Expressed *LuxAB* from this single vector links *LuxA* with a Strep tag II at the N-terminus. Light emission in *E. coli* expression cultures was initiated by the addition of chemically reduced flavin and decanal, resulting in visible luminescence. Hence, active luciferase was expressed successfully. The followed cell disruption and affinity purification are illustrated in sections 2.7.3 and 2.7.4.1. The purity of *LuxAB* was further analyzed by SDS-Page. The expressed luciferase subunits *LuxA*, including the linked Strep tag II, and *LuxB* have molecular weights of 43.2 kDa and 37.3 kDa, respectively. However, SDS-Page only showed very little presence of *LuxAB* with less than 0.2 mg per g cell material. Changes in IPTG concentration and expression temperature did not result in any improvement concerning the luciferase concentration.

As a consequence, a secondary cloning experiment was performed, in which the gene complex *luxAB* was cloned into the vector pPR-IBA1. This constitution resulted in the expression of *LuxAB* with a C-terminal Strep tag II linked to the subunit *LuxB*

(Figure 3-11). This vector was named IBA1*luxAB*. Primers *luxAB_strep_for* and *luxAB_strep2_rev* for gen amplification by PCR were annealed at 56 °C. The latter primer includes the restriction site *Sall*, mutating the *luxB* stop codon for attachment of Strep tag II. The PCR product of the first cloning experiment (*vide supra*) was used as DNA template for this secondary PCR. After heterologous expression and affinity purification, SDS-Page showed a predominantly presence of the expressed protein in the soluble fraction, indicating the accumulation of the protein in the cytoplasm and not in the membrane. The presence of expressed protein in the insoluble fraction was relatively low and may be the result of the accumulation of inclusion bodies during expression. In general, the expression from T7 promotor, like it appears in pPR-IBA1 and pPR-IBA2, results in a very high protein synthesis rate, which enhances the built-up of inclusion bodies [216]. The formation of inclusion bodies in the present study, after the expression with vector IBA1*luxAB*, was insignificantly low. Since their formation could not be positively influenced by the change of expression temperature or IPTG concentration, their presence was neglected. The expressed luciferase subunits LuxA and LuxB, including the linked Strep tag II, have molecular weights of 42.1 kDa and 39.5 kDa, respectively. Resolution of SDS-Page does not enable the separate identification of both subunits with absolute certainty. MALDI spectrometry, however, generally results in distinct signals for individual protein subunits. In this case, it only confirmed the presence of LuxB with a signal at 39.49 kDa. Hence, LuxA was not expressed and the formation of homodimeric LuxAB did not occur.

As a continuing approach, *luxA* was additionally cloned into vector pET-28c and coexpressed with IBA1*luxAB*. Primers *luxA_long_Vf_for* and *luxA_long_Vf_rev* including restriction sites *NcoI* and *Sall*, respectively, were annealed at 51 °C. DNA of the previous cloning experiment was used as PCR template. Figure 3-10 shows the clean PCR product of amplified gene *luxA*. The constructed vector was named pET*luxA* and analyzed by DNA sequencing and restriction using *XhoI*. This vector was used for the expression of the LuxA subunit without tag (Figure 3-11) and a molecular weight of 40.4 kDa.

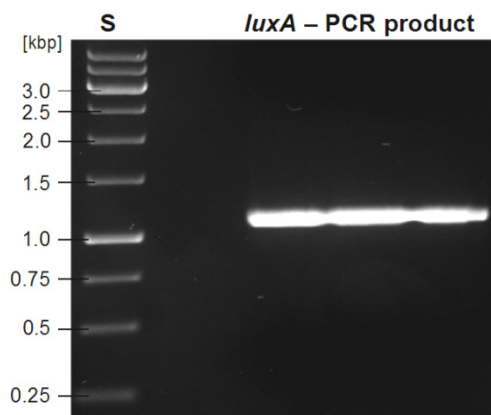


Figure 3-10: Electrophoresis gel of *V. fischeri* luciferase gene *luxA* amplified by PCR. Amplified *luxA* shows a molecular weight of 1120 Da. MW: molecular weight; S: standard.

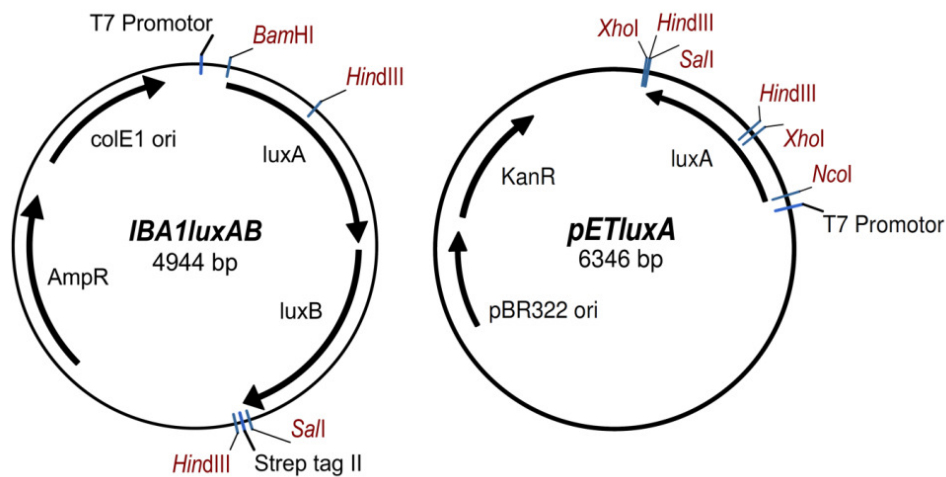


Figure 3-11: Maps of the bacterial luciferase expression vectors. *IBA1luxAB* (left) contains the genes *luxA* and *luxB*, which is linked to the gene for Strep tag II. Vector *pETluxA* (right) contains *luxA*. The included arrows indicate the direction of transcription. AmpR: Ampicillin resistance gene, KanR: Kanamycin resistance gene.

For the simultaneous expression of both vectors, IBA1*luxAB* and pET*luxA*, from the same *E. coli* cell, the following steps were performed: firstly, IBA1*luxAB* was transformed into *E. coli* BL21. These cells were then treated chemically with calcium chloride in order to make them competent again. A secondary transformation with the pET*luxA* vector resulted in *E. coli* cells carrying both vectors. These cells were cultivated in LB medium containing both ampicillin and kanamycin to prevent the loss of the vectors. Using the approach of coexpression, incompatibility of plasmids needed to be considered. Plasmids that contain the same origin of replication, also known as replicon, are thought to be incompatible, since they cannot stably co-exist in the same cell [217–219]. The same origin of replication may lead to competition between the plasmids, in favor of the one with faster replication due to e.g. smaller size, rapidly outgrowing of other plasmids. In this study, the origins of replication in the vectors IBA1*luxAB* and pET*luxA* were *colE1* (replicon *colE1*) and pBR322 (replicon pMB1), respectively, and belong to the same incompatibility group. Though, the same copy number of 15-20 per cell and per cell generation decreases the pressure of competition. Velappen and coworkers found that with plasmids containing the same origin of replication and different antibiotic resistance genes, persistence of all vectors occurs to a significant degree [220]. In this study, the pressure to replicate both vectors during coexpression was sustained by the two different antibiotic resistance genes on each vector. The presence of both vectors was confirmed by restriction analysis with *Hind*III of the isolated vector DNA from cells after expression. Figure 3-12 shows the DNA gel of this restriction fragments.

All fragments of the single digests (lane 2 and 3) of each vector, IBA1*luxAB* and pET*luxA*, can be located in the digest of the isolated DNA from the expressed cells. Hence both vectors were still present and were coexpressed in *E. coli*.

For purification of recombinant protein the harvested cells were disrupted and the protein was isolated by affinity chromatography. LuxAB eluted in all six fractions, as provided by SDS-electrophoresis (Figure 3-13, left). The gel shows a high purity of the two luciferase subunits. LuxA, expressed from pET*luxA*, at 40.4 kDa and LuxB, expressed from IBA1*luxAB*, at 39.5 kDa and a negligible intensity of other proteins.

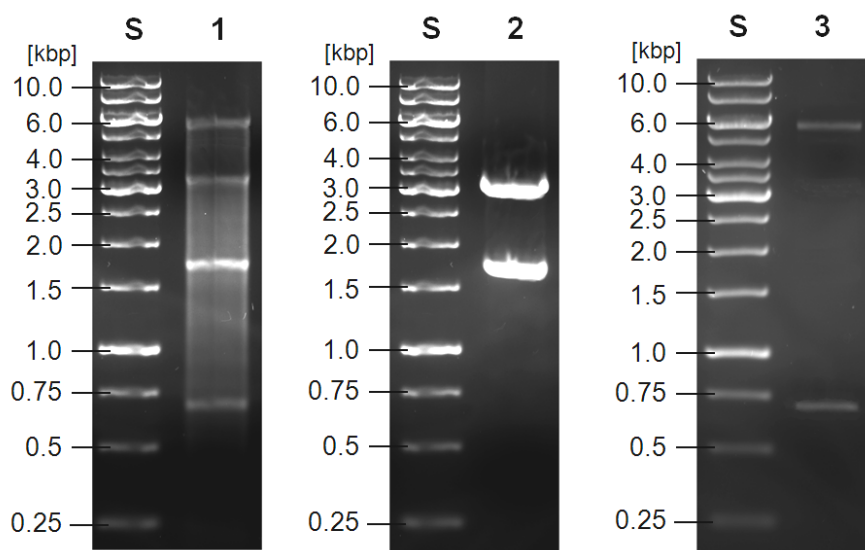


Figure 3-12: Electrophoresis gel of restriction fragments of the vectors IBA1luxAB and pETluxA using HindIII. 1: digest of cell DNA after expression; 2: digest of IBA1luxAB with fragments of 3212 and 1732 Da; 3: digest of pETluxA with fragments of 5670 and 676 Da. MW: molecular weight; S: standard.

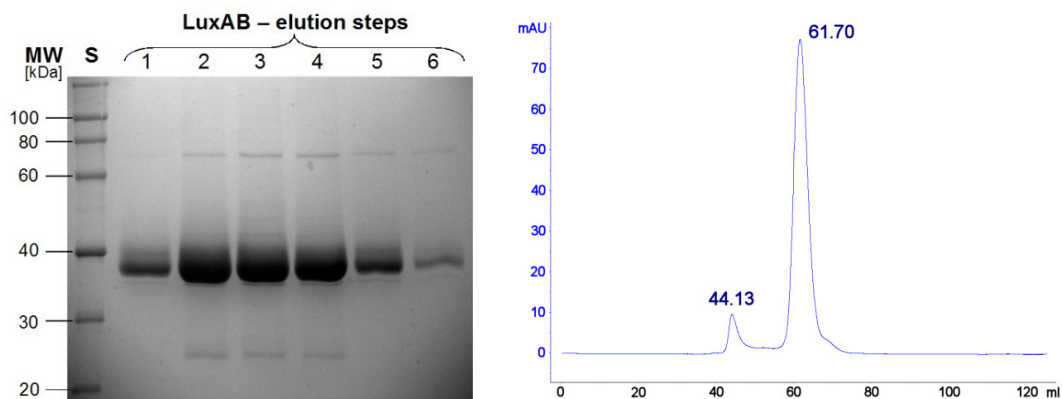


Figure 3-13: Analysis of purified recombinant LuxAB. Left: SDS gel (Coomassie-stained) showing the affinity chromatography elution steps of heterologous, recombinant LuxAB. MW: molecular weight; S: standard. Right: Elution profile of the gel filtration of the heterologous, recombinant LuxAB. mAU: milli Absorption Units (relative units).

Additionally, MALDI-TOF was performed to determine the exact molecular weight of each subunit. The MALDI spectrum in Figure 3-14 displays the presence of both subunits. A possible interpretation of the spectrum is shown as a fitting curve, consisting of four impulses with different maxima. The maximum at 39.43 kDa corresponds with the subunit LuxB and the one at 40.38 kDa corresponds with the subunit LuxA. The maxima at 39.9 kDa and 41.92 kDa are products of peak tailing. Peak tailing to higher molecular weights generally results from multiple cluster formation of the molecules with sodium, potassium or matrix molecules and depends on the modulation of the used laser energy.

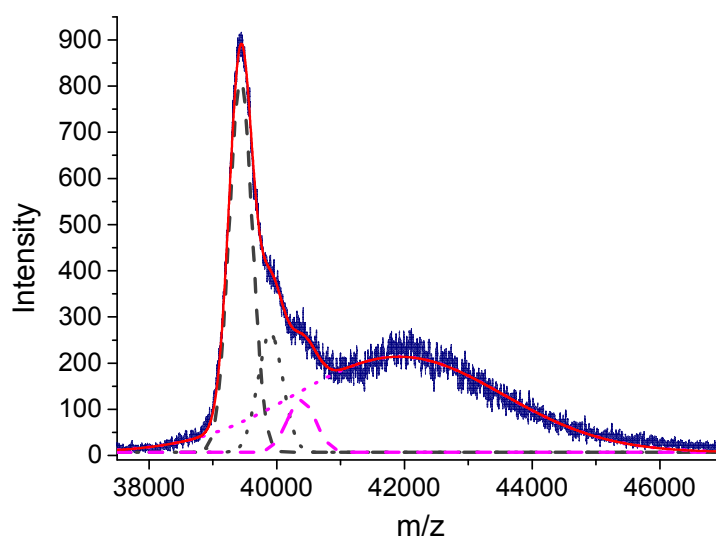


Figure 3-14: MALDI-TOF of heterologous, recombinant LuxAB using a DHAP matrix (blue line). The fit (red line) consists of 4 impulses with maxima at 39.43 kDa (grey dashed line), 39.9 kDa (grey dotted line), 40.38 kDa (pink dashed line) and 41.92 kDa (pink dotted line).

Gel filtration chromatography was additionally carried out in order to determine the molecular weight of the apoprotein. The molecules were separated according to their size as they pass through the gel matrix. The elution of the protein was monitored as absorption at 280 nm. The expressed protein eluted in one clear peak at an elution

volume of 61.70 ml (Figure 3-13, right), which corresponds to a molecular mass of 76.1 kDa. This is in excellent agreement with the expected 79.9 kDa of heterodimeric, recombinant LuxAB. The small deviation of 3.8 kDa is within the range of tolerance of this method. The second absorption peak at 44.13 ml elution volume was present in all gel filtration experiments and can be ascribed to a noise signal of the used chromatographic system. Since mass spectrometry additionally revealed the presence of both subunits, LuxA and LuxB, the heterodimeric protein complex must have formed and was successfully purified. The used Strep tag strategy enabled the purification of up to 2.2 mg protein with very high purity from 1 g cell material.

3.2.2 Homologous purification of LuxAB

Besides the heterologously expressed, recombinant luciferase the native protein was homologously purified from *V. fischeri* cells by means of ion exchange chromatography. Generally, proteins carry both negatively and positively charged groups. The net charge of a protein depends on the applied pH. At its isoelectric point (pI), the net charge of a protein is zero and no binding to any type of ion-exchange gel matrix will occur. The analysis of the *V. fischeri* ATCC 7744 luciferase subunits with the Vector NTI software yielded a pI of 4.92 and a net charge of -13.5 at pH 7.0 for LuxA and a pI of 4.94 and a net charge of -16.2 at pH 7.0 for LuxB. Since LuxA and LuxB are negatively charged at neutral pH, an anion exchanger was used as matrix for the purification of native LuxAB. Anion exchangers dispose different utilities depending on the applied matrix material. DEAE sephadex ion exchanger A-25 is more cross-linked than A-50, which results in a greater rigidity. Therefore A-25 is best suited for small molecules up to 30 kDa, whereas A-50 is best used for proteins in the molecular weight range of 30-100 kDa. LuxAB did not bind to either one of these two sephadex materials, which was derived from luminescence-induced experiments. All luminescent activity was only present in the flowthrough. Compared to DEAE sephadex, which contains a mix of weak and strong anion exchanger particles, Q sepharose is an exclusively strong anion exchanger. Hereby no LuxAB eluted until a phosphate buffer concentration of 600 mM. Besides a very low visual protein activity in the 600 mM elution fraction, all higher buffer concentrations showed no protein

activity whatsoever. The high salt concentration probably led to the inactivation of the protein. DEAE cellulose is a weak anion exchanger and showed the presence of active LuxAB in all elution fractions, including the flowthrough. Hence, Q sepharose and DEAE cellulose were not suited for the purification of native luciferase.

DEAE sepharose showed excellent separation of LuxAB and represented the optimum anion exchanger for the purification of homologous luciferase. The flowthrough and the 150 mM elution fraction with phosphate buffer revealed no luminescence. All luciferase proteins eluted with 450 mM from the column matrix and showed high luminescent activity. However, luciferase only bound unspecifically to the matrix material, which made a complete isolation of luciferase from all other present proteins unlikely. Therefore a determination of the protein concentration would have contained no information about the exact luciferase concentration and was not determined. A secondary purification step was performed by means of ammonium sulfate precipitation. Derived from SDS-Page, the addition of solid ammonium sulfate only led to poorly increased purity of LuxAB. After dialysis over night the purified homologous luciferase was stored until used in fluorescence and EPR experiments.

3.2.3 Optimum activity of LuxAB *in vitro*

The bacterial bioluminescence reaction with reduced flavin as luciferin, aldehyde and molecular oxygen is catalyzed by the luciferase protein. Emission spectra confirmed the activity of the purified, recombinant protein (Figure 3-15). A broad emission spectrum appears from 410 to 650 nm with a maximum at 490 nm.

It is important to note that in all fluorescent measurements the protein was associated with the reduced flavin before addition of the aldehyde, because a partly inhibiting complex can be formed, if the luciferase is first exposed to the aldehyde prior to the flavin [186,187]. Additionally, the binding of FMN results in a structural change of the luciferase protein, protecting the complex from proteolytic inactivation [128,129].

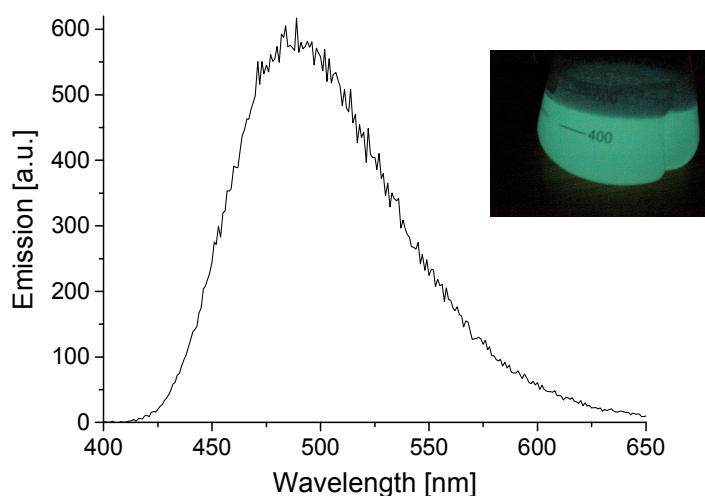


Figure 3-15: Emission spectrum of bacterial bioluminescence with purified recombinant luciferase; reaction was conducted in phosphate buffer pH 7.5 with 1 μM LuxAB, 150 μM FMN, 20 mM $\text{Na}_2\text{S}_2\text{O}_4$, 2 mM octanal. The inset shows a photograph of a luminescent *V. fischeri* culture.

As one product of the bacterial bioluminescence the corresponding acid of the applied aldehyde concentrates in the reaction solution, which results in a continuously decreasing pH. A stable pH during measurements was preserved by the use of adequate buffers. Furthermore, unfolding and denaturing of the protein was inhibited under buffered conditions. Most proteins are stable and most active at pH 7.0 – 8.0, which mimics biological conditions, whereas others are soluble and stable at a broad range of pH, but show changing activity at different pH values, e.g. firefly luciferase. In order to determine conditions for optimum activity of bacterial luciferase the luminescence was detected over a pH range of 5.5 – 9.0. The measurements were performed as described in section 2.8.2 using four different buffers (citrate, phosphate, HEPES, Tris-HCl) to cover a broad buffer range, since every buffer has its own specific buffering capacity. Additionally, the use of at least 100 mM buffer concentration ensured a stable pH, which was confirmed by pH determinations before and after emission measurements. Emission at different pH was monitored at 490 nm, the maximum of the emission

spectrum (cf. Figure 3-15). The emission values after 15 sec are plotted in Figure 3-16. Beyond the lowest emission intensities at pH 5.5 and 9.0, no luminescence was detected. The optimum of the protein activity was observed to be at pH 7.5 in phosphate buffer. Hence all following fluorescence and EPR measurements were performed in phosphate buffer at pH 7.5.

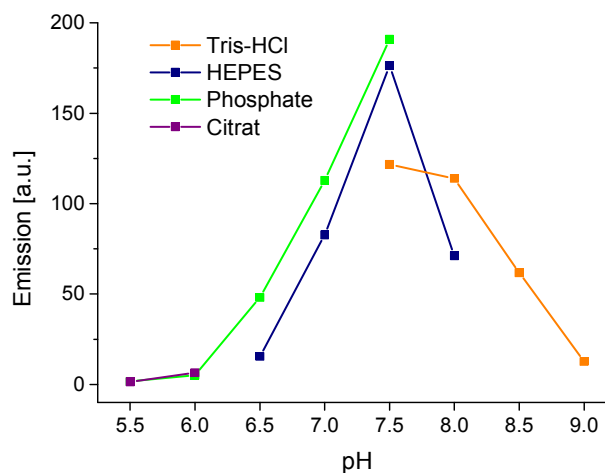


Figure 3-16: pH optimum of recombinant luxAB in vitro; reaction was conducted in different buffers with 1 μM LuxAB, 150 μM FMN, 20 mM $\text{Na}_2\text{S}_2\text{O}_4$, 10 mM acetaldehyde.

In all measurements the aldehyde was previously diluted in water. Aldehydes in aqueous solutions exist as a mixture of the hydrated and unhydrated species [150], which may influence the emission intensity. Hence, the aldehyde was additionally diluted in different ethanol concentrations, in order to increase solubility. However, emission was slightly decreased with ethanol. The same observation holds for the additional use of Tween 20 (Polysorbate 20), which is a non-ionic tenside and often used for oil-in-water emulsions and solubilization of membrane proteins, and Triton X-100 (Octoxinol 9), which is used to stabilize the native conformation of proteins. Henceforth, aldehyde was diluted in water in all measurements. Due to the necessity of O_2 for the bioluminescent reaction the sample was air-bubbled during measurements.

Switching off the gas bubbling led to immediate loss of light emission, which restarted with applied gas flow. The use of pure oxygen resulted in no change of emission intensity, whereas argon displayed a 90 % decreased light emission. A change of bubbling volume to more than 18 ml/min exhibited no change in emission; a lower volume displayed a diminished emission. In summary, the optimum conditions for maximum luciferase activity and the following kinetic measurements were determined to be in phosphate buffer pH 7.5, with water-diluted aldehyde and constant air-bubbling of 18 ml/min flow rate.

3.2.4 Different substrates for bacterial bioluminescence

In order to further validate the activity of the recombinant and homologous luciferases, measurements with different aldehydes were performed. The relative emission values 15 sec after initiation were compared. A threefold determination in random order was performed to ensure reproducibility.

The relative emission values are listed in Table 3-5. For heterologous luciferase, the aldehyde dodecanal induces the highest emission values, followed by decanal with 40 % less emission and octanal with half the emission intensity. Addition of acetaldehyde, the only water-soluble aldehyde in the series, also led to protein activity. Cinnamaldehyde and hydrocinnamaldehyde induced some bioluminescent activity, though at very low levels and likely related to the poor solubility. Activity was absent when vanillin was used. In experiments with homologous luciferase the emission measured in the presence of different aldehydes was approximately the same as for the heterologously expressed protein.

Variations of the flavin substrate in combination with recombinant luciferase were also examined. FAD resulted in a decreased light emission by a factor of ten, whereas RIF even showed no measurable bioluminescence whatsoever (Table 3-6). In all experiments with different aldehydes as well as with different flavins, the wavelength of maximum emission and the shape of the emission spectrum were identical and very similar to the fluorescence emission spectrum of FMN and lumiflavin in solution [221,222], thus confirming the isoalloxazine moiety as the light-emitting species.

Table 3-5: Relative bioluminescent emission, determined 15 sec after initiation at 490 nm for different aldehydes using the sodium dithionite assay.

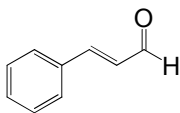
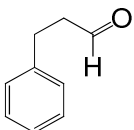
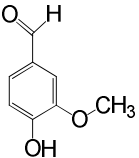
Aldehyde	Emission at 490 nm [%]		
	Heterologous luciferase	Homologous luciferase	
Dodecanal	$\text{CH}_3 (\text{CH}_2)_9 \text{CH}_2 \text{C}(=\text{O})\text{H}$	100	100
Decanal	$\text{CH}_3 (\text{CH}_2)_7 \text{CH}_2 \text{C}(=\text{O})\text{H}$	59	65
Octanal	$\text{CH}_3 (\text{CH}_2)_5 \text{CH}_2 \text{C}(=\text{O})\text{H}$	45	51
Acetaldehyde	$\text{H}_3\text{C}-\text{C}(=\text{O})\text{H}$	14	17
Cinnamaldehyde		6	6
Hydrocinnamaldehyde		2	3
Vanillin		0	0

Table 3-6: Relative bioluminescent emission, determined 15 sec after initiation at 490 nm for different flavins under $\text{Na}_2\text{S}_2\text{O}_4$ conditions and with heterologous protein.

Flavin	Emission at 490 nm [%]
FMN	100
FAD	10
RIF	0

Emission experiments, monitored as scan over 400 – 650 nm at distinct time intervals, additionally showed an increase of emission over time and a shift of maximum emission (Figure 3-17) from 490 to 510 nm after 4.5 min. The change in emission intensity was further analyzed and described in more detail later (section 3.2.5).

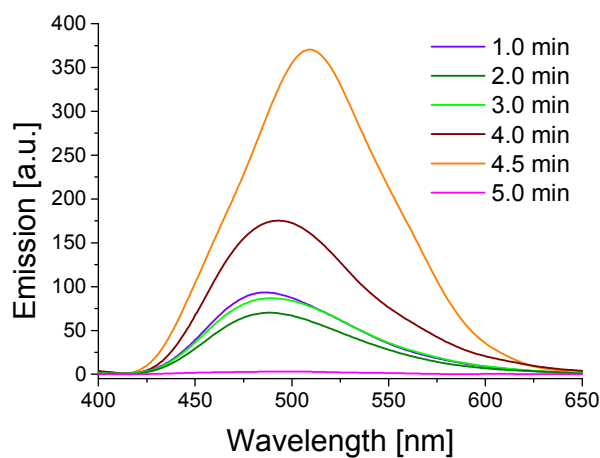


Figure 3-17: Emission scans over 5 min showing the emission shift from 490 to 510 nm (Fourier filtered using the Origin Pro software – original spectra are shown in appendix Figure 0-1). Luminescence was induced with octanal.

The shift of maximum emission was observed at all pH and with different concentrations of different aldehydes or flavins. The maximum shift can be explained by further investigations of oxidized and reduced FMN by means of UV/VIS and

fluorescence spectroscopy. FMN was photochemically reduced in the presence of EDTA using UV light (see section 2.8.1).

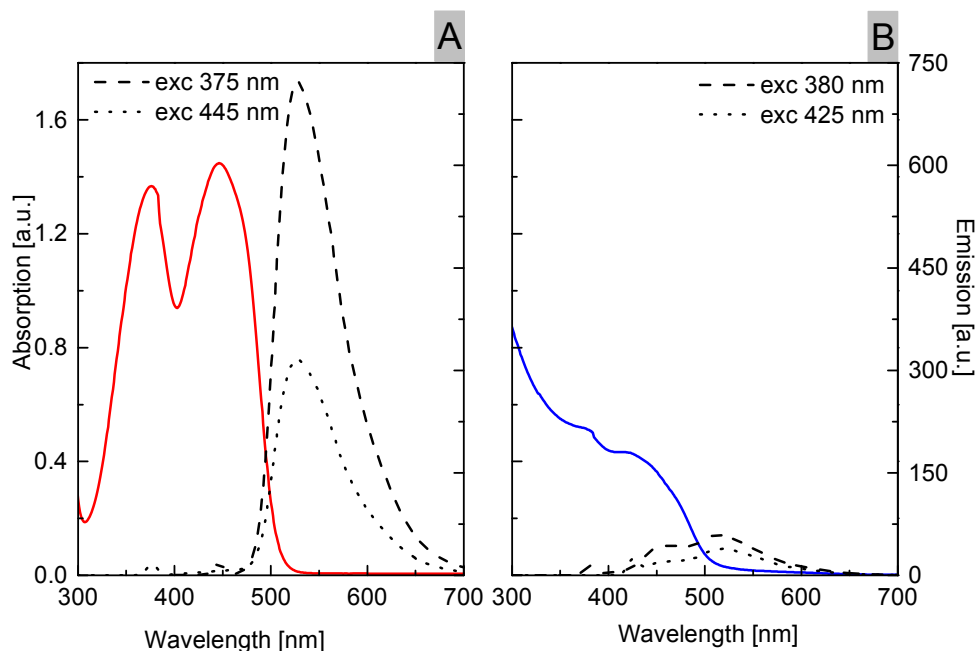


Figure 3-18: UV/VIS (colored) and fluorescence spectra (black) of FMN (A) and FMNH₂ (B).

Oxidized FMN displays the known absorption maxima at 375 and 445 nm in UV/VIS. These maxima wavelengths were used as excitation energies for fluorescence measurements (Figure 3-18, A). Both fluorescence spectra showed a maximum emission at 530 nm, whereas the amplitude of the 375 nm excited spectrum is less than 50 % of the 445 nm excited spectrum. In reduced FMN, the maxima visible in oxidized FMN decrease drastically in amplitude (Figure 3-18, B). Two shoulders remain at 380 nm and 425 nm. The fluorescence spectra at these excitation wavelengths show maximum emissions at 510 nm and shoulders at 465 nm (Figure 3-18, B). Hence the protonation state of the flavin has a major impact on the fluorescence. The shift of maximum emission from 490 to 510 nm during measurements probably originates from the emission of flavin at different protonation states.

3.2.5 Kinetic assays with LuxAB *in vitro*

In the following data, an assay, in which FMN is reduced by dithionite, was used for kinetic measurements. In this assay, the luciferase was incubated with FMNH₂, chemically reduced by sodium dithionite, followed by the rapid injection of aldehyde [223]. A strong dependence of the luminescent reaction regarding the presence of sodium dithionite was noticed. In particular, all chronometric emission curves (Figure 3-19) showed a delay after mixing ($t = 0$) before reaching maximum light emission that depends on the concentration of sodium dithionite (Figure 3-19, A); at a fivefold larger dithionite concentration it took more than five times as long for the point of maximum emission to appear, whereas the amplitude at maximum emission decreased by almost 60 % (Table 3-7). Also the aldehyde concentration affected the time of maximum emission, but in the opposite way. With diminished concentrations the maximum emission was increased (cf. Figure 3-19, B; Table 3-7). The amplitude dropped to 50 % at five-fold reduced aldehyde concentration.

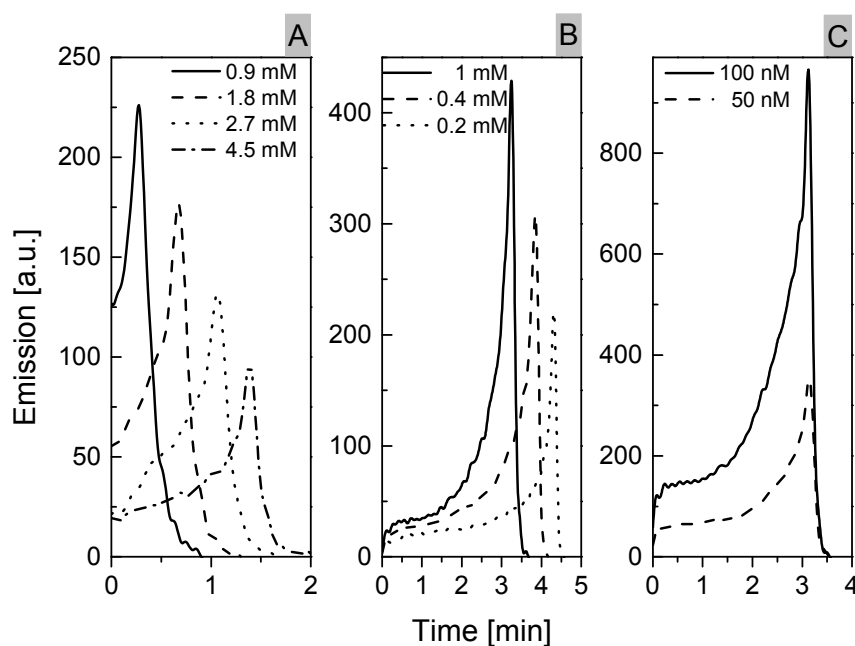


Figure 3-19: Chronometric emission spectra of bacterial bioluminescence at 490 nm with varying concentrations of (A) Na₂S₂O₄: 0.9, 1.8, 2.7, 4.5 mM (0.1 μM luxAB, 25 μM FMN, 260 μM decanal), (B) decanal: 0.2, 0.4, 1 mM (0.5 μM luxAB, 100 μM FMN, 260 μM decanal), (C) luxAB: 100 nM, 50 nM (0.5 μM luxAB, 100 μM FMN, 260 μM decanal).

20 mM Na₂S₂O₄) and (C) luxAB: 0.1, 0.05 μM (100 μM FMN, 20 mM Na₂S₂O₄, 2 mM dodecanal). Spectra are Fourier filtered using the Origin Pro software.

Table 3-7: Values of overall photon emission, amplitude and maximum emission of bacterial bioluminescence at 490 nm with varying concentrations of Na₂S₂O₄, decanal and LuxAB. Emission values were recorded with a time interval of 0.01 min. Values have been determined from spectra that are shown in Figure 3–19.

	Overall photon emission [emission a.u.]	Emission amplitude [emission a.u.]	Time of maximum emission [sec]
Na₂S₂O₄ variation			
0.9 mM	7634	226	15.7
1.8 mM	8586	181	39.7
2.7 mM	7924	132	63.1
4.5 mM	6205	97	82.9
Decanal variation			
1.0 mM	30973	418	195.7
0.4 mM	26526	298	229.3
0.2 mM	17855	213	259.3
Luciferase variation			
100 nM	97429	937	186.7
50 nM	37806	344	186.7

With increasing aldehyde to sodium dithionite ratio, the time of maximum emission occurred earlier. At this time the increased amount of available aldehyde substrate led to

increased luminescence. A change in the luciferase concentration (Figure 3-19, C) did not affect the time of maximum emission, though it did give rise to a drop in the amplitude and the overall photon emission. With a halved luciferase concentration the amplitude of maximum emission dropped to 37 % and the overall photon emission to 39 %. The correlation between increasing luciferase concentration and amplitude of light emission has already been detected for *V. harveyi* [224]. With the results presented here, this correlation can additionally be assigned to the luciferase of *V. fischeri*. Interestingly, all spectra show a sudden break down of emission without having reached a consistent emission plateau.

After completion of the luminescent assay, spin trapping in combination with EPR experiments were performed, which help to explain the strong dependence of the luminescent reaction regarding the presence of sodium dithionite. Samples with sodium dithionite, different aldehydes and DMPO as spin trap revealed the presence of DMPO adducts, characteristically with six signals (Figure 3-20). The spectra containing the aldehydes dodecanal, decanal and octanal are very similar. Two sets of three signals, marked 1 and 2, can be identified with a hyperfine coupling constant of approximately $a_H = 1.6$ mT, whereas the three signals of one set are separated by the hyperfine coupling constant of the nitroxide nitrogen atom of $a_N = 1.5$ mT. For acetaldehyde the spectrum is broader: the signals within each set have a distance of 1.7 mT (a_N) to each other and both sets are separated by 2.3 mT (a_H). The amplitude of the EPR signals is comparable to that for octanal, even though the solubility of the two aldehydes was quite different. DMPO adducts established during oxidation of FMN, visible by the change of color from pale to strong orange. However, adduct signals vanished within the first hour, which prohibited further investigations by mass spectrometry. EPR signals were even present in samples that only contained DMPO, dithionite and the aldehyde. Since the EPR spectra changed with changing identity of the aldehyde, aldehyde radicals must have formed. Thus, dithionite did not only reduce FMN, but also directly reacted with the aldehyde. This side reaction has an unwanted impact on the bioluminescent reaction, visible by the delayed time of maximum emission during kinetic measurements.

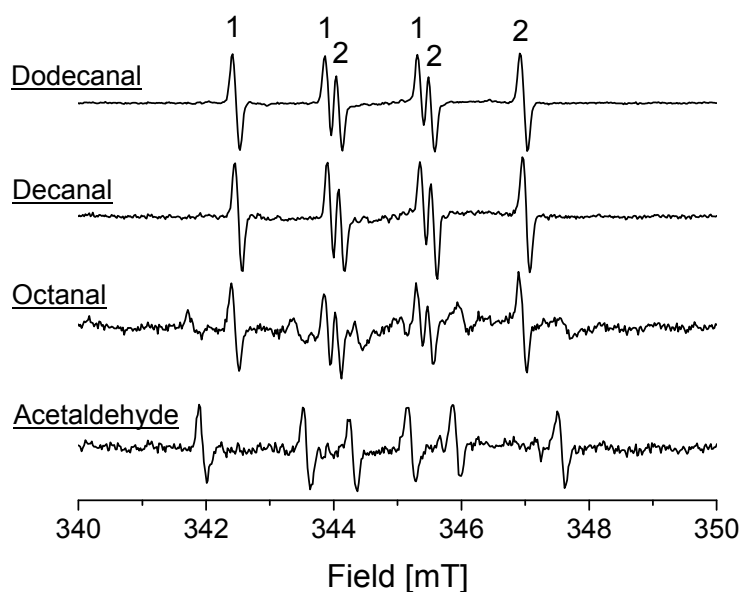


Figure 3-20: CW EPR of DMPO adducts generated by aldehyde radicals.

3.2.6 Radical intermediates in bacterial bioluminescence

In order to examine the presence of radical intermediates during bacterial bioluminescence, spin trapping in combination with EPR spectroscopy was performed. For this series of experiments the FMN was reduced photochemically and not chemically with the above mentioned sodium dithionite. The present study already showed that the presence of dithionite leads to aldehyde radicals, which originate from a side reaction and would adulterate the spin trapping measurements. The photochemical reduction and sample preparation was performed as already described (cf. section 2.8.3.3). DMPO was used as spin trap in all experiments. All samples containing luciferase displayed emission of light in the presence of DMPO. At concentrations of DMPO larger than 20 mM, the protein activity decreased drastically. Therefore the formation of detectable DMPO adducts was limited.

The EPR spectra of formed DMPO adducts are presented in Figure 3-21. The spectra show two sets of signals. The first set displays two groups of three signals and is present

in samples with and without luciferase (Figure 3-21, marked 1 and 2). An additional set of three signals, marked with 3, was present in all samples as well, but with significantly increased amplitude in samples containing luciferase, as indicated in grey. Control experiments without luciferase and with buffer W, in which the purified luciferase was stored, instead of phosphate buffer did not result in the increased formation of grey-marked DMPO adducts. The EPR spectra did not change as different aldehydes were used, except for the amplitude of the signals sets 1 and 2. These signals sets are separated by a hyperfine coupling constant $a_H = 2.2$ mT, whereas the three signals of one set are separated by a hyperfine coupling constant of $a_N = 1.6$ mT. As for the signals marked with 3 the separation between the signals is 1.5 mT.

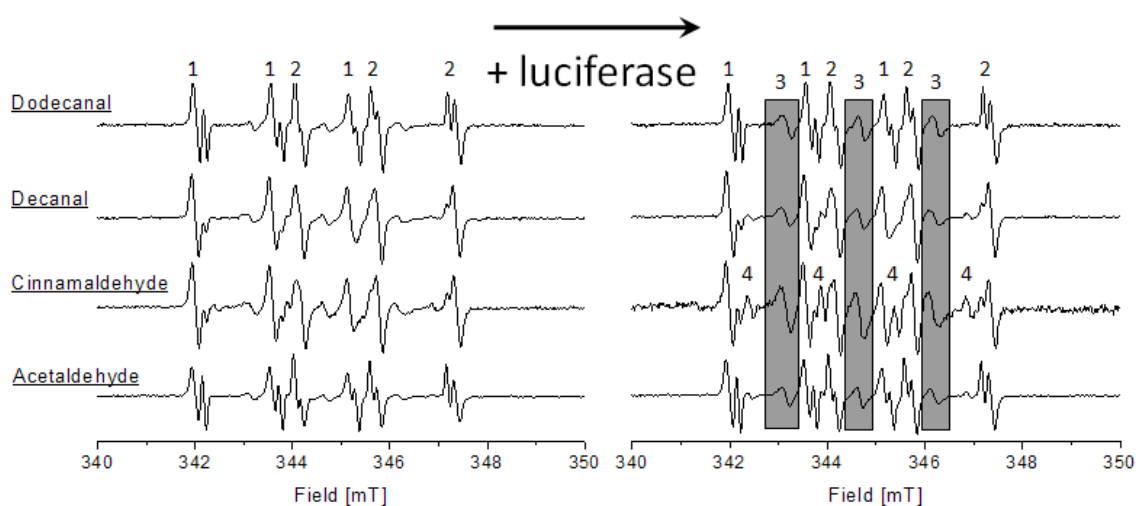


Figure 3-21: EPR spectra of generated DMPO radicals that appear during bioluminescence. Signals that change in the presence of luciferase are highlighted.

In order to elucidate, whether the DMPO adducts originate from EDTA, experiments with another reducing agent for the photoreduction of FMN were performed. During irradiation with UV or blue light the lowest excited triplet state of FMN is generated, which subsequently abstracts electrons from a reducing agent like EDTA or NADH [74,197]. Hence NADH was applied as electron donor for the photoreduction. Experiments resulted in the same DMPO adduct formation as with EDTA (Figure 3-22), thus DMPO adducts do not originate from EDTA radicals. The visual reduction of FMN

(change of color from strong to pale orange) in the presence of NADH during illumination occurred not as quickly as in the presence of EDTA, leading to decreased signals of DMPO adducts. An increase of FMN and EDTA concentrations resulted in incomplete reduction of FMN and did not lead to an increase of EPR signals. Control experiments without illumination or with illumination and without either FMN or EDTA showed no build-up of DMPO adducts. Since the storage buffer of the luciferase, buffer W, contains 1 mM EDTA, a secondary control experiment with buffer W without luciferase was performed, but did not result in the formation of DMPO adducts. This additionally confirms that the DMPO adducts do not originate from EDTA.

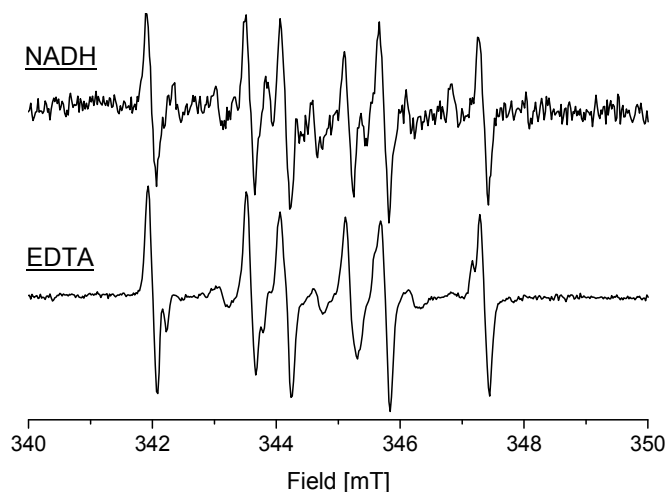


Figure 3-22: CW EPR of DMPO adducts generated in the presence of either NADH or EDTA. Illuminated samples contained 200 μ M FMN, 2 mM decanal, 20 mM DMPO and 8 mM NADH or EDTA.

The signals marked with 3 increase significantly in amplitude when luciferase is present. This increase was analyzed in relation to signal 1 to exclude fluctuation effects of sample preparation, e.g. inconsistent air-bubbling. With increasing luciferase concentration, the amplitude of signal 3 increases relative to signal 1 (Figure 3-23) and even indicates a saturation. The increase of the DMPO adducts thus directly correlates with the protein concentration. Despite the saturation with heterologous protein, the addition of homologous luciferase leads to even larger amplitudes (Figure 3-24).

Here an additional signal set, marked with 4, appears with a separation of 1.5 mT. This signal set was only observed in the sample containing homologous luciferase and the sample containing heterologous luciferase in combination with cinnamaldehyde (Figure 3-21).

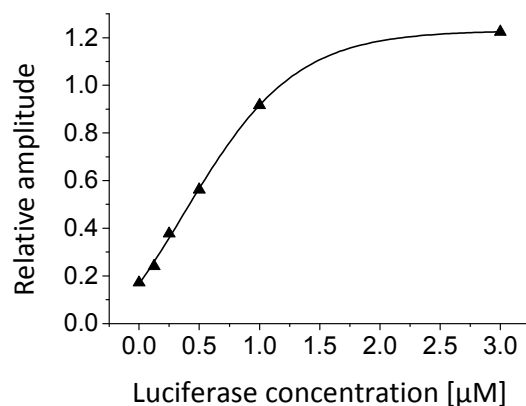


Figure 3-23: Plot of luciferase concentration against DMPO adduct amplitude of signal 3 generated by bioluminescent reaction with dodecanal. These values have been calculated in relation to the amplitude of DMPO adduct signal 1 (cf. Figure 3-24).

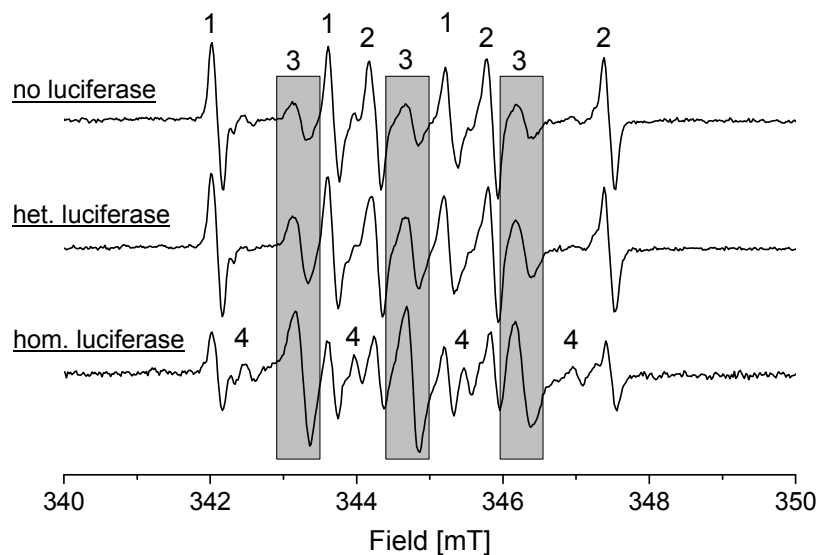


Figure 3-24: EPR of generated DMPO radicals that appear during bioluminescence in the absence of luciferase (upper), catalyzed by heterologous luciferase (middle) and catalyzed by homologous luciferase (lower). Signals that change significantly are highlighted.

DMPO adducts have been further analyzed by mass spectrometry. Here, HEPES buffer was used for sample preparation instead of phosphate buffer, since phosphate buried all signals with higher molecular weights. Apart from that, mass spectrometry samples have been prepared equally and analyzed before and after illumination. Before illumination ESI negative spectra show strong signals for HEPES and EDTA ions. A peak at m/z 455 displays the presence of FMN ($-H^+$) ions (Appendix Figure 0-2). DMPO ions were only detectable in ESI positive spectra at m/z 114 ($+H^+$). After illumination the signals for DMPO and FMN were clearly decreased. The used aldehyde dodecanal is not ESI sensitive and therefore showed no mass peak. However, the concentration of DMPO adducts remains too low for explicit attribution of mass signals to DMPO adducts.

Illumination of some flavins in aqueous solutions can cause photodegradation to the primary photoproducts lumichrome and lumiflavin derivatives. These photoproducts may not function as luminescent substrates. Hence, photodegradation has been analyzed by UV/VIS spectroscopy. FMN was illuminated in the presence of EDTA and DMPO and under the same conditions as performed for EPR samples (cf. section 2.8.3). Figure 3-25 shows absorption spectra before and after illumination.

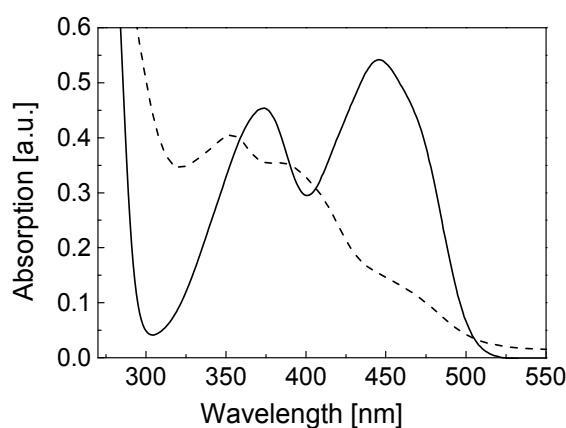


Figure 3-25: UV/VIS spectra of 50 μ M FMN before (solide line) and after (dotted line) air-bubbling and illumination for 20 min additionally containing 2 mM EDTA and 5 mM DMPO.

After illumination the maximum at 375 nm splits into one maximum at 355 nm and a shoulder at 385 nm. The absorption at 445 nm is strongly decreased. The additional presence of aldehyde and luciferase did not lead to a change of spectra. These measurements indicate the degradation of FMN caused by illumination, which may have limited the formation of DMPO adducts in EPR experiments.

3.3 Selective production and characterization of Luc from *P. pyralis*

The chemical reaction of firefly luciferase has been investigated by EPR spectroscopy in combination with spin trapping in order to detect radical intermediates of the reaction. Therefore the *luc* gene from *P. pyralis* was cloned and heterologously expressed in *E. coli*. The recombinant luciferase protein was purified by means of affinity chromatography.

3.3.1 Heterologous expression of recombinant Luc from *P. pyralis*

For the heterologous expression of firefly luciferase, the gene *luc*, which encodes for the monomeric luciferase protein, was cloned into an expression vector. The mutagenic oligonucleotides *luc_for* and *luc_rev* were used for the amplification of *luc* by means of PCR, whereas vector pGEM-*luc* was used as template DNA. The oligonucleotides include restriction sites *Bam*HI and *Sal*I and were annealed at 58 °C. The *luc* gene of 1699 Da was successfully amplified as derived from DNA gel electrophoresis (Figure 3-26). Plasmid pPR-IBA 2 was digested with the same restriction enzymes as the amplified *luc* DNA. *Luc* was then cloned into pPR-IBA2, resulting in a vector named IBA2*luc* (Figure 3-26), which was analyzed by DNA sequencing. An enzyme digest with *Eco*RI ensured the correct ligation of the gene and the plasmid matrix. The created vector was transformed into *E. coli* BL21 for the expression of Luc with N-terminal Strep tag II. Previous cloning experiments including a C-terminal Strep tag II did not lead to successful expression of Luc at any chosen conditions.

The expression and purification steps of Luc were subsequently analyzed by SDS-Page (Figure 3-27). The gel shows the presence of Luc at 63.5 kDa with high purity. The

highest protein yield was achieved with 0.5 mM IPTG induction and an expression at 22 °C for 6 h. Slight changes in expression temperature or IPTG concentration resulted in the formation of inclusion bodies or no heterologous protein expression at all. Luc was purified with up to 2.1 mg protein per g cell material with very high purity.

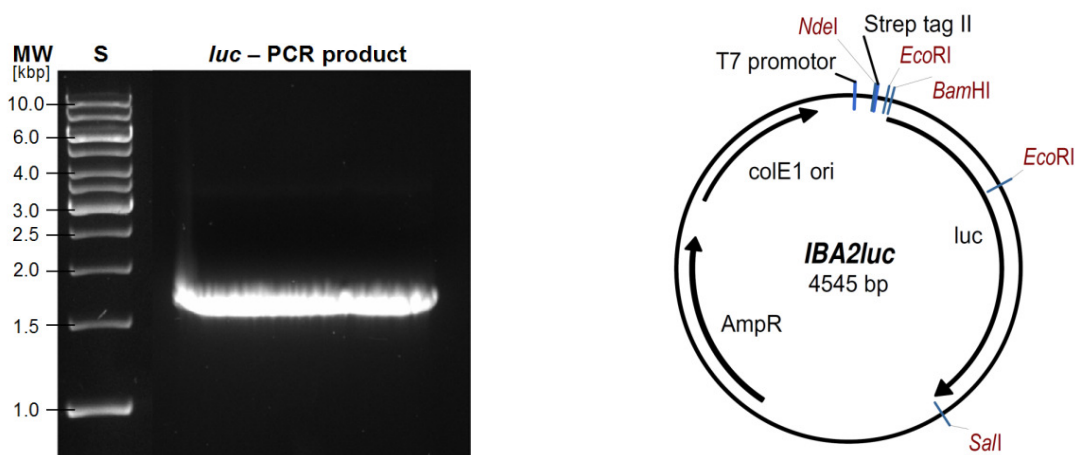


*Figure 3-26: Cloning of luc. Left: Electrophoresis gel of *P. pyralis* luciferase gene *luc* amplified by PCR. Primers *fireluc_for* and *fireluc_rev* were used to amplify the *luc* gene with a molecular weight (MW) of 1699 Da; S: standard. Right: Vector map of the constructed IBA2luc vector for heterologous expression of the *P. pyralis* luciferase with N-terminal Strep tag II in *E. coli* BL21. Luc was cloned into pPR-IBA2 using restriction sites *Bam*HI and *Sall*. AmpR: ampicillin resistance gene; *colE1 ori*: origin of replication.*

Additionally, gel filtration was performed to determine the exact molecular mass of Luc and to detect any oligomerization of the protein. Superdex 75 matrix was used for gel filtration and the elution of the protein was monitored as absorption at 280 nm. Luc eluted in one distinct absorption peak at an elution volume of 65.56 ml (Figure 3-27). This volume corresponds to a molecular mass of 59.2 kDa, which is in good agreement with the expected 63.5 kDa. The absorption peak at 44.57 ml elution volume can be ascribed to a noise signal of the used chromatographic system. Since no other

significant absorption peak appeared in the elution spectrum, multimerization of Luc can be excluded.

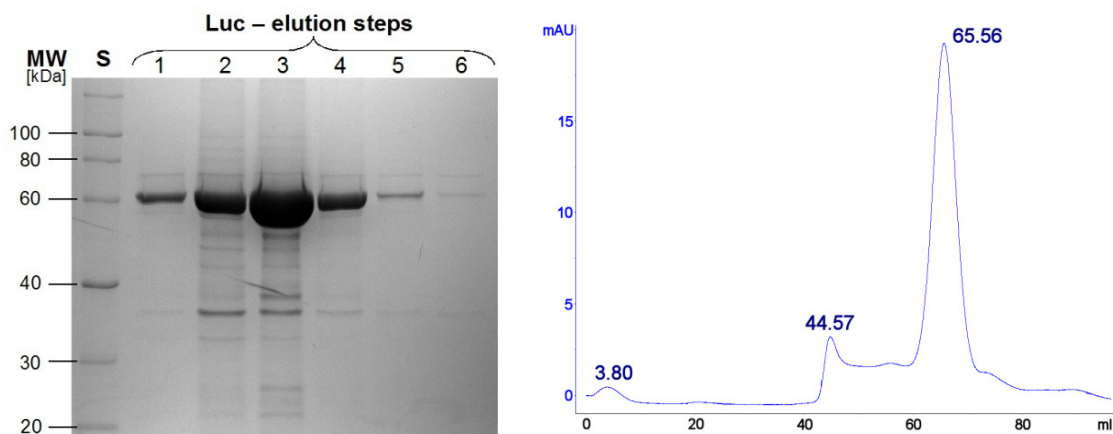
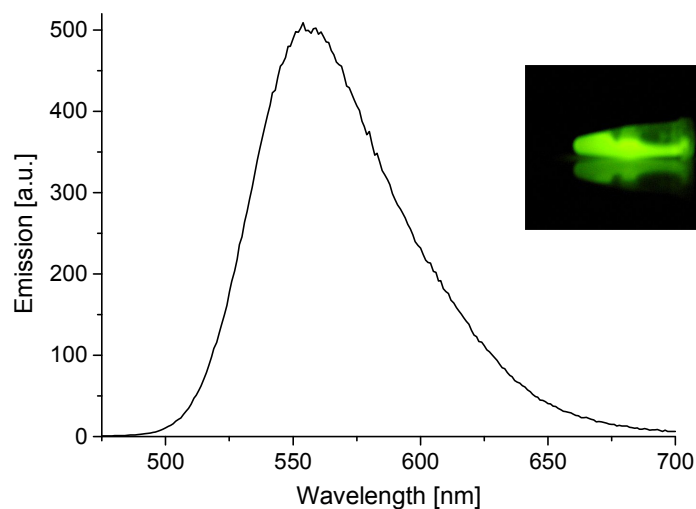


Figure 3-27: Analysis of purified Luc. Left: SDS gel (Coomassie-stained), showing the affinity chromatography elution steps of heterologous, recombinant Luc. MW: molecular weight; S: standard. Right: Elution profile of the gel filtration of heterologous, recombinant Luc. mAU: milli Absorption Units (relative units).

In the reaction of firefly bioluminescence the luciferin is oxidized in the presence of ATP and Mg^{2+} by molecular oxygen. Luminescence was recorded at pH 8.0 with heterologously expressed recombinant Luc (Figure 3-28). The spectrum shows a broad, asymmetric emission peak from 490 to 700 nm with a maximum at 555 nm. According to McElroy and Seliger [169] the highest quantum yields of *P. pyralis* luciferase can be observed at pH 8.0 or higher, resulting in the emission of yellow-green light. Hence the optimum buffer conditions for recombinant Luc in this study was tested for pH ≥ 7.5 . The emission maximum did not show any shift under pH conditions ≥ 7.5 . Tris-HCl, HEPES and phosphate buffer were tested within their corresponding buffer range. The maximum emission was achieved in Tris-HCl at pH 8.0.



*Figure 3-28: Emission spectrum of firefly bioluminescence with purified recombinant luciferase; luminescence was induced in Tris-HCl buffer pH 8.0 with 0.5 μM Luc, 100 μM luciferin, 250 μM ATP, 5 mM MgCl_2 . The inset shows a photograph of induced luminescence in *E. coli* expression culture in a lying reaction tube.*

3.3.2 No radical intermediate detected

In order to detect radical intermediates during the bioluminescent reaction of fireflies, the light emitting reaction was induced in the presence of the spin trapping agent DMPO. In the presence of MgCl_2 the luciferase catalyzes the emission of light. D-luciferin is decarboxylated as ATP gets dephosphorylated and forms an AMP derivative of luciferin. After the subsequent reaction with molecular oxygen the molecule decomposes under the emission of light. CW EPR measurements of the prepared spin trapping samples in Tris-HCl pH 8.0, however, did not show any presence of DMPO adducts. Therefore no further information can be derived using this method.

4 Discussion

4.1 Electronic structure of the lowest triplet state of bacterial luciferin

One main aim of the present work was the characterization of electronic structure of the bacterial luciferin, FMN. It has been investigated at different protonation states and in the presence of AgNO_3 by UV/VIS spectroscopy, EPR spectroscopy of the light-induced triplet state and by DFT and TDDFT calculations. Studies on photoexcited triplet states of FMN are not easy to accomplish due to the low spin polarization of the excited triplet state and the exceeding long lifetime of one of the triplet sublevels of 100 ms, which results in very time-consuming measurements [96]. By the addition of silver nitrate in this study, the ISC has been successfully enhanced and the triplet lifetimes decreased simultaneously by increasing the SOC interaction. Since SOC becomes larger for heavier atoms, the introduction of such atoms causes the following: (1) the absolute triplet yield is increased, since ISC more effectively competes with radiative and non-radiative decay of the singlet excited state; (2) the triplet lifetime is decreased to the microsecond range, which makes it more accessible for measurements; (3) the spin polarization of the triplet state is increased. Indeed, in liquid solutions, Ag^+ , Tl^+ , Ni^+ , Co^{2+} , Tb^{3+} , Sm^{3+} and Dy^{3+} were all found to significantly enhance ISC of organic chromophores and thereby act as triplet sensitizers [225–228]. For FMN, the binding of heavy atoms and in particular the concomitant fluorescence quenching is known as well [211,212,229,230]. In this study, an enhancement is achieved for frozen solutions of FMN in the presence of highly soluble AgNO_3 , though at the expense of high concentrations of the latter. A significant change of the polarization pattern was observed as well as a change in the triplet lifetimes. The signal amplitude, however, still remains too low for ENDOR experiments of the triplet state of FMN and for direct examination of the hyperfine coupling constants of the nitrogen atoms and the protons of FMN.

The UV/VIS spectrum of FMN at high pH shows bands at 355 and 450 nm. The calculated electron transition are in somewhat poor agreement with experiment,

indicating that the simple model of an FMN anion with a Na^+ counterion for the high pH case does not yet capture all interactions with the environment that influence the electronic structure. The UV/VIS maxima change with decreasing pH in such a way that they come together and give rise to one strong band at 397 nm. This observation of pH dependency is very consistent with the findings of Beinert [81], Nakamura [82] and Drössler [231] for riboflavin. Compared to riboflavin, the remaining absorption at about 400 nm at acidic conditions is more narrow and intense in case of FMN. The changes with pH in the UV/VIS spectrum have been ascribed to a protonation of nitrogen atom N1 (cf. Figure 3-5), which stabilizes all orbitals that carry $2p_z$ density at N1. Upon addition of AgNO_3 , all bands in the spectrum display a bathochromic shift. This occurrence has been attributed to the coordination of Ag^+ to nitrogen atom N5, which stabilizes the LUMO. The appearance of a band at wavelengths longer than 500 nm after the addition of AgNO_3 has been observed before and has been extensively studied by Baarda and Metzler [212]. They assign the band at 520 nm to the formation of a complex and ascribe the appearance of red color to an Ag-FMN adduct, containing one or possibly two Ag^+ ions bound to FMN. Centrifugation experiments with varying incubation times led to the conclusion that the red-shifted absorption derives from Ag-FMN complexes with a high degree of polymerization [212]. Under conditions of AgNO_3 in excess, as used here, the observation of a yellow color suggests that monomeric Ag-FMN complexes may be present. This is further concluded from the observation that the UV/VIS spectra are highly similar to that of FMN without AgNO_3 , whereas the polymerized complex displays an absorption maximum at 400 nm [212]. Given that the red complex resembles the absorption spectrum of an FMN radical, the formation of a diradical Ag^{2+} -FMN complex was suggested [211]. EPR measurements, however, were not able to confirm the existence of such a species at large AgNO_3 concentrations. Bamberg and Hemmerich furthermore argue that the bathochromic shift in the UV/VIS spectra of the flavin is not restricted to the presence of silver salts, but is also characteristic for copper(I) and mercury ions or basically for all d^{10} ions with a small energy difference between d^9s^1 and d^{10} electronic configurations [211]. They ascribe the red shifted complex to being a chelated trigonal complex, in which the metal binds to N5, the neighboring keto-oxygen atom and one solvent molecule.

The ZFS parameters, on the other hand, change only slightly upon pH change, which can be explained by a HOMO and LUMO that remain virtually the same upon pH change. However, the doubly occupied orbitals that are lower in energy react stronger to pH change, in particular, the first six doubly occupied orbitals directly below the HOMO.

For the FMN anion, the calculated HOMO and LUMO change considerably depending on how the excess anionic charge is stabilized. Interestingly, not only the isoalloxazine moiety contributes, but also the ribose chain. Apparently, some ribose orbitals are similar in energy to the isoalloxazine orbitals. The addition of explicit two water molecules and incorporation of a COSMO salvation model resulted in a frontier orbital structure as found for pH neutral conditions. These findings confirm earlier observations that environmental effects have a large influence on the electronic structure of FMN [63,85] and that the simplest model seems to be one where the negative charge is explicitly stabilized by a sodium counterion. Since light excitation in flavins induces phosphorylation processes in phototropins [232], it is tempting to speculate that the excitation may be transferred from the aromatic part to the ribose chain and the phosphate group in this way.

The calculated ZFS parameters D for high and low pH cases are larger than at neutral conditions, which was also observed in experiment. This indicates that the interaction of FMN with its environment in the form of hydrogen bonds slightly affects the frontier orbitals of the aromatic part of the molecule. At high pH the width of the Q-band EPR spectrum of FMN, and therefore the ZFS parameter D , is smaller ($D = 541 \cdot 10^{-4} \text{ cm}^{-1}$) than at low pH ($D = 603 \cdot 10^{-4} \text{ cm}^{-1}$), indicating that the effective distance between the triplet electrons is largest at high pH. The change of the effective distance is a direct consequence of slightly changed frontier orbitals of the isoalloxazine moiety depending on the protonation state of the isoalloxazine moiety. Compared to the values recorded at X-band by Kowalczyk and coworkers [96], who determined $D = 565 \cdot 10^{-4} \text{ cm}^{-1}$ at high pH and $D = 629 \cdot 10^{-4} \text{ cm}^{-1}$ at low pH, the values derived from the X-band spectra are systematically larger by about $25 \cdot 10^{-4} \text{ cm}^{-1}$. The reason is hyperfine broadening of

about 60 MHz (cf. section 3.1.2), to which the X-band spectra are much more sensitive than the Q-band spectra. Upon addition of AgNO_3 , the simulated ZFS parameters D and E slightly increase, owing to a contribution by SOC of Ag^+ . The altered SOC is directly visible in the EPR spectrum, since the polarization pattern has changed (EAEAEA) compared to the spectrum of neutral FMN (EEEAAA). The D and E parameters are furthermore similar to those observed by Kowalczyk and coworkers [96] and are characteristic for an organic triplet state with basically no spin density at silver. Upon exchange of H_2O to D_2O , the widths of the spectra remain the same, indicating that the line width is not dominated by unresolved ^1H hyperfine interaction.

4.2 Purification and optimum activity conditions of bacterial luciferase

The main aim of the present work was to gain further insights into the reaction of bacterial bioluminescence. Therefore the catalyzing protein of this reaction, LuxAB, was homologously purified from *V. fischeri* as well as recombinantly expressed in *E. coli*. The heterologous expression of a bacterial protein is best performed in a bacterial expression environment. The labeling of proteins for affinity purification, however, as performed here with Strep tag II, can influence protein folding and accordingly cause lowering or even inhibition of the expressed protein activity [233–235]. The first expression strategy in this study included the linkage of the Strep tag to the N-terminus of LuxA. Even though strong light emission could be induced in *E. coli* expression cultures, only a small amount of the luciferase could be purified by chromatography. However, both subunits must have been successfully expressed here and must have formed the active, homodimeric LuxAB apoprotein, since only the heterodimer shows biologically significant activity [121]. The three-dimensional structure of luciferase from *V. harveyi* shows an extensively close packing of the $\alpha 2$ helices from each subunit, which are involved in the formation of the dimer interface [119]. The $\alpha 2$ helices are located close to the N-terminus in both subunits. These structural results can be assigned to luciferase of *V. fischeri*, since the LuxA subunits of *V. harveyi* and *V. fischeri* are homologous in this region, confirmed by amino acid sequence analysis of the N-termini [113]. Hence, the accessibility of the N-terminal

Strep tag for chromatographic purification was probably prohibited by protein folding and dimer formation of LuxAB.

The second cloning strategy resulted in the expression of LuxAB with a C-terminal linkage of the Strep tag to LuxB (vector IBA1*luxAB*). The adherence of the tag at this end of the protein holds one advantage compared to the linkage of the tag at the N-terminus. An N-terminal tag ensures no complete protein expression, since even the aborted expressions result in tagged protein moieties, which are purified by chromatography. The purified proteins with C-terminal tag can be assumed to be expressed completely, whereas proteins derived from aborted expression possess no tag and are not purified by chromatography. Induced luminescence in expression cultures of *E. coli* with IBA1*luxAB* only resulted in weak light emission. The formation of heterodimeric LuxAB was questionable, since mass spectra showed only the presence of LuxB. Moreover, though the heterodimer LuxAB is the preferred product with respect to kinetic observation [236,237], LuxB was shown to be able to form a weakly luminescent homodimer [238]. The coexpression of LuxA (vector pET*luxA*) finally led to the formation of heterodimeric LuxAB, as shown by intense luminescence in light-induced *E. coli* expression cells and mass spectrometry. The presence of peak tailing products in the MALDI spectrum can be attributed to multiple cluster formation of the subunits with sodium, potassium or matrix molecules. Moreover, the broad tail associated with LuxA (cf. Figure 3-14) probably results from different conformational states of the subunit. Compared to LuxB, LuxA is known to run through conformational changes due to substrate binding in the active center [239,240].

The optimum activity of bacterial luciferases differs for different species. Luciferase from the terrestrial bacterium *Photobacterium luminescens* is strikingly heat stable, compared to other bacterial luciferases, with a maximum activity at about 40 °C [241]. Since Tyulkova and Sandalova determined a maximum activity for the *V. fischeri* luciferase at 28 - 30 °C [242], kinetic experiments in this study with luciferase from *V. fischeri* were performed at RT. During kinetic assays with heterologous luciferase in this study a shift of maximum emission from 490 to 510 nm during measurements has been observed. With FMN being the excited emitter in bacterial bioluminescence

[42], this emission shift probably originates from the emission of flavin at different protonation states. The photons, which are emitted by the bioluminescent reaction, excite other flavin molecules in the sample. The simultaneous emission of photons by both excited flavin species results in an emission shift during bioluminescent measurements.

4.3 Affinity for different substrates

It is well known that bacterial bioluminescence is visible only in the presence of a second substrate, a long chain aliphatic aldehyde, such as nonanal, octanal and decanal. These aldehydes are oxygenated into their corresponding carboxylic acid [108]. The present study shows that in *V. fischeri* even acetaldehyde causes luminescence. The aldehyde group thus seems to be the active part involved in the reaction. The aliphatic chain, however, has a large influence on the intensity, since maximum light emission increases with extending chain length, in native as well as in recombinant protein.

The emission kinetics of bacterial bioluminescence has been investigated until now using mainly the luciferase from *V. harveyi*. The recombinant luciferase from this bacterium displayed tenfold higher specific activity for nonanal and decanal than for octanal, undecanal and dodecanal [121,131]. In contrast, measurements in the present study for luciferase from *V. fischeri* yielded a little less than two times more activity for dodecanal than for decanal (cf. Table 3-5). Hence, concerning the chain length of the aldehyde substrate, the activity of recombinant luciferases from different organisms differs drastically. Moreover, for *V. harveyi* the maximum light emission does not increase with extending chain length as shown for *V. fischeri* in the present study. The activity of homologous luciferase from *V. fischeri* with octanal and dodecanal has been reported to be the same [243], whereas this study shows about two times less activity for octanal than for dodecanal. Hence, even for the luciferase of the same organism, the activity ratios concerning the aldehyde chain length obviously vary for different studies and need to be carefully compared. Experiments with mutants from MAV, a luminous bacterium described by Hastings [243], revealed that the activity with decanal in mutant AK-20 with a S227F mutation is approximately half of that for dodecanal [244], similar

to the heterologous luciferase from *V. fischeri*. The activity with octanal in this mutant is 2.3 times larger than that for dodecanal. The wild-type MAV protein, however, shows a ten times larger activity for decanal compared to octanal and dodecanal. Despite the fact that many mutations of the luciferase protein have been investigated that result in a change in correlation of activity and the aldehyde chain-length, an explanation on a molecular level still has not yet been formulated [245,246]. Additionally, the structure of the aldehyde has an impact. Cinnamaldehyde, hydrocinnamaldehyde and vanillin possess an aromatic moiety close to the aldehyde group. Cinnamaldehyde and hydrocinnamaldehyde induce weak luminescence, whereas with vanillin no light emission was observed, most likely due to steric effects. Steric analysis, however, is hindered by the fact that no crystal structure of a protein with bound aldehyde is available. Presumably, the aldehyde becomes more strongly bound to the enzyme as the carbon chain length in the aldehyde increases and as it becomes more hydrophobic, since the hydrophobic groups of the luciferase determine the affinity of the aldehyde [30,247].

With regard to the identity of the flavin substrate, FMN and FAD lead to luminescence, whereas riboflavin did not. FAD, which has an additional AMP, only inhibits the light emission partly. This indicates that the phosphate group, that is absent in riboflavin, seems to be important for the enzymatic process, either on an electronic level or sterically for the binding to the luciferase itself. The affinity for the flavin molecule seems to be connected to the activity of the luciferase. The dissociation constant of the flavin-luciferase complex in *V. fischeri* has been reported to be 60 times higher for riboflavin than for FMN [248]. The activity of riboflavin is only 0.5 % of that for FMN. The dissociation constants for flavin vary in different bacteria. In *Photobacterium phosphoreum* the dissociation constant for the binding of reduced FMN is reported to be 0.6 μM , for *V. harveyi* 0.3 μM and for *V. fischeri* even 10 μM [249]. Flavins with negatively charged side chains, such as FMN and FAD, lead to higher fluorescent yields and are bound more tightly to the protein. Flavins with an uncharged side chain, e.g. those without phosphate residues like riboflavin, do not bind as tightly to the luciferase as FMN and FAD [250,251]. Lin and coworkers present a detailed study on

the steric binding of FMN in *V. harveyi* luciferase [252]. The isoalloxazine moiety of FMN binds with the alanine 74-75 (A74, A75) *cis*-peptide bond and with the cysteine 106 (C106) side chain in the α subunit (Figure 4-1). The phosphate moiety of the FMN forms seven intermolecular hydrogen-bonds with the LuxA subunit. Three bonds are formed with the guanidinium moiety of arginine 107 (R107), two bonds are linked to the NH groups of glutamate 175 (E175) and serine 176 (S176), respectively. The last two bonds are formed with the hydroxyl groups of serine 176 and threonine 179 (T179) [252]. The manifold linkage between the phosphate moiety and the luciferase is obligatory for the luminescent reaction, which becomes apparent when riboflavin is used as substrate and no light emission occurs.

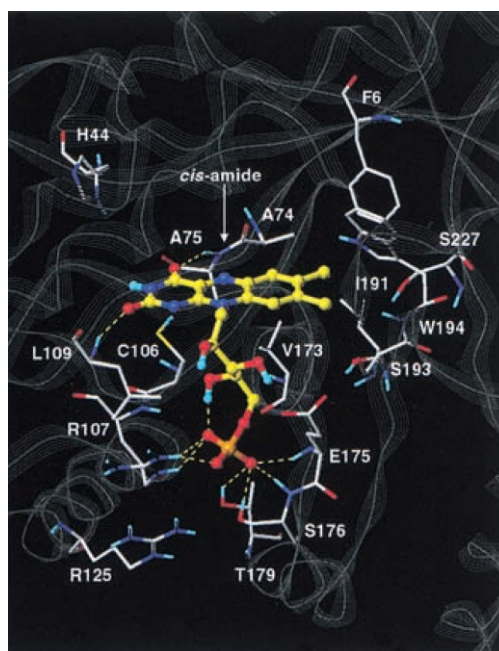


Figure 4-1: Modeled complex of the α subunit of bacterial luciferase with bound FMN. The protein is shown as grey line-ribbon. Selected and involved protein residues are labeled and plotted as capped-sticks. Formed inter- and intramolecular hydrogen bonds between FMN and luciferase are displayed in yellow dashed lines [252].

4.4 Kinetic assays in vitro; aldehyde radicals and dithionite

In the reaction of bacterial bioluminescence reduced flavin reacts with molecular oxygen and an aldehyde, resulting in the emission of photons. The amount of emitted photons during bioluminescence provides direct information about the activity of the catalyzing protein. Two commonly used assay methods have been established for the quantification of the kinetics of the bacterial luciferase. In the first assay, the luciferase is incubated with the aldehyde and the luminescent reaction is started by the rapid injection of photochemically reduced FMNH₂ [253,254]. Lei and coworkers showed that enzyme-binding of the aldehyde prior to FMNH₂ inhibits the reaction partly [186]. High concentrations of dodecanal were shown to inhibit the luminescence in MAV strongly and slightly in *V. fischeri* [243], which makes the first method unsuitable for the determination of rate constants. In the second assay, FMN is reduced chemically with sodium dithionite and subsequently incubated with luciferase, which leads to light emission almost twice as large as in the first assay. However, sodium dithionite is known to react with aldehydes and ketones in aqueous solutions [255]. At high temperatures, aldehydes are reduced to the corresponding alcohol, whereas at RT the reaction can lead to α -hydroxy sulfinates. For instance, the ratio of benzaldehyde and benzyl alcohol at room temperature was determined to be 35/65 [255], since the formation of an α -hydroxy sulfinate is reversible [256]. Owing to these additional reaction pathways for the aldehyde, the availability of aldehyde for the luminescent reaction is considerably decreased in the presence of sodium dithionite in the second assay, which explains the observed initial delay in light emission. While the dithionite is being used up to reduce FMN, the equilibrium of the aldehyde-sulfinate reaction shifts and more aldehyde becomes available for the luminescent reaction. Then, after depletion of dithionite, FMN is no longer reduced to FMNH₂, resulting in a sudden breakdown of bioluminescence. Since dithionite both reduces FMN and reacts with aldehydes in an equilibrium reaction, the dithionite concentration largely determines the time resolved emission characteristics.

The reaction of dithionite with aldehyde has been shown in the present study by means of spin trapping. The presence of aldehyde-originated DMPO adducts in samples that

only contained the aldehyde, DMPO and sodium dithionite, without FMN, can be explained as follows. $S_2O_4^{2-}$ is known to disproportionate into two $SO_2^{\bullet-}$ radicals. It was found that SO_2 spin adducts are not detectable using DMPO with sodium dithionite [257,258]. As schematized in Figure 4-2, $SO_2^{\bullet-}$ can react with an aldehyde resulting in the formation of α -hydroxy sulfinate with a radical intermediate and the radical being located at the α -carbon as suggested by de Vries and Kellogg [255].

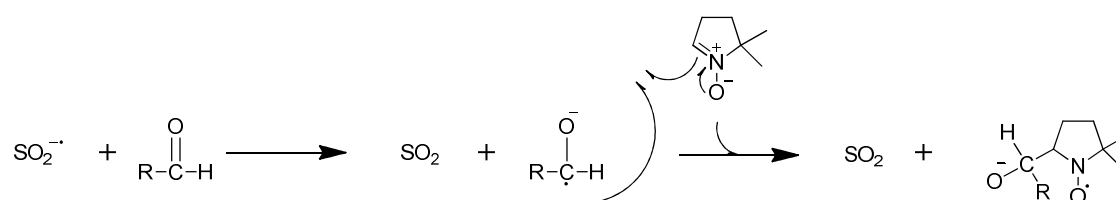


Figure 4-2: Proposed reaction scheme of sulfur dioxide radical anion ($SO_2^{\bullet-}$) and aldehyde spin adduct.

This aldehyde spin adduct formation is confirmed by the observation that different aldehydes give rise to different EPR signals in the presence of sodium dithionite. The path in which dithionite induces aldehyde radicals is another reaction pathway that may lead to a large impact on the rate constants of the bioluminescent reaction in quantitative assays. These findings indicate that the widely used dithionite assay needs to be carefully applied when performing kinetic measurements and determining kinetic constants. Additionally, both mentioned assays require the constant supply of molecular oxygen as an obligatory component of the reaction. Moreover, this study showed that the bubbling-motion increases *in vitro* luminescence, due to a improved mixing of all components, especially when poorly soluble aldehydes are used. Reduced flavin is rapidly oxidized by molecular oxygen, which additionally needs to be considered when kinetic constants are determined.

A more accurate determination of kinetic constants can be achieved by the simultaneous enzymatic reduction of FMN by flavin reductase. The affinity constant, Michaelis constant, has been determined for FMN, using the NAD(P)H:flavin oxidoreductase

from *E. coli* in combination with the luciferase from *V. harveyi* [259]. The use of *V. harveyi* flavin reductase (FRP) instead results in the reduced formation of FMNH₂. The *V. harveyi* cellular ratio of luciferase and FRP at maximal *in vivo* bioluminescence was estimated to be 57:1 [260]. Furthermore, FRP has optimal activity at low micromolar concentrations in luciferase coupled assays. A replacement of the reductase with *V. fischeri* FRase I also needs to be carefully applied, since the 10% sequence identity between FRP and FRase I is relatively low [126], which makes their activities hardly comparable. Hence, the determination of kinetic constants in the presence of a flavin reductase is possible, but only comparable for assays with the same reductase protein.

4.5 Bacterial bioluminescence runs via a radical intermediate

The presence of a radical intermediate in the bacterial bioluminescence reaction has been proposed by several groups, but no experimental evidence has been provided yet. If radicals are short-lived, spin trapping is an ideal method to stabilize them so that they can be detected by EPR spectroscopy. Bacterial bioluminescence DMPO experiments led to the formation of DMPO adducts. In firefly bioluminescence, however, no DMPO adducts were detected.

Adducts of DMPO radicals were observed in all samples upon addition of FMNH₂ to the solution containing DMPO and the aldehyde, even without the presence of luciferase (cf. Figure 3-24). It is unlikely that the trapped radicals originate from the aldehyde, since identical EPR spectra have been measured for different aldehydes and, moreover, the EPR signals do not correspond to those measured for the reaction of aldehydes with dithionite. In order to avoid the formation of aldehyde radicals, experiments have been performed by the photoreduction of FMN in the presence of EDTA. Control experiments with FMN, EDTA and DMPO without illumination and experiments with illumination and without either FMN or EDTA showed no build-up of DMPO adducts. In the presence of luciferase, one EPR signal systematically changes in amplitude depending on the concentration of luciferase. For dodecanal, the relative amplitude of this signal, as a function of luciferase concentration, is shown in Figure

3-23 and indicates a saturation curve. The spin trapping experiments thus give rise to an EPR signal that is directly correlated with the concentration of the luciferase. It therefore must be related to a radical intermediate in the bioluminescent reaction catalyzed by the protein.

At present, observed EPR signals do not give information about the identity of the detected radical species. No significant information can be extracted from mass spectrometry either. Indeed, carbon- and oxygen centered DMPO spin adducts have already been analyzed by mass spectrometry [261], the formation of spin adducts in this study, however, is too low. Neither the increase of DMPO concentration, nor of FMN and EDTA concentrations resulted in an increased formation of DMPO adducts. Most likely, the trapped radicals derive from FMN, since changing EDTA to NADH gave rise to identical EPR spectra. It is known that in the process of photoreduction the lowest triplet state of FMN abstracts an electron from EDTA to generate the semiquinone anion radical $\text{FMN}^{\bullet-}$ [197]. DMPO adducts generated from these radicals may be present in all illuminated samples and may correspond to the signals that are not luciferase-specific. The amount of bioluminescence-originated DMPO adducts becomes even more pronounced when homologous luciferase is used (cf. Figure 3-24). Homologously purified luciferase additionally contains NAD(P)H:FMN oxidoreductase, FRase I [176]. FRase I from *V. fischeri* binds FMN with a ratio of 1:1 as a prosthetic group [125] and was shown to form a functional complex with luciferase [224]. The complex formation enables the direct transfer of FMNH_2 to the luciferase for the bioluminescent reaction [262]. This observation may suggest that this direct transfer of FMNH_2 due to the formation of a luciferase-FRase I-complex somewhat leads a more frequently reaction rate of FMNH_2 and luciferase compared to assays without reductase. This explains the raised formation of DMPO adducts when homologous luciferase is used.

The low yield of DMPO adducts and the saturation of the bioluminescence-originated signals may be explained by the photodegradation of FMN. It has been shown that illumination can cause photodegradation to the primary photoproducts lumichrome and lumiflavin derivatives [75]. Tabata and coworkers found that the activity of the

flavoprotein geranyltransferase from the plant *Lithospermum erythrorhizon*, is strongly inhibited by light-treated FMN due to the accumulation of lumiflavin [263]. These photodegradation products do not function as luminescent substrates due to their lack of the phosphate moiety, which is obligatory for protein-binding as already discussed. The accumulation of the photoproducts during sample preparation thus inhibits the bioluminescence reaction and the formation of further DMPO adducts. Furthermore, the decreasing concentration of FMN leads to an increased luciferase-binding of aldehyde prior to flavin. The accumulation of an aldehyde-enzyme complex subsequently results in a partly inhibiting complex [186,187], yet additionally leading to a reduced formation of DMPO adducts.

Nevertheless the luminescence-derived DMPO adducts shown in this study are the first experimental evidence for a radical intermediate in bacterial bioluminescence. Based on this finding, the proposed reactions mechanisms from the literature can be compared. Since radical intermediates have been indirectly detected in this study, McCapra's approach of a non radical transformation with a second aldehyde molecule seems to be not applicable [145]. In the proposed mechanism by Kosower the excited state for light emission results from dissociative electron transfer from a flavin semiquinone [146]. This proposition, however, is highly unlikely, since the formation of 4a-hydroperoxyflavin as first intermediate (cf. Figure 1-7, II) is not considered, though its existence has been proven by NMR [141]. The most applicable approach has been given by Mager and Addink with a mechanism adapted to CIEEL [147]. CIEEL consists of two main steps: firstly, a peroxide reacts with an electron donor and subsequently forms a radical ion pair and secondly the radical anion transforms into a carboxyl radical. A reverse electron transfer gives rise to an excited fluorophore. The idea of Mager and Addink comprises the formation of flavin peroxyhemiacetal (Figure 4-3, IIIa), which has widely been accepted as presumably required step in the reaction.

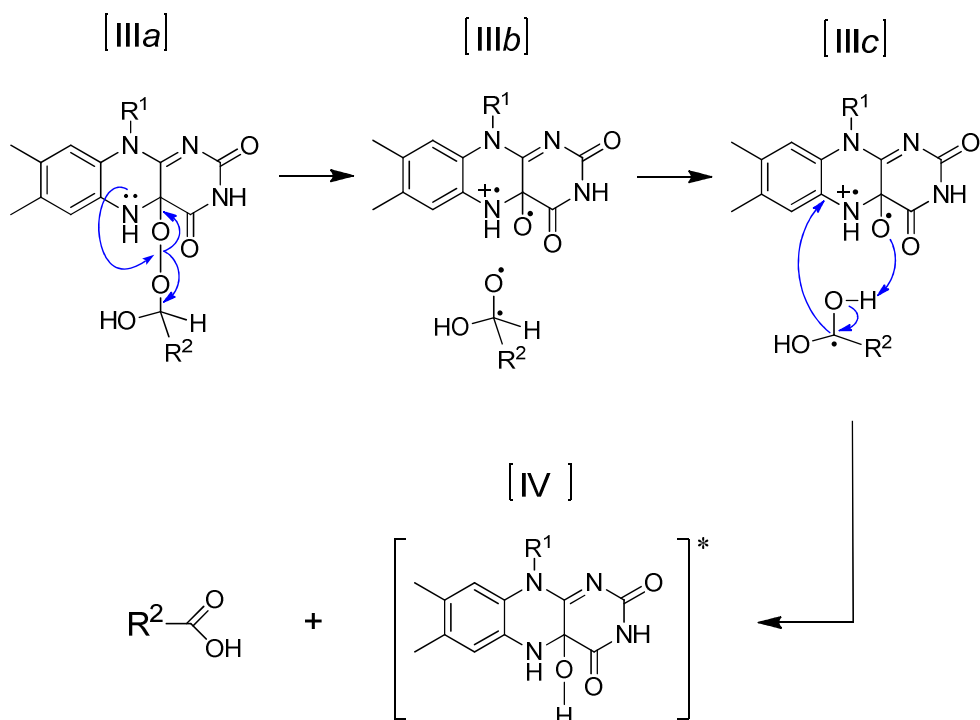


Figure 4-3: Proposed formation of the excited emitter state [IV] of FMN by CIEEL in bacterial bioluminescence, including a hydroxyflavin radical cation [IIIb] (illustration adapted from Nemtseva & Kudryasheva [264]). R^1 : side chain in FMN, R^2 : long chained aliphatic compound.

Intramolecular relocations of single-electrons form a hydroxyflavin radical cation (Figure 4-3, IIIb). These relocations start with the transfer of an electron from atom N(5) of the isoalloxazine moiety to one oxygen atom of the peroxide component. The peroxide bond is splitted by hemolytic cleavage. The following reverse electron transfer results in an excited hydroxyflavin and a carboxylic acid (Figure 4-3, IV). In summary, this proposed reaction mechanism by Mager and Addink [147] with a radical intermediate of FMN correlates with the findings of the present study, which makes it the most probable reaction mechanism from the literature.

5 Summary and outlook

The light emitting reaction of bioluminescence is one of the most visible processes in nature. Many open questions are still present, in particular with respect to the reaction mechanism. The present work provides new significant information about the bioluminescent reaction in bacteria. A radical intermediate during the catalytic process was detected by means of spin trapping in combination with EPR spectroscopy. In the presence of luciferase, the relative amplitude of the EPR signal of this spin adduct correlates with the protein concentration. Since the radical most likely derived from FMN, the proposed reaction mechanisms from the literature can be narrowed down to the ones including a radical species of FMN. The mechanism proposed by Mager and Addink, including a hydroxyflavin radical cation, presents the most probable one. As to the identity of the observed radical species, the EPR signals contain no information at present. For future research in this field, an increased formation of DMPO adducts needs to be achieved to enable further investigations by ENDOR and mass spectrometry. The exact mass would provide information about the formed DMPO species and ENDOR spectroscopy would elucidate information on an electronic level about the hyperfine interactions of the unpaired electron with surrounding nuclei. Even small hyperfine interactions, such as weakly coupled protons from the luciferase protein, may be detectable and provide information about the luciferase-FMN interaction. Moreover, a more extensive characterization of spin adducts should comprise the use of alternative spin traps like phenylbutylnitron (PBN) or TEMPO, which are used more frequently to capture alkyl radicals.

The kinetic assays in the present work provide direct information about the activity of the luciferase and the effect of different substrates. The phosphate moiety of the flavin-cofactor was shown to be obligatory for the process of bacterial bioluminescence. With regard to the aldehyde cosubstrate, kinetic measurements provide evidence for the important role of the aldehyde moiety. Moreover, the light emission increased with extending chain length of the aliphatic aldehyde. An explanation on a molecular level for the correlation of luciferase activity and the aldehyde chain length, however, still has

not yet been formulated. Additionally, the presence of an aromatic compound in the structure of the aldehyde has a negative impact on the luciferase activity, most likely owing to steric effects. Future kinetic assays should include an extensive variety of aldehydes to elucidate the steric influence. Secondary, crystal structures of the luciferase with bound aldehyde may hold indispensable information about the interaction of the individual aldehyde components with the protein. The commonly used assay including a chemically reduced FMN by sodium dithionite was found to have a high impact on the bioluminescence efficiency. Sodium dithionite is involved in additional reaction pathways and induces the formation of aldehyde radicals, making interpretation of rate constants difficult.

The electronic structure of FMN has been investigated at different pH values and in the presence of AgNO_3 by UV/VIS spectroscopy, EPR spectroscopy of the triplet state, DFT and TDDFT calculations. The bands at 355 and 450 nm in UV/VIS spectrum of FMN change with lowering of the pH such that they come together and form one intense band at 397 nm. These changes have been attributed to a protonation of nitrogen atom N1, which stabilizes all orbitals that carry $2p_z$ density at N1. ZFS parameters change only slightly upon pH change, since the HOMO and LUMO remain virtually the same. The first six doubly occupied orbitals that are in energy below the HOMO react stronger to the pH change. Upon addition of AgNO_3 , all UV/VIS bands display a bathochromic shift, which originates from the coordination of Ag^+ to nitrogen atom N5, stabilizing the LUMO. In the presence of AgNO_3 , the ZFS parameters slightly increase and the polarization pattern changes, owing to a contribution by SOC of Ag^+ . The addition of AgNO_3 did not lead to an increase of signal, which would be large enough to perform pulsed ENDOR experiments of the triplet state for direct examination of the hyperfine coupling constants of the nitrogen atoms and the protons of FMN. Nevertheless, the decrease of the lifetimes of the triplet sublevels by up to several hundred microseconds by the increased SOC is an advance, since it allows excitation and detection with a larger rate than previously possible. Additionally, the interpretation of the electronic structure of free FMN may be useful when compared

with the same investigations of enzyme-bound FMN. A high concentration of the latter is indispensable, however, hardly accessible for bacterial luciferase.

The results in this study contribute to a better understanding of the catalytic cycle of bacterial bioluminescence and its high efficiency. Detailed knowledge about this and other luminescent processes may lead to the development of model systems, in which chemical energy is utilized as an alternative light source without the concomitant loss of energy as heat. In the long term, the adaption of natural system such as bioluminescence is indispensable for the future projects of energy conservation.

6 References

1. Harvey E.N. (1957) A history of luminescence from the earliest times until 1900. American Philosophical Society Philadelphia.
2. Wiedemann E. (1888) Über Fluorescenz und Phosphorescenz I. Abhandlung. *Ann. Phys.* **270**: 446-463.
3. Harvey E.N. (1916) The mechanism of light production in animals. *Science* **44**: 208-209.
4. Haddock S.H.D., Moline M.A., Case J.F. (2009) Bioluminescence in the sea. *Annu. Rev. Marine. Sci.* **2**: 443-493.
5. Lee J. (2008) Bioluminescence: the first 3000 years (Review). *J. SibFU Biol.* **3**: 194-205.
6. Squirrell D.J., Price R.L., Murphy M.J. (2002) Rapid and specific detection of bacteria using bioluminescence. *Anal. Chim. Acta* **457**: 109-114.
7. Shimomura O., Johnson F.H., Saiga Y. (1962) Extraction, purification and properties of aequorin, a bioluminescent protein from the luminous Hydromedusan, *Aequorea*. *J. Cell. Comp. Physiol.* **59**: 223-239.
8. Hastings J.W., Gibson Q.H. (1963) Intermediates in the bioluminescent oxidation of reduced flavin mononucleotide. *J. Biol. Chem.* **238**: 2537-2554.
9. Bowie L.J., Irwin R., Loken M., DeLuca M., Brand L. (1973) Excited-state proton transfer and the mechanism of action of firefly luciferase. *Biochemistry* **12**: 1852-1857.
10. DeLuca M., McElroy W.D. (1978) Purification and properties of firefly luciferase. In *Methods in Enzymology*. New York: Academic Press. pp. 3-15.
11. Gates B.J., DeLuca M. (1975) The production of oxyluciferin during the firefly luciferase light reaction. *Arch. Biochem. Biophys.* **169**: 616-621.
12. Henry J.P., Monny C., Michelson A.M. (1975) Characterization and properties of *Pholas* luciferase as a metalloprotein. *Biochemistry* **14**: 3458-3466.
13. DeLuca M. (1976) Firefly luciferase. In *Advances in Enzymology and Related Areas of Molecular Biology*. John Wiley & Sons, Inc. pp. 37-68.
14. Dubois R. (1885) Note sur la physiologie des Pyrophores. *Cr. Soc. Biol.* **37**: 559-562.

15. Harvey E.N. (1952) Bioluminescence. Academic Press.
16. Waters C.M., Bassler B.L. (2005) Quorum sensing: cell-to-cell communication in bacteria. *Annu. Rev. Cell Dev. Biol.* **21**: 319-346.
17. Nealson K.H., Hastings J.W. (2006) Quorum Sensing on a Global Scale: Massive Numbers of Bioluminescent Bacteria Make Milky Seas. *Appl. Environ. Microb.* **72**: 2295-2297.
18. Fuqua C., Winans S.C., Greenberg E.P. (1996) Census and consensus in bacterial ecosystems: the LuxR-LuxI family of quorum-sensing transcriptional regulators. *Annu. Rev. Microbiol.* **50**: 727-751.
19. Engebrecht J., Nealson K., Silverman M. (1983) Bacterial bioluminescence: Isolation and genetic analysis of functions from *Vibrio fischeri*. *Cell* **32**: 773-781.
20. Hastings J.W. (1986) Bioluminescence in bacteria and dinoflagellates. In *Light emission by plants and bacteria*. Govindjee A.J., Fork D.C. (eds). Academic Press. pp. 363-398.
21. McFall-Ngai M.J., Ruby E.G. (1998) Sepiolid and vibrios: when first they meet. *BioScience* **48**: 257-265.
22. Beijerinck M.W. (1889) Le *Photobacterium luminosum*, bactérie lumineuse de la Mer du Nord. *Arch. Neerl. Sci. Exact. Nat.* **23**: 401-427.
23. Lee K.H., Ruby E.G. (1994) Effect of the squid host on the abundance and distribution of symbiotic *Vibrio fischeri* in nature. *Appl. Environ. Microb.* **60**: 1565-1571.
24. Ruby E.G., Asato L.M. (1993) Growth and flagellation of *Vibrio fischeri* during initiation of the sepiolid squid light organ symbiosis. *Arch. Microbiol.* **159**: 160-167.
25. Ruby E.G., Urbanowski M., Campbell J., Dunn A., Faini M., Gunsalus R., Lostroh P., Lupp C., McCann J., Millikan D., Schaefer A., Stabb E., Stevens A., Visick K., Whistler C., Greenberg E.P. (2005) Complete genome sequence of *Vibrio fischeri*: A symbiotic bacterium with pathogenic congeners. *P. Natl. Acad. Sci. USA* **102**: 3004-3009.
26. Milne L., Milne M., Rayfield S. (1980) Audubon society field guide to North American insects and spiders. New York: Alfred A. Knopf.
27. Lloyd J.E. (1984) Occurrence of aggressive mimicry in fireflies. *Fla. Entomol.* **67**: 368-376.

28. Green A.A., McElroy W.D. (1956) Crystalline firefly luciferase. *Biochim. Biophys. Acta* **20**: 170-176.
29. Hastings J.W., Balny C., Peuch C.L., Douzou P. (1973) Spectral properties of an oxygenated luciferase-flavin intermediate isolated by low-temperature chromatography. *P. Natl. Acad. Sci.* **70**: 3468-3472.
30. Hastings J.W., Krause K.L. (2004) Luciferases and light-emitting accessory proteins: structural biology. In *Nature Encyclopedia of Life Sciences (eLS)*. John Wiley & Sons, Ltd, online
31. Shimomura O., Johnson F.H. (1975) Chemical nature of bioluminescence systems in coelenterates. *P. Natl. Acad. Sci.* **72**: 1546-1549.
32. Morise H., Shimomura O., Johnson F.H., Winant J. (1974) Intermolecular energy transfer in the bioluminescent system of *Aequorea*. *Biochemistry* **13**: 2656-2662.
33. Kendall J.M., Badminton M.N. (1998) *Aequorea victoria* bioluminescence moves into an exciting new era. *Trends Biotechnol.* **16**: 216-224.
34. Shimomura O., Inoue S., Johnson F.H., Haneda Y. (1980) Widespread occurrence of coelenterazine in marine bioluminescence. *Comp. Biochem. Phys. B - Comp. Biochem.* **65**: 435-437.
35. Thomson C.M., Herring P.J., Campbell A.K. (1997) The widespread occurrence and tissue distribution of the imidazolopyrazine luciferins. *J. Biolumin. Chemilumin.* **12**: 87-91.
36. Morse D.S., Fritz L., Hastings J.W. (1990) What is the clock? Translational regulation of circadian bioluminescence. *Trends Biochem. Sci.* **15**: 262-265.
37. Stanley P.E., Kricka L.J. (2002) Bioluminescence & chemiluminescence. World Scientific Publishing Company.
38. Tagami A., Ishibashi N., Kato D., Taguchi N., Mochizuki Y., Watanabe H., Ito M., Tanaka S. (2009) Ab initio quantum-chemical study on emission spectra of bioluminescent luciferases by fragment molecular orbital method. *Chem. Phys. Lett.* **472**: 118-123.
39. Bitler B., McElroy W.D. (1957) The preparation and properties of crystalline firefly luciferin. *Arch. Biochem. Biophys.* **72**: 358-368.
40. White E.H., McCapra F., Field G.F., McElroy W.D. (1961) The structure and synthesis of firefly luciferin. *J. Am. Chem. Soc.* **83**: 2402-2403.

41. White E.H., McCapra F., Field G.F. (1963) The structure and synthesis of firefly luciferin. *J. Am. Chem. Soc.* **85**: 337-343.
42. McElroy W.D., Green A.A. (1955) Enzymatic properties of bacterial luciferase. *Arch. Biochem. Biophys.* **56**: 240-255.
43. Nakamura H., Kishi Y., Shimomura O., Morse D., Hastings J.W. (1989) Structure of dinoflagellate luciferin and its enzymic and nonenzymic air-oxidation products. *J. Am. Chem. Soc.* **111**: 7607-7611.
44. Hori K., Cormier M.J. (1973) Structure and chemical synthesis of a biologically active form of *Renilla* (sea pansy) luciferin. *P. Natl. Acad. Sci.* **70**: 120-123.
45. Hardeland R., Zsizsik B.K., Poeggeler B., Fuhrberg B., Holst S., Coto-Montes A. (1999) Indole-3-pyruvic and -propionic acids, kynurenic acid, and related metabolites as luminophores and free-radical scavengers. In *Tryptophan, Serotonin, and Melatonin*. Huether G., Kochen W., Simat T., Steinhart H. (eds). Springer US. pp. 389-395.
46. Li G., Sichula V., Glusac K.D. (2008) Role of adenine in thymine-dimer repair by reduced flavin-adenine dinucleotide. *J. Phys. Chem. B* **112**: 10758-10764.
47. Heelis P.F. (1982) The photophysical and photochemical properties of flavins (isoalloxazines). *Chem. Soc. Rev. b* **11**: 15-39.
48. Massey V. (2000) The chemical and biological versatility of riboflavin. *Biochem. Soc. T.* **28**: 283-296.
49. Fraaije M.W., Mattevi A. (2000) Flavoenzymes: diverse catalysts with recurrent features. *Trends Biochem. Sci.* **25**: 126-132.
50. Weber S. (2005) Light-driven enzymatic catalysis of DNA repair: a review of recent biophysical studies on photolyase. *BBA-Bioenergetics* **1707**: 1-23.
51. Kondoh M., Hitomi K., Yamamoto J., Todo T., Iwai S., Getzoff E.D., Terazima M. (2011) Light-induced conformational change and product release in DNA repair by (6-4) photolyase. *J. Am. Chem. Soc.* **133**: 2183-2191.
52. Carneiro P., Duarte M., Videira A. (2012) Characterization of apoptosis-related oxidoreductases from *Neurospora crassa*. *PloS one* **7**: e34270.
53. Losi A., Gärtner W. (2012) The evolution of flavin-binding photoreceptors: an ancient chromophore serving trendy blue-light sensors. *Annu. Rev. Plant Biol.* **63**: 49-72.

54. Henriques J., Olsen K., Bross P., Gomes M. (2010) Emerging roles for riboflavin in functional rescue of mitochondrial-oxidation flavoenzymes. *Curr. Med. Chem.* **17**: 3842-3854.
55. Hines R.N., Prough R.A., Lyubimov A.V. (2011) Amine oxidases and reductases. In *Encyclopedia of Drug Metabolism and Interactions*. John Wiley & Sons, Inc.
56. Miura R. (2001) Versatility and specificity in flavoenzymes: control mechanisms of flavin reactivity. *Chem. Record* **1**: 183-194.
57. Massey V., Hemmerich P. (1980) Active-site probes of flavoproteins. *Biochem. Soc. T.* **8**: 246-257.
58. Bock M., Lubitz W., Kurreck H., Fenner H., Grauert R. (1981) ^{14}N and ^1H ENDOR and TRIPLE resonance experiments of flavin and thiaflavin radical cations in liquid solution. *J. Am. Chem. Soc.* **103**: 5567-5568.
59. Kurreck H., Bock M., Bretz N., Elsner M., Kraus H., Lubitz W., Mueller F., Geissler J., Kroneck P.M.H. (1984) Fluid solution and solid-state electron nuclear double resonance studies of flavin model compounds and flavoenzymes. *J. Am. Chem. Soc.* **106**: 737-746.
60. Fuchs M.R., Schleicher E., Schnegg A., Kay C.W.M., Törring J.T., Bittl R., Bacher A., Richter G., Möbius K., Weber S. (2002) G-Tensor of the neutral flavin radical cofactor of DNA photolyase revealed by 360-GHz electron paramagnetic resonance spectroscopy. *J. Phys. Chem. B* **106**: 8885-8890.
61. Schleicher E., Kowalczyk R.M., Kay C.W.M., Hegemann P., Bacher A., Fischer M., Bittl R., Richter G., Weber S. (2004) On the reaction mechanism of adduct formation in LOV domains of the plant blue-light receptor phototropin. *J. Am. Chem. Soc.* **126**: 11067-11076.
62. Kay C.W.M., Bittl R., Bacher A., Richter G., Weber S. (2005) Unambiguous determination of the g-matrix orientation in a neutral flavin radical by pulsed electron-nuclear double resonance at 94 GHz. *J. Am. Chem. Soc.* **127**: 10780-10781.
63. Weber S., Kay C.W.M., Bacher A., Richter G., Bittl R. (2005) Probing the N(5)-H bond of the isoalloxazine moiety of flavin radicals by X- and W-band pulsed electron-nuclear double resonance. *ChemPhysChem* **6**: 292-299.
64. Barquera B., Ramirez-Silva L., Morgan J.E., Nilges M.J. (2006) A new flavin radical signal in the Na^+ -pumping NADH:quinone oxidoreductase from *Vibrio cholerae*: An EPR/electron nuclear double resonance investigation

- of the role of the covalently bound flavins in subunits b and c. *J. Biol. Chem.* **281**: 36482-36491.
65. Schnegg A., Kay C.W.M., Schleicher E., Hitomi K., Todo T., Möbius K., Weber S. (2006) The g-tensor of the flavin cofactor in (6-4) photolyase: a 360 GHz/12.8 T electron paramagnetic resonance study. *Mol. Phys.* **104**: 1627-1633.
 66. Kay C.W.M., Mkami H.E., Molla G., ollegioni L., amsay R.R. (2007) Characterization of the covalently bound anionic flavin radical in monoamine oxidase A by electron paramagnetic resonance. *J. Am. Chem. Soc.* **129**: 16091-16097.
 67. Okafuji A., Schnegg A., Schleicher E., Möbius K., Weber S. (2008) G-tensors of the flavin adenine dinucleotide radicals in glucose oxidase: a comparative multifrequency electron paramagnetic resonance and electron-nuclear double resonance study. *J. Phys. Chem. B* **112**: 3568-3574.
 68. Schleicher E., Bittl R., Weber S. (2009) New roles of flavoproteins in molecular cell biology: Blue-light active flavoproteins studied by electron paramagnetic resonance. *FEBS J.* **276**: 4290-4303.
 69. Schleicher E., Weber S. (2012) Radicals in flavoproteins. In *EPR Spectroscopy*. Drescher M., Jeschke G. (eds). Springer Berlin Heidelberg, pp. 41-65.
 70. Karthikeyan S., Zhou Q., Mseeh F., Grishin N.V., Osterman A.L., Zhang H. (2003) Crystal structure of human riboflavin kinase reveals a beta barrel fold and a novel active site arch. *Structure* **11**: 265-273.
 71. Sandoval F.J., Roje S. (2005) An FMN hydrolase is fused to a riboflavin kinase homolog in plants. *J. Biol. Chem.* **280**: 38337-38345.
 72. Yankovskaya V., Horsefield R., Törnroth S., Luna-Chavez C., Miyoshi H., Léger C., Byrne B., Cecchini G., Iwata S. (2003) Architecture of succinate dehydrogenase and reactive oxygen species generation. *Science* **299**: 700-704.
 73. Radda G.K., Calvin M. (1964) Chemical and photochemical reductions of flavin nucleotides and analogs. *Biochemistry* **3**: 384-393.
 74. Penzer G.R. (1970) The chemistry of flavins and flavoproteins. Aerobic photochemistry. *Biochem. J.* **116**: 733-743.
 75. Holzer W., Shirdel J., Zirak P., Penzkofer A., Hegemann P., Deutzmann R., Hochmuth E. (2005) Photo-induced degradation of some flavins in aqueous solution. *Chem. Phys.* **308**: 69-78.

76. Friedrich W. (1988) Vitamins. Berlin: Walter de Gruyter.
77. Müller F. (1992) Chemistry and biochemistry of flavoenzymes. Boca Raton: CRC Press.
78. Briggs W.R., Huala E. (1999) Blue-light photoreceptors in higher plants. *Annu. Rev. Cell Dev. Biol.* **15**: 33-62.
79. Hefti M.H., Vervoort J., van Berkel W.J.H. (2003) Deflavination and reconstitution of flavoproteins. *Eur. J. Biochem.* **270**: 4227-4242.
80. van der Horst M.A., Hellingwerf K.J. (2003) Photoreceptor proteins, "Star Actors of Modern Times": a review of the functional dynamics in the structure of representative members of six different photoreceptor families. *Acc. Chem. Res.* **37**: 13-20.
81. Beinert H. (1956) Spectral characteristics of flavins at the semiquinoid oxidation level. *J. Am. Chem. Soc.* **78**: 5323-5328.
82. Nakamura S., Nakamura T., Ogura Y. (1963) Absorption spectrum of flavin mononucleotide semiquinone. *J. Biochem.* **53**: 143-146.
83. Neiss C., Saalfrank P., Parac M., Grimme S. (2002) Quantum chemical calculation of excited states of flavin-related molecules. *J. Phys. Chem. A* **107**: 140-147.
84. Choe Y.K., Nagase S., Nishimoto K. (2007) Theoretical study of the electronic spectra of oxidized and reduced states of lumiflavin and its derivative. *J. Comput. Chem.* **28**: 727-739.
85. Cannuccia E., Pulci O., Sole R.D., Cascella M. (2011) Optical properties of flavin mononucleotide: a QM/MM study of protein environment effects. *Chem. Phys.* **389**: 35-38.
86. Cavelier G., Amzel L.M. (2001) Mechanism of NAD(P)H:quinone reductase: ab initio studies of reduced flavin. *Proteins* **43**: 420-432.
87. Eweg J.K., Müller F., Visser A.J.W.G., Veeger C., Bebelaar D., Voorst J.D.W. (1979) Molecular luminescence of some isoalloxazines in apolar solvents at various temperatures. *Photochem. Photobiol.* **30**: 463-471.
88. Yagi K., Ohishi N., Nishimoto K., Choi J.D., Song P.S. (1980) Effect of hydrogen bonding on electronic spectra and reactivity of flavins. *Biochemistry* **19**: 1553-1557.
89. Dutta P.K., Spiro T.G. (1978) Resonance CARS line shapes: excited state parameters for flavin adenine dinucleotide. *J. Chem. Phys.* **69**: 3119-3123.

-
90. Song P.S., Kurtin W.E. (1969) The nature of the triplet states of flavins: a further study. *Photochem. Photobiol.* **10**: 211-214.
 91. Di Valentin M., Tait C., Salvadori E., Ceola S., Scheer H., Hiller R.G., Carbonera D. (2011) Conservation of spin polarization during triplet-triplet energy transfer in reconstituted peridinin-chlorophyll-protein complexes. *J. Phys. Chem. B* **115**: 13371-13380.
 92. Marchanka A., Savitsky A., Lubitz W., Möbius K., van Gestel M. (2010) B-branch electron transfer in the photosynthetic reaction center of a *Rhodobacter sphaeroides* quadruple mutant. Q- and W-band electron paramagnetic resonance studies of triplet and radical-pair cofactor states. *J. Phys. Chem. B* **114**: 14364-14372.
 93. Carbonera D., Di Valentin M., Corvaja C., Agostini G., Giacometti G., Liddell P.A., Kuciauskas D., Moore A.L., Moore T.A., Gust D. (1998) EPR investigation of photoinduced radical pair formation and decay to a triplet state in a carotene-porphyrin-fullerene triad. *J. Am. Chem. Soc.* **120**: 4398-4405.
 94. Lewis G.N., Kasha M. (1944) Phosphorescence and the triplet state. *J. Am. Chem. Soc.* **66**: 2100-2116.
 95. McClure D.S. (1949) Triplet-singlet transitions in organic molecules. Lifetime measurements of the triplet state. *J. Chem. Phys.* **17**: 905-913.
 96. Kowalczyk R.M., Schleicher E., Bittl R., Weber S. (2004) The photoinduced triplet of flavins and its protonation states. *J. Am. Chem. Soc.* **126**: 11393-11399.
 97. Shiga T., Piette L.H. (1964) Triplet state studies of flavins by electron paramagnetic resonance. *Photochem. Photobiol.* **3**: 213-222.
 98. Moore W.M., McDaniels J.C., Hen J.A. (1977) The photochemistry of riboflavin-VI. The photophysical properties of isoalloxazines. *Photochem. Photobiol.* **25**: 505-512.
 99. Wall L.A., Byers D.M., Meighen E.A. (1984) In vivo and in vitro acylation of polypeptides in *Vibrio harveyi*: identification of proteins involved in aldehyde production for bioluminescence. *J. Bacteriol.* **159**: 720-724.
 100. Lee C.Y., O'Kane D.J., Meighen E.A. (1994) Riboflavin synthesis genes are linked with the lux operon of *Photobacterium phosphoreum*. *J. Bacteriol.* **176**: 2100-2104.

101. Engebrecht J., Silverman M. (1987) Nucleotide sequence of the regulatory locus controlling expression of bacterial genes for bioluminescence. *Nucleic Acids Res.* **15**: 10455-10467.
102. Swartzman E., Silverman M., Meighen E.A. (1992) The luxR gene product of *Vibrio harveyi* is a transcriptional activator of the lux promoter. *J. Bacteriol.* **174**: 7490-7493.
103. Mok K.C., Wingreen N.S., Bassler B.L. (2003) *Vibrio harveyi* quorum sensing: a coincidence detector for two autoinducers controls gene expression. *EMBO J.* **22**: 870-881.
104. Milton D.L. (2006) Quorum sensing in vibrios: complexity for diversification. *Int. J. Med. Microbiol.* **296**: 61-71.
105. Ast J.C., Dunlap P.V. (2004) Phylogenetic analysis of the lux operon distinguishes two evolutionarily distinct clades of *Photobacterium leiognathi*. *Arch. Microbiol.* **181**: 352-361.
106. Dunlap P.V. (1999) Quorum regulation of luminescence in *Vibrio fischeri*. *J. Mol. Microbiol. Biotechnol.* **1**: 5-12.
107. Visick K.L., Foster J., Doino J., McFall-Ngai M., Ruby E.G. (2000) *Vibrio fischeri* lux genes play an important role in colonization and development of the host light organ. *J. Bacteriol.* **182**: 4578-4586.
108. Lee J. (1989) Bioluminescence. In *The Science of Photobiology*. Smith K. (ed). Springer US. pp. 391-417.
109. Legocki R.P., Legocki M., Baldwin T.O., Szalay A.A. (1986) Bioluminescence in soybean root nodules: demonstration of a general approach to assay gene expression in vivo by using bacterial luciferase. *P. Natl. Acad. Sci.* **83**: 9080-9084.
110. Belas R., Mileham A., Cohn D., Hilman M., Simon M., Silverman M. (1982) Bacterial bioluminescence: isolation and expression of the luciferase genes from *Vibrio harveyi*. *Science* **218**: 791-793.
111. Zenno S., Saigo K., Kanoh H., Inouye S. (1994) Identification of the gene encoding the major NAD(P)H-flavin oxidoreductase of the bioluminescent bacterium *Vibrio fischeri* ATCC 7744. *J. Bacteriol.* **176**: 3536-3543.
112. Angell P., Langley D., Chamberlain A.H.L. (1989) Localisation of luciferase in luminous marine bacteria by gold immunocytochemical labelling. *FEMS Microbiol. Lett.* **65**: 177-181.

113. Baldwin T.O., Ziegler M.M., Powers D.A. (1979) Covalent structure of subunits of bacterial luciferase: NH₂-terminal sequence demonstrates subunit homology. *P. Natl. Acad. Sci.* **76**: 4887-4889.
114. Baldwin T.O., Christopher J.A., Raushel F.M., Sinclair J.F., Ziegler M.M., Fisher A.J., Rayment I. (1995) Structure of bacterial luciferase. *Curr. Opin. Struc. Biol.* **5**: 798-809.
115. Fisher A.J., Thompson T.B., Thoden J.B., Baldwin T.O., Rayment I. (1996) The 1.5 Å resolution crystal structure of bacterial luciferase in low salt conditions. *J. Biol. Chem.* **271**: 21956-21968.
116. Sparks J.M., Baldwin T.O. (2001) Functional implications of the unstructured loop in the (β/α)₈ barrel structure of the bacterial luciferase α subunit. *Biochemistry* **40**: 15436-15443.
117. Low J.C., Tu S.C. (2002) Functional roles of conserved residues in the unstructured loop of *Vibrio harveyi* bacterial luciferase. *Biochemistry* **41**: 1724-1731.
118. Clark A.C., Raso S.W., Sinclair J.F., Ziegler M.M., Chaffotte A.F., Baldwin T.O. (1997) Kinetic mechanism of luciferase subunit folding and assembly. *Biochemistry* **36**: 1891-1899.
119. Fisher A.J., Raushel F.M., Baldwin T.O., Rayment I. (1995) Three-dimensional structure of bacterial luciferase from *Vibrio harveyi* at 2.4 Å resolution. *Biochemistry* **34**: 6581-6586.
120. Huang S., Tu S.C. (1997) Identification and characterization of a catalytic base in bacterial luciferase by chemical rescue of a dark mutant. *Biochemistry* **36**: 14609-14615.
121. Baldwin T.O., Ziegler M.M. (1991) The biochemistry and molecular biology of bacterial bioluminescence. In *Chemistry and Biochemistry of Flavoenzymes*. Müller F. (ed). Boca Raton: CRC Press. pp. 467-530.
122. Bourgois J.J., Sluse F.E., Baguet F., Malfet J. (2001) Kinetics of light emission and oxygen consumption by bioluminescent bacteria. *J. Bioenerg. Biomembr.* **33**: 353-363.
123. Jablonski E., DeLuca M. (1978) Studies of the control of luminescence in *Beneckea harveyi*: properties of the NADH and NADPH:FMN oxidoreductases. *Biochemistry* **17**: 672-678.
124. Lei B., Liu M., Huang S., Tu S.C. (1994) *Vibrio harveyi* NADPH-flavin oxidoreductase: cloning, sequencing and overexpression of the gene and

- purification and characterization of the cloned enzyme. *J. Bacteriol.* **176**: 3552-3558.
125. Inouye S. (1994) NAD(P)H-flavin oxidoreductase from the bioluminescent bacterium, *Vibrio fischeri* ATCC 7744, is a flavoprotein. *FEBS Lett.* **347**: 163-168.
126. Koike H., Sasaki H., Kobori T., Zenno S., Saigo K., Murphy M.E.P., Adman E.T., Tanokura M. (1998) 1.8 Å crystal structure of the major NAD(P)H:FMN oxidoreductase of a bioluminescent bacterium, *Vibrio fischeri*: overall structure, cofactor and substrate-analog binding, and comparison with related flavoproteins. *J. Mol. Biol.* **280**: 259-273.
127. Jeffers C.E., Tu S.C. (2001) Differential transfers of reduced flavin cofactor and product by bacterial flavin reductase to luciferase. *Biochemistry* **40**: 1749-1754.
128. Holzman T.F., Baldwin T.O. (1980) Proteolytic inactivation of luciferases from three species of luminous marine bacteria, *Beneckea harveyi*, *Photobacterium fischeri*, and *Photobacterium phosphoreum*: evidence of a conserved structural feature. *P. Natl. Acad. Sci.* **77**: 6363-6367.
129. Baldwin T.O., Hastings J.W., Riley P.L. (1978) Proteolytic inactivation of the luciferase from the luminous marine bacterium *Beneckea harveyi*. *J. Biol. Chem.* **253**: 5551-5554.
130. Strehler B.L., Cormier M.J. (1954) Isolation, identification, and function of long chain fatty aldehydes affecting the bacterial luciferin-luciferase reaction. *J. Biol. Chem.* **211**: 213-225.
131. Lin L.Y.-C., Sulea T., Szittner R., Kor C., Purisima E.O., Meighen E.A. (2002) Implications of the reactive thiol and the proximal non-proline cis-peptide bond in the structure and function of *Vibrio harveyi* luciferase. *Biochemistry* **41**: 9938-9945.
132. Langridge W.H.R., Fitzgerald K.J., Koncz C., Schell J., Szalay A.A. (1989) Dual promoter of *Agrobacterium tumefaciens* mannopine synthase genes is regulated by plant growth hormones. *P. Natl. Acad. Sci.* **86**: 3219-3223.
133. Lee J. (1985) The mechanism of bacterial bioluminescence. In *Chemiluminescence and Bioluminescence*. Dekker M. (ed). New York: Marcel Dekker. pp. 401-437.
134. Shimomura O., Johnson F.H., Kohama Y. (1972) Reactions involved in bioluminescence systems of limpet (*Latia neritoides*) and luminous bacteria. *P. Natl. Acad. Sci.* **69**: 2086-2089.

135. McCapra F., Hysert D.W. (1973) Bacterial bioluminescence - identification of fatty acid as product, its quantum yield and a suggested mechanism. *Biochem. Bioph. Res. Co.* **52**: 298-304.
136. Dunn D.K., Michalyszyn G.A., Bogacki I.G., Meighen E.A. (1973) Conversion of aldehyde to acid in the bacterial bioluminescent reaction. *Biochemistry* **12**: 4911-4918.
137. Meighen E.A. (1991) Molecular biology of bacterial bioluminescence. *Microbiol. Rev.* **55**: 123-142.
138. Sirokman G., Wilson T., Hastings J.W. (1995) A bacterial luciferase reaction with a negative temperature coefficient attributable to protein-protein interaction. *Biochemistry* **34**: 13074-13081.
139. Lin L.Y.-C., Szittner R., Friedman R., Meighen E.A. (2004) Changes in the kinetics and emission spectrum on mutation of the chromophore-binding platform in *Vibrio harveyi* luciferase. *Biochemistry* **43**: 3183-3194.
140. Tu S.C. (1979) Isolation and properties of bacterial luciferase-oxygenated flavin intermediate complexed with long-chain alcohols. *Biochemistry* **18**: 5940-5945.
141. Vervoort J., Müller F., Lee J., Van den Berg W.A.M., Moonen C.T.W. (1986) Identifications of the true carbon-13 nuclear magnetic resonance spectrum of the stable intermediate II in bacterial luciferase. *Biochemistry* **25**: 8062-8067.
142. Kurfuerst M., Macheroux P., Ghisla S., Hastings J.W. (1987) Isolation and characterization of the transient, luciferase-bound flavin-4a-hydroxide in the bacterial luciferase reaction. *BBA-Gen. Subjects* **924**: 104-110.
143. Lee J., O'Kane D.J., Gibson B.G. (1988) Dynamic fluorescence properties of the bacterial luciferase intermediates. *Biochemistry* **27**: 4862-4870.
144. Vervoort J., Müller F., O'Kane D.J., Lee J., Bacher A. (1986) Bacterial luciferase: a carbon-13, nitrogen-15, and phosphorus-31 nuclear magnetic resonance investigation. *Biochemistry* **25**: 8067-8075.
145. McCapra F. (2000) Chemical generation of excited states: the basis of chemiluminescence and bioluminescence. In *Methods in Enzymology: Bioluminescence and Chemiluminescence Part C*. Academic Press. pp. 3-47.
146. Kosower E.M. (1980) A proposed mechanism for light emission by bacterial luciferase involving dissociative electron transfer. *Biochem. Bioph. Res. Co.* **92**: 356-364.

147. Mager H.I.X., Addink R. (1984) On the role of some flavin adducts as one-electron donors. In *Flavins and Flavoproteins*. Bray R.C., Engel P.C., Mayhew S.C. (eds). pp. 37-40.
148. Raushel F.M., Baldwin T.O. (1989) Proposed mechanism for the bacterial bioluminescence reaction involving a dioxirane intermediate. *Biochem. Biophys. Res. Co.* **164**: 1137-1142.
149. Kudryasheva N.S., Belobrov P.I., Kratasyuk V.A., Shigorin D.N. (1991) Electron-excited states in bioluminescence. *Dokl. Akad. Nauk SSSR* **321**: 837-841.
150. Francisco W.A., Abu-Soud H.M., DelMonte A.J., Singleton D.A., Baldwin T.O., Raushel F.M. (1998) Deuterium kinetic isotope effects and the mechanism of the bacterial luciferase reaction. *Biochemistry* **37**: 2596-2606.
151. Baldwin T.O., Ziegler M.M., Müller F. (1992) Chemistry and biochemistry of flavoenzymes. Boca Raton: CRC Press.
152. Merenyi G., Lind J., Mager H.I.X., Tu S.C. (1992) Properties of 4a-hydroxy-4a,5-dihydroflavin radicals in relation to bacterial bioluminescence. *J. Phys. Chem.* **96**: 10528-10533.
153. Tu S.C., Mager H.I.X. (1995) Biochemistry of bacterial bioluminescence. *Photochem. Photobiol.* **62**: 615-624.
154. Hopkins T.A., Seliger H.H., White E.H., Cass M.W. (1967) Chemiluminescence of firefly luciferin. Model for the bioluminescent reaction and identification of the product excited state. *J. Am. Chem. Soc.* **89**: 7148-7150.
155. White E.H., Miano J.D., Umbreit M. (1975) Mechanism of firefly luciferin luminescence. *J. Am. Chem. Soc.* **97**: 198-200.
156. Koo J.A., Schmidt S.P., Schuster G.B. (1978) Bioluminescence of the firefly: key steps in the formation of the electronically excited state for model systems. *P. Natl. Acad. Sci.* **75**: 30-33.
157. de Wet J.R., Wood K.V., Helinski D.R., DeLuca M. (1985) Cloning of firefly luciferase cDNA and the expression of active luciferase in *Escherichia coli*. *P. Natl. Acad. Sci.* **82**: 7870-7873.
158. Ye L., Buck L.M., Schaeffer H.J., Leach F.R. (1997) Cloning and sequencing of a cDNA for firefly luciferase from *Photuris pennsylvanica*. *BBA-Protein Struct. M.* **1339**: 39-52.
159. Viviani V.R., Arnoldi F.G.C., Brochetto-Braga M., Ohmiya Y. (2004) Cloning and characterization of the cDNA for the Brazilian *Cratomorphus*

- distinctus* larval firefly luciferase: similarities with European *Lampyrus noctiluca* and Asiatic *Pyrocoelia* luciferases. *Comp. Biochem. Phys. B - Biochem. Mol. Biol.* **139**: 151-156.
160. Devine J.H., Kutuzova G.D., Green V.A., Ugarova N.N., Baldwin T.O. (1993) Luciferase from the East European firefly *Luciola mingrelica*: Cloning and nucleotide sequence of the cDNA, overexpression in *Escherichia coli* and purification of the enzyme. *BBA-Gene Struct. Expr.* **1173**: 121-132.
161. Sala-Newby G.B., Thomson C.M., Campbell A.K. (1996) Sequence and biochemical similarities between the luciferases of the glow-worm *Lampyrus noctiluca* and the firefly *Photinus pyralis*. *Biochem. J.* **313**: 761-767.
162. Said Alipour B., Hosseinkhani S., Nikkhah M., Naderi-Manesh H., Chaichi M.J., Osaloo S.K. (2004) Molecular cloning, sequence analysis, and expression of a cDNA encoding the luciferase from the glow-worm, *Lampyrus turkestanicus*. *Biochem. Bioph. Res. Co.* **325**: 215-222.
163. Tatsumi H., Kajiyama N., Nakano E. (1992) Molecular cloning and expression in *Escherichia coli* of a cDNA clone encoding luciferase of a firefly, *Luciola lateralis*. *BBA-Gene Struct. Expr.* **1131**: 161-165.
164. Ohmiya Y., Ohba N., Toh H., Tsuji F.I. (1995) Cloning, expression and sequence analysis of cDNA for the luciferases from the Japanese fireflies, *Pyrocoelia tniyako* and *Hotaria parvula*. *Photochem. Photobiol.* **62**: 309-313.
165. Choi Y.S., Lee K.S., Bae J.S., Lee K.M., Kim S.R., Kim I., Lee S.M., Sohn H.D., Jin B.R. (2002) Molecular cloning and expression of a cDNA encoding the luciferase from the firefly, *Hotaria unmunzana*. *Comp. Biochem. Phys. B - Biochem. Mol. Biol.* **132**: 661-670.
166. Wood K.V., de Wet J.R., Dewji N., DeLuca M. (1984) Synthesis of active firefly luciferase by in vitro translation of RNA obtained from adult lanterns. *Biochem. Bioph. Res. Co.* **124**: 592-596.
167. Conti E., Franks N.P., Brick P. (1996) Crystal structure of firefly luciferase throws light on a superfamily of adenylate-forming enzymes. *Structure* **4**: 287-298.
168. Branchini B.R., Magyar R.A., Murtiashaw M.H., Portier N.C. (2001) The role of active site residue arginine 218 in firefly luciferase bioluminescence. *Biochemistry* **40**: 2410-2418.

-
169. McElroy W.D., Seliger H.H. (1961) Mechanisms of bioluminescent reactions. In *Light and Life*. McElroy W.D., Glass B. (eds). Johns Hopkins Press. pp. 219-257.
170. Seliger H.H., McElroy W.D. (1964) The colors of firefly bioluminescence: enzyme configuration and species specificity. *P. Natl. Acad. Sci. USA* **52**: 75-81.
171. Wood K.V. (1990) Firefly luciferase: A new tool for molecular biologists. *Promega Notes* **28**: 1-2.
172. Hanahan D. (1983) Studies on transformation of *Escherichia coli* with plasmids. *J. Mol. Biol.* **166**: 557-580.
173. Studier F.W., Moffatt B.A. (1986) Use of bacteriophage T7 RNA polymerase to direct selective high-level expression of cloned genes. *J. Mol. Biol.* **189**: 113-130.
174. Miller J.H. (1972) Assay of β -galactosidase. In *Experiments in Molecular Genetics*. Miller J.H. (ed). Cold Spring Harbor Laboratory. pp. 352-355.
175. Maniatis T., Fritsch E.F., Sambrook J. (1982) *Molecular cloning: a laboratory manual*. New York: C.S.H.
176. Gunsalus-Miguel A., Meighen E.A., Nicoli M.Z., Nealson K.H., Hastings J.W. (1972) Purification and properties of bacterial luciferases. *J. Biol. Chem.* **247**: 398-404.
177. Dagert M., Ehrlich S.D. (1979) Prolonged incubation in calcium chloride improves the competence of *Escherichia coli* cells. *Gene* **6**: 23-28.
178. Bazaral M., Helinski D.R. (1968) Circular DNA forms of colicinogenic factors E1, E2 and E3 from *Escherichia coli*. *J. Mol. Biol.* **36**: 185-194.
179. Saiki R.K., Scharf S., Faloona F., Mullis K.B., Horn G.T., Erlich H.A., Arnheim N. (1985) Enzymatic amplification of β -globin genomic sequences and restriction site analysis for diagnosis of sickle cell anemia. *Science* **230**: 1350-1354.
180. Mullis K., Faloona F., Scharf S., Saiki R., Horn G., Erlich H. (1986) Specific enzymatic amplification of DNA in vitro: the polymerase chain reaction. *Cold Spring Harb. Sym.* **51**: 263-273.
181. Saiki R.K., Bugawan T.L., Horn G.T., Mullis K.B., Erlich H.A. (1986) Analysis of enzymatically amplified β -globin and HLA-DQ α DNA with allele-specific oligonucleotide probes. *Nature* **324**: 163-166.

-
182. Embury S.H., Scharf S.J., Saiki R.K., Gholson M.A., Golbus M., Arnheim N., Erlich H.A. (1987) Rapid prenatal diagnosis of sickle cell anemia by a new method of DNA analysis. *N. Engl. J. Med.* **316**: 656-661.
183. Bradford M.M. (1976) A rapid and sensitive method for the quantitation of microgram quantities of protein utilizing the principle of protein-dye binding. *Anal. Biochem.* **72**: 248-254.
184. Laemmli U.K. (1970) Cleavage of structural proteins during the assembly of the head of bacteriophage T4. *Nature* **227**: 680-685.
185. Blum H., Beier H., Gross H.J. (1987) Improved silver staining of plant proteins, RNA and DNA in polyacrylamide gels. *ELECTROPHORESIS* **8**: 93-99.
186. Lei B., Cho K.W., Tu S.C. (1994) Mechanism of aldehyde inhibition of *Vibrio harveyi* luciferase. Identification of two aldehyde sites and relationship between aldehyde and flavin binding. *J. Biol. Chem.* **269**: 5612-5618.
187. Francisco W.A., Abu-Soud H.M., Baldwin T.O., Raushel F.M. (1993) Interaction of bacterial luciferase with aldehyde substrates and inhibitors. *J. Biol. Chem.* **268**: 24734-24741.
188. Gerlach W., Stern O. (1922) Der experimentelle Nachweis des magnetischen Moments des Silberatoms. *Z. Physik* **8**: 110-111.
189. Berliner L.J. (1998) Spin labeling: the next millenium. In *Biological Magnetic Resonance*. New York: Plenum Press
190. Root K.S., Hill C.L., Lawrence L.M., Whitesides G.M. (1989) The mechanism of formation of Grignard reagents: trapping of free alkyl radical intermediates by reaction with tetramethylpiperidine-N-oxyl. *J. Am. Chem. Soc.* **111**: 5405-5412.
191. Barton D.H.R., Le Gloahec V.N., Smith J. (1998) Study of a new reaction: trapping of peroxy radicals by TEMPO. *Tetrahedron Lett.* **39**: 7483-7486.
192. Finkelstein E., Rosen G.M., Rauckman E.J. (1980) Spin trapping. Kinetics of the reaction of superoxide and hydroxyl radicals with nitrones. *J. Am. Chem. Soc.* **102**: 4994-4999.
193. Chen Y.R., Chen C.L., Yeh A., Liu X., Zweier J.L. (2006) Direct and indirect roles of cytochrome b in the mediation of superoxide generation and NO catabolism by mitochondrial succinate-cytochrome c reductase. *J. Biol. Chem.* **281**: 13159-13168.

-
194. Bosnjakovic A., Schlick S. (2006) Spin trapping by 5,5-dimethylpyrroline-N-oxide in fenton media in the presence of nafion perfluorinated membranes: limitations and potential. *J. Phys. Chem. B* **110**: 10720-10728.
195. Ueda J., Saito N., Ozawa T. (1996) ESR spin trapping studies on the reactions of hydroperoxides with Cu (II) complex. *J. Inorg. Biochem.* **64**: 197-206.
196. Castelhana A.L., Perkins M.J., Griller D. (1983) Spin trapping of hydroxyl in water: decay kinetics for the $\bullet\text{OH}$ and $\text{CO}_2^{\bullet-}$ adducts to 5,5-dimethyl-1-pyrroline-N-oxide. *Can. J. Chem.* **61**: 298-299.
197. Sakai M., Takahashi H. (1996) One-electron photoreduction of flavin mononucleotide: time-resolved resonance Raman and absorption study. *J. Mol. Struct.* **379**: 9-18.
198. Neese F. (2006) Importance of direct spin-spin coupling and spin-flip excitations for the zero-field splittings of transition metal complexes: a case study. *J. Am. Chem. Soc.* **128**: 10213-10222.
199. Dauw X.L.R., Poluektov O.G., Warntjes J.B.M., Bronsveld M.V., Groenen E.J.J. (1998) Triplet-state dynamics of C_{70} . *J. Phys. Chem. A* **102**: 3078-3082.
200. Hahn E.L. (1950) Spin echoes. *Phys. Rev.* **80**: 580-594.
201. Karas M., Hillenkamp F. (1988) Laser desorption ionization of proteins with molecular masses exceeding 10,000 daltons. *Anal. Chem.* **60**: 2299-2301.
202. Tanaka K., Waki H., Ido Y., Akita S., Yoshida Y., Yoshida T., Matsuo T. (1988) Protein and polymer analyses up to m/z 100 000 by laser ionization time-of-flight mass spectrometry. *Rapid Commun. Mass Spectrom.* **2**: 151-153.
203. Fenn J.B., Mann M., Meng C.K., Wong S.F., Whitehouse C.M. (1989) Electrospray ionization for mass spectrometry of large biomolecules. *Science* **246**: 64-71.
204. Neese F. (2008) ORCA - an *ab initio*, density functional and semiempirical program package, Version 2.6. Bonn: University of Bonn.
205. Weigend F., Ahlrichs R. (2005) Balanced basis sets of split valence, triple zeta valence and quadruple zeta valence quality for H to Rn: design and assessment of accuracy. *Phys. Chem. Chem. Phys.* **7**: 3297-3305.
206. Becke A.D. (1988) Density-functional exchange-energy approximation with correct asymptotic behavior. *Phys. Rev. A* **38**: 3098-3100.
207. Becke A.D. (1993) Density-functional thermochemistry. III. The role of exact exchange. *J. Chem. Phys.* **98**: 5648-5652.

-
208. Sinnecker S., Neese F. (2006) Spin-spin contributions to the zero-field splitting tensor in organic triplets, carbenes and biradicals - a density functional and ab initio study. *J. Phys. Chem. A* **110**: 12267-12275.
209. van Gastel M. (2009) The effect of spin polarization on zero field splitting parameters in paramagnetic π -electron molecules. *J. Chem. Phys.* **131**: 124111-124117.
210. McConnell H.M., Chesnut D.B. (1958) Theory of isotropic hyperfine interactions in π -electron radicals. *J. Chem. Phys.* **28**: 107-117.
211. Bamberg P., Hemmerich P. (1961) Farbe und Konstitution der Isoalloxazin-Silber-Komplexe. Zum Verhalten des Riboflavins gegen Metallionen II. *Helv. Chim. Acta* **44**: 1001-1011.
212. Baarda I.F., Metzler D.E. (1961) Complexes of riboflavin with silver and other metal ions. *Biochim. Biophys. Acta* **50**: 463-471.
213. Klamt A., Schüürmann G. (1993) COSMO: a new approach to dielectric screening in solvents with explicit expressions for the screening energy and its gradient. *J. Chem. Soc., Perkin Trans. 2*: 799-805.
214. Vijayakumar M., Gopinathan M.S. (1996) Spin-orbit coupling constants of transition metal atoms and ions in density functional theory. *J. Mol. Struct.-Theochem.* **361**: 15-19.
215. Neiss C., Saalfrank P. (2003) *Ab initio* quantum chemical investigation of the first steps of the photocycle of phototropin: a model study. *Photochem. Photobiol.* **77**: 101-109.
216. Studier F.W., Rosenberg A.H., Dunn J.J., Dubendorff J.W. (1990) Use of T7 RNA polymerase to direct expression of cloned genes. *Methods Enzymol.* **185**: 60-89.
217. Novick R.P. (1987) Plasmid incompatibility. *Microbiol. Rev.* **51**: 381-395.
218. Nordström K., Austin S.J. (1989) Mechanisms that contribute to the stable segregation of plasmids. *Annu. Rev. Genet.* **23**: 37-69.
219. Austin S., Nordström K. (1990) Partition-mediated incompatibility of bacterial plasmids. *Cell* **60**: 351-354.
220. Velappan N., Sblattero D., Chasteen L., Pavlik P., Bradbury A.R.M. (2007) Plasmid incompatibility: more compatible than previously thought? *Protein Eng. Des. Sel.* **20**: 309-313.

-
221. Eley M., Lee J., Lhoste J.M., Cormier M.J., Hemmerich P. (1970) Bacterial bioluminescence. Comparisons of bioluminescence emission spectra, the fluorescence of luciferase reaction mixtures, and the fluorescence of flavin cations. *Biochemistry* **9**: 2902-2908.
222. Kolesnikov M.P., Kritsky M.S. (2001) Study of chemical structure and of photochemical activity of abiogenic flavin pigment. *J. Evol. Biochem. Phys.* **37**: 507-514.
223. Meighen E.A., Hastings J.W. (1971) Binding site determination from kinetic data: reduced flavin mononucleotide binding to bacterial luciferase. *J. Biol. Chem.* **246**: 7666-7674.
224. Lei B., Tu S.C. (1998) Mechanism of reduced flavin transfer from *Vibrio harveyi* NADPH-FMN oxidoreductase to luciferase. *Biochemistry* **37**: 14623-14629.
225. Ehrenberg A., Eriksson L., Müller F. (1966) Electron spin resonance hyperfine splittings from zinc and cadmium in flavin radical chelates. *Nature* **212**: 503-504.
226. Nakamura T., Kira A., Imamura M. (1982) Enhancement of the intersystem crossing of pyrene by metal ions in sodium dodecyl sulfate micelle solutions. *J. Phys. Chem.* **86**: 3359-3363.
227. Samanta A., Fessenden R.W. (1989) Sensitized and heavy atom induced production of acenaphthylene triplet: a laser flash photolysis study. *J. Phys. Chem.* **93**: 5823-5827.
228. Liao H.H., Yang C.M., Wu C.H., Sheng-Fu H., Lee W.S., Hsin-Fei M., Jow-Tsong S., Chain-Shu H. (2007) Large enhancement of intersystem crossing in polyfluorenes by iridium-complex doping. *Appl. Phys. Lett. b* **90**: 013504-013504-3.
229. Weber G. (1950) Fluorescence of riboflavin and flavin-adenine dinucleotide. *Biochem. J.* **47**: 114-121.
230. Varnes A.W., Dodson R.B., Wehry E.L. (1972) Interactions of transition-metal ions with photoexcited states of flavines. Fluorescence quenching studies. *J. Am. Chem. Soc.* **94**: 946-950.
231. Drössler P., Holzer W., Penzkofer A., Hegemann P. (2003) Fluorescence quenching of riboflavin in aqueous solution by methionin and cystein. *Chem. Phys.* **286**: 409-420.
232. Christie J.M. (2007) Phototropin blue-light receptors. *Annu. Rev. Plant Biol.* **58**: 21-45.

-
233. Malhotra A. (2009) Tagging for protein expression. In *Methods in Enzymology: Guide to Protein Purification*. Burgess R.R., Murray P. (eds). Academic Press. pp. 239-258.
234. Woestenenk E.A., Hammarström M., van den Berg S., Härd T., Berglund H. (2004) His tag effect on solubility of human proteins produced in *Escherichia coli*: a comparison between four expression vectors. *J. Struct. Func. Genom.* **5**: 217-229.
235. Terpe K. (2003) Overview of tag protein fusions: from molecular and biochemical fundamentals to commercial systems. *Appl. Microbiol. Biotech.* **60**: 523-533.
236. Thoden J.B., Holden H.M., Fisher A.J., Sinclair J.F., Wesenberg G., Baldwin T.O., Rayment I. (1997) Structure of the β_2 homodimer of bacterial luciferase from *Vibrio harveyi*: X-ray analysis of a kinetic protein folding trap. *Protein Sci.* **6**: 13-23.
237. Inlow J.K., Baldwin T.O. (2002) Mutational analysis of the subunit interface of *Vibrio harveyi* bacterial luciferase. *Biochemistry* **41**: 3906-3915.
238. Sinclair J.F., Waddle J.J., Waddill E.F., Baldwin T.O. (1993) Purified native subunits of bacterial luciferase are active in the bioluminescence reaction but fail to assemble into the $\alpha\beta$ structure. *Biochemistry* **32**: 5036-5044.
239. Noland B.W., Dangott L.J., Baldwin T.O. (1999) Folding, stability, and physical properties of the α subunit of bacterial luciferase. *Biochemistry* **38**: 16136-16145.
240. Noland B.W., Baldwin T.O. (2003) Demonstration of two independently folding domains in the α subunit of bacterial luciferase by preferential ligand binding-induced stabilization. *Biochemistry* **42**: 3105-3112.
241. Colepicolo P., Cho K.W., Poinar G.O., Hastings J.W. (1989) Growth and luminescence of the bacterium *Xenorhabdus luminescens* from a human wound. *Appl. Environ. Microb.* **55**: 2601-2606.
242. Tyulkova N.A., Sandalova T.P. (1996) Comparative study of temperature effects on bacterial luciferases. *Biochemistry* **61**: 205-214.
243. Hastings J.W., Weber K., Friedland J., Eberhard A., Mitchell G., Gunsalus A. (1969) Structurally distinct bacterial luciferases. *Biochemistry* **8**: 4681-4689.
244. Cline T.W., Hastings J.W. (1972) Mutationally altered bacterial luciferase. Implications for subunit functions. *Biochemistry* **11**: 3359-3370.

245. Chen L.H., Baldwin T.O. (1989) Random and site-directed mutagenesis of bacterial luciferase: investigation of the aldehyde binding site. *Biochemistry* **28**: 2684-2689.
246. Hosseinkhani S., Szittner R., Meighen E.A. (2005) Random mutagenesis of bacterial luciferase: critical role of Glu¹⁷⁵ in the control of luminescence decay. *Biochem. J.* **385**: 575-580.
247. Gitel'zon I.I., Rodicheva É.K., Medvedeva S.I., Primakova G.A., Bartsev S.I., Kratasyuk G.A., Petushkov V.N., Mezhevikin V.V., Vysotskii E.S., Zavoruev V.V. (1984) Luminous bacteria. Novosibirsk: Nauka.
248. Meighen E.A., MacKenzie R.E. (1973) Flavine specificity of enzyme-substrate intermediates in the bacterial bioluminescent reaction. Structural requirements of the flavine side chain. *Biochemistry* **12**: 1482-1491.
249. Eckstein J.W., Hastings J.W., Ghisla S. (1993) Mechanism of bacterial bioluminescence: 4a,5-Dihydroflavin analogs as models for luciferase hydroperoxide intermediates and the effect of substituents at the 8-position of flavin on luciferase kinetics. *Biochemistry* **32**: 404-411.
250. Baldwin T.O., Riley P.L. (1980) Anion binding to bacterial luciferase: evidence for binding associated changes in enzyme structure. In *Flavins and Flavoproteins*. Yagi K., Yamano T. (eds). Tokyo and Baltimore: Japan Scientific Societies Press and University Park Press. pp. 139-147.
251. Moore C., Lei B., Tu S.C. (1999) Relationship between the conserved α subunit arginine 107 and effects of phosphate on the activity and stability of *Vibrio harveyi* luciferase. *Arch. Biochem. Biophys.* **370**: 45-50.
252. Lin L.Y.-C., Sulea T., Szittner R., Vassilyev V., Purisima E.O., Meighen E.A. (2001) Modeling of the bacterial luciferase-flavin mononucleotide complex combining flexible docking with structure-activity data. *Protein Sci.* **10**: 1563-1571.
253. Hastings J.W., Baldwin T.O., Nicoli M.Z. (1978) Bacterial luciferase: assay, purification, and properties. In *Methods in Enzymology: Bioluminescence and Chemiluminescence*. Marlene A.D. (ed). Academic Press. pp. 135-152.
254. Tu S.C., Hastings J.W. (1975) Differential effects of 8-anilino-1-naphthalenesulfonate upon binding of oxidized and reduced flavines by bacterial luciferase. *Biochemistry* **14**: 4310-4316.
255. De Vries J.G., Kellogg R.M. (1980) Reduction of aldehydes and ketones by sodium dithionite. *J. Org. Chem.* **45**: 4126-4129.

-
256. Yarmolinsky M.B., Colowick S.P. (1956) On the mechanism of pyridine nucleotide reduction by dithionite. *Biochim. Biophys. Acta* **20**: 177-189.
257. Zamora P.L., Villamena F.A. (2012) Theoretical and experimental studies of the spin trapping of inorganic radicals by 5,5-dimethyl-1-pyrroline N-oxide (DMPO). 3. Sulfur dioxide, sulfite, and sulfate radical anions. *J. Phys. Chem. A* **116**: 7210-7218.
258. Ohya-Nishiguchi H., Packer L. (1995) Bioradicals detected by ESR spectroscopy. Berlin: Birkhäuser.
259. Campbell Z.T., Baldwin T.O. (2009) Fre is the major flavin reductase supporting bioluminescence from *Vibrio harveyi* luciferase in *Escherichia coli*. *J. Biol. Chem.* **284**: 8322-8328.
260. Jeffers C.E., Nichols J.C., Tu S.C. (2002) Complex formation between *Vibrio harveyi* luciferase and monomeric NADPH:FMN oxidoreductase. *Biochemistry* **42**: 529-534.
261. Reis A., Domingues M.R.M., Amado F.M.L., Ferrer-Correia A.J.V., Domingues P. (2003) Detection and characterization by mass spectrometry of radical adducts produced by linoleic acid oxidation. *J. Am. Soc. Mass. Spectr.* **14**: 1250-1261.
262. Tu S.C. (2008) Activity coupling and complex formation between bacterial luciferase and flavin reductases. *Photochem. Photobiol. Sci.* **7**: 183-188.
263. Tabata M., Yazaki K., Nishikawa Y., Yoneda F. (1993) Inhibition of shikonin biosynthesis by photodegradation products of FMN. *Phytochemistry* **32**: 1439-1442.
264. Nemtseva E.V., Kudryasheva N.S. (2007) The mechanism of electronic excitation in the bacterial bioluminescent reaction. *Russ. Chem. Rev.* **76**: 91-100.

Appendix figures

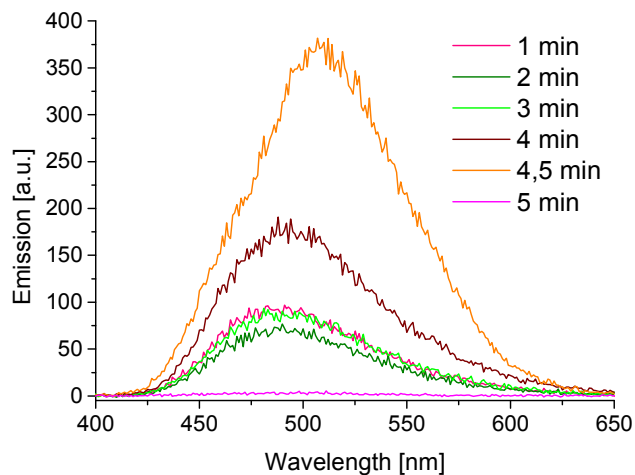


Figure 0-1: Emission scans over 5 min showing the emission shift from 490 to 510 nm. Luminescence was induced with octanal.

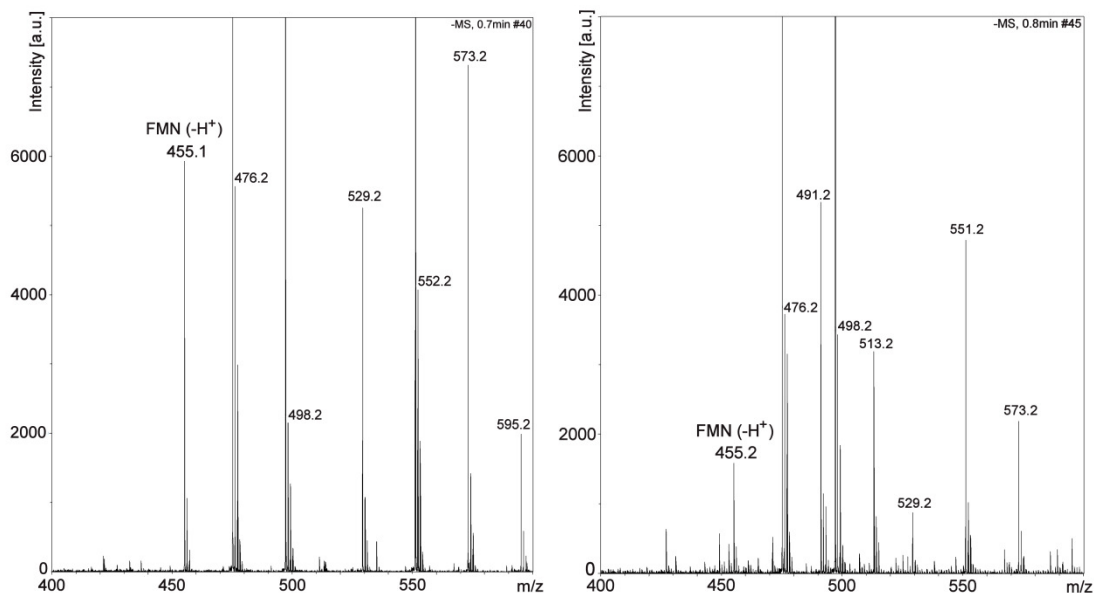


Figure 0-2: Mass spectra of the not illuminated (left) and illuminated (right) sample. FMN ions are present at 455.2 m/z. Signal for FMN is conspicuously weaker in the illuminated sample.

Publications

Parts of this thesis have already been published in

Kammler, L., van Gastel, M. (2012) Electronic Structure of the Lowest Triplet State of Flavin Mononucleotide. *J. Phys. Chem. A* **116**: 10090–10098.

Oral presentations:

Kammler, L., van Gastel, M. (2009) Light by Spin Centers. A Magnetic Resonance Study of Bioluminescence in Bacteria. *SFB 813 workshop – Chemistry at Spin Centers: Concepts, Mechanisms, Functions, Schleiden, Germany.*

Kammler, L., van Gastel, M. (2011) Bacterial Bioluminescence - Molecular Biology and Spectroscopy. *SFB 813 workshop – Chemistry at Spin Centers: Concepts, Mechanisms, Functions, Schleiden, Germany.*

Posters:

Kammler, L., Marchanka, A., van Gastel, M. (2009) Light by Spin Centers. A Magnetic Resonance Study of Bioluminescence in Bacteria. SFB 813 workshop – Chemistry at Spin Centers: Concepts, Mechanisms, Functions, *Schleiden, Germany.*

Kammler, L., Marchanka, A., van Gastel, M. (2010) Light by Spin Centers. A Magnetic Resonance Study of Bioluminescence in Bacteria. 3rd Joint Conference of the German Society for Hygiene and Microbiology (DGHM) and the Association for General and Applied Microbiology (VAAM), *Hannover, Germany.*

Kammler, L., Marchanka, A., van Gastel, M. (2010) Light by Spin Centers. A Magnetic Resonance Study of Bioluminescence in Bacteria. Workshop on multi-frequency EPR in the biosciences at the Lorentz Center, *Leiden, The Netherlands*.

Kammler, L., van Gastel, M. (2010) Light by Spin Centers. A Magnetic Resonance Study of Bioluminescence in Bacteria. Joint EUROMAR 2010 and 17th ISMAR Conference, *Florence, Italy*.

Kammler, L., van Gastel, M. (2010) Bacterial bioluminescence investigated by EPR spectroscopy. International Symposium 2010 - Chemistry at Spin Centers (SFB 813), *Bad Honnef, Germany*.

Kammler, L., van Gastel, M. (2012) Spin trapping of a radical intermediate in the light emitting reaction of bacterial bioluminescence. Poster, 54th Rocky Mountain Conference on Analytical Chemistry, *Copper Mountain, Colorado, USA*.

Acknowledgment

This thesis is the result of years of work at the Institute of Physical and Theoretical Chemistry in Bonn and the Max Planck Institute for Chemical Energy Conversion. I am thankful to all the people who had a share in any way during these years. I would like to express my special thanks to the ones mentioned below:

First, I owe my deepest gratitude to my supervisor, PD Dr. Maurice van Gestel, for his patient guidance and leadership during my entire PhD studies. His courtesy in giving constant advice and help in various questions were always a strong and encouraging support for me. Without him this thesis would not have been possible. I appreciate the opportunity to work on such an exciting and demanding project and to attend several national and international conferences and workshops.

I am sincerely thankful to Prof. Dr. Peter Vöhringer for being part of the main dissertation committee.

I would like to express my gratitude to Prof. Dr. Ulrich Kubitscheck and Prof. Dr. Olav Schiemann. They kindly offered me to perform parts of my experiments in their laboratories.

Dr. Marianne Engeser and her staff members are gratefully acknowledged for performing mass spectrometry analyses.

Professional help on the topics of molecular biology and protein kinetics were given by Dr. Jan-Peter Siebrasse. I deeply value his suggestions. I would like to thank Yvonne Stockdreher, Claudio Nietzel and Julia Hockling for their kind help with gel chromatography.

The Max Planck Institute for Chemical Energy Conversion gave me the opportunity to perform numerous EPR and fluorescence experiments. I would like to thank everybody at this institute for a pleasant working atmosphere.

I thank the SFB 813 “Chemistry at Spin Centers” (DFG) at the University of Bonn for their financial support.

All my former EPR group members are gratefully mentioned for providing an enjoyable environment with fruitful discussions. Dr. Alexander Marchanka is especially noted for his patience of a saint and advanced training ‘up kölsch’. Andreas Meyer was a pleasant conversationalist, especially concerning vital matters of lunch and current movies.

The discussion group on the first floor of the Institute of Physical Chemistry in Bonn is joyfully acknowledged. All these scientific and nonscientific conversations with Katharina Scherer, Claudio Nietzel and Lisa Büttner during coffee breaks will be remembered forever.

Whenever needed, I was welcome in Christina Reuter’s office; our numerous constructive discussions of everyday commodities always cheered me up. Anne Kirschfink and Rolf Paulig are thanked for cheerful chit-chats and for incessantly providing goodies.

Finally, I would like to express my heartfelt gratitude to my family for the love and caring support they have given me. They have always motivated and encouraged me through out my studies and constantly believed in me.